Analysis of Desertification Situation Using Remote Sensing and GIS –A Case Study in Ongniud Banner, Horqin Sandy Land

February, 2017

Chiba University
Graduate School of Science
Division of Geosystem and Biological Sciences
Department of Earth Sciences

Bai Xiulian

（千葉大学審査学位論文）

Analysis of Desertification Situation Using Remote Sensing and GIS –A Case Study in Ongniud Banner, Horqin Sandy Land

2017 年 2 月

千葉大学大学院理学研究科
地球生命圏科学専攻 地球科学コース

白　秀蓮

Table of Contents

Abstract

Desertification is a crucial environmental issue in the Horqin Sandy Land, Inner Mongolia Autonomous Region of China. The Horqin Sandy Land is an important grain base region of northern China, thus there is increasing necessity to monitor the situation for better understanding of desertification processes. Therefore, in this study, we analyzed desertification from 2000 onward by utilizing remote sensing technology in Ongniud Banner in the western part of the Horqin Sandy Land.

In order to recognize desertification through land use changes, in this research we attempted to extract classification categories representing the state of the land, which we subdivided into the normal classification categories. For that purpose, we performed the land use classification by combining multiple spectral indices that can be calculated from satellite data to each spectral band of the Landsat satellite to construct multi-band input data for a Support Vector Machine-based supervised classification approach. Applying this method to Landsat archive images in 2000, 2009, and 2015, we made land use maps of the three time periods and clarified the desertification situation. Over the past 16 years, irrigated farmlands and salinized areas were expanded, whereas water bodies shrank, and exposed sandy lands were replaced by sparse grass and moderate grass converted to sparse grass.

At the same time, we calculated ground surface variations to analyze the state of desertification. In addition, we tried comprehensive understanding of land use change accompanied with desertification of the research area based on socioeconomic situations and policy of Horqin Sandy Land discussed in the study period. As a result, a 3051 km2 area suffered from desertification in the study area from 2000 to 2015, and desertification of moderate grass was the most common type of desertification (21% of total desertified area), followed by desertification of other forest, sparse grass, and forest areas at 19%, 16%, and 15% respectively. And less desertification occurred in dense grass (8%) and dry land (6%) areas. New knowledge was achieved in this study, such as that the area of sandy land decreased during the analysis period, but the deterioration of land was progressing.

Acknowledgements

This thesis would not have been completed without the immense help form many people, I would like to thank all those people who gave me help.

First, I would like to express my sincere gratitude to my supervisor Professor Ryutaro Tateishi and Akihiko Kondoh for the support my Ph.D. study and research work. I appreciate their guidance and valuable suggestions helped me to write of this thesis.

I also would like to thank other members of a reviewer committee of my thesis: Prof. Hiroaki Kuze, Prof. Chiharu Hongo and Prof. Makoto Ito, for their encouragement, insightful comments and suggestions.

My sincere thanks also go to Dr. Ram C. Sharma for checking English Grammar and organizing my paper publication. Dr. Hasi Bagan, and Has Baator, Eerdeni, Jian Xu gave the valuable comments for my publication.

I appreciate the help received from Dr. Bayan Alsaaideh, Haireti Alifu, Saieed for their valuable comments and the stimulating discussions. Buhe with preparing Climate data for me.

I thank my colleagues in Tateishi Laboratory and Kondoh Laboratory for all the fun we have had together.

Special thanks given to my Senior Gegen Tana and Husi Letu gave me help for my study and life.

I would also like to thank the Japan Student Services Organization (JASSO) offers the honors scholarship to me for one year.

Finally, I thank to my family members which include my parents, elder brother, sister- in-law and my nephew, for their financial support, encouragement and funny communication throughout my life. Without their support, it is impossible for me to

finish my Ph.D. course.

List of Tables

List of Figures

Chapter 1. Introduction

1.1 Research background

Desertification is a crucial environmental issue restricting social, economic, and political development in arid and semi-arid areas (Warren, 1988; Chen, 2005). Desertification has been defined in several ways, but the most widely accepted one is from the Conference on Environment and Development （UNCED）, which was held in 1992 and defined desertification as land degradation in arid, semi-arid, and dry sub-humid areas resulting from various factors, including climate variations and human activities (WHO, 1992; Sciortino, 2001; Darkoh, 1998; Secretariat, 1977). Desertification has affected about 35 million km^2 of land globally and overall, 35% of the Earth's land surface was at risk of undergoing similar changes (Nicholson, 1998).

In recent years, many problems affecting the environment and population have emerged, such as land shortages, environmental deterioration, and reduction of biological and economic productivity. Water scarcity, poverty, and migration have all increased due to the rapid spread of desertification. These problems have threatened human survival and sustainable economic development (Wang, 2004; El-Karouri, 1986; Bullock, 1996). It is argued that sustainability will be a great challenge facing human society in coming decades in fragile ecological zones, particularly in the transitional and marginal zones of agriculture and animal husbandry, which have been affected by intensive and irrational human activities (Pink, 2016; Lik, 2015; Hasi, 2010).

China is a developing country with large population and scarce arable land, and is plagued by long-term and large-scale desertification (Wang, 2013). Investigation of China's deserts and sandy lands began in the late 1950s (Zhu, 1989). Desert areas in

China are expanding by between 2460 and 10,400 km^2 per year. As much as 3.317 million km^2 (34.6 % of the total land area) in China is affected by desertification, and up to 400 million people are struggling with unproductive agricultural land and water shortages. This is mostly distributed in the arid, semi-arid, and sub-humid areas in the western part of northeast China, the northern part of northern China, and most parts of northwest China (Plit, 1995; Jun, 2012).

Since 1994, China's State Forestry Administration (SFA) has conducted a national desertification survey at the country level every 5 years. The 1994 survey indicated that the area affected by desertification was 262.23 million km^2 in 1994, 267.41 million km^2 in 1999, 263.62 million km^2 in 2004, and 262.37 million km^2 in 2009. Desertified area increased by 10,400 km^2 yearly from 1996 to 1999, and decreased by 7,585 km^2 yearly from 1999 to 2004. The desertification affected area covered 18 provinces and 508 counties, mainly including Beijing, Tianjian, Heibei, Shanxi, Inner Monglia, Liaoning, Jilin, Shandong, Henan, Hainan, Sichuan, Yunnan, Tibet, Shaanxi, Gansu, Qinghai, Ningxia, and Xinjiang. The second largest desertification affected area occurred in the Inner Mongolia Autonomous Region (SFA, 2011). Desertification mainly occurred in five provinces or autonomous regions, whose total desertified area accounts for 95.48% of China's total land area, while the other 13 provinces, autonomous regions, and municipalities account for the remaining 4.52% (Wang, 2012).

The Horqin Sandy Land, one of the four largest sandy lands in northern China, has a long history of desertification and land degradation. Feng (2015) reported that socio-economic factors were the dominant driving forces affecting desertification in this region. A rapid increase of population and inappropriate human activities, such as agricultural reclamation and dry farmland abundance, overgrazing, excessive fuel wood cutting, blind collection of medicinal herbs, poorly managed tourism, over-

consumption of water resources, mining, and road cutting have induced desertification continuously in the Horqin Sandy Land (Huang, 2008; Han, 2010; Duan, 2014). Moreover, climate change in recent decades has severely intensified desertification (Fan, 2001). In addition to global warming, intensive land use and land cover changes coupled with frequent long-duration droughts have resulted in a significant decline in the groundwater table (Zhao, 2016).

During the Liao Dynasty (907–1125 A.D.), the Horqin Sandy Land was full of tall forests and dense grasslands that sustained nomadic herders. Since the nineteenth century, a rapid increase of agricultural migrants into this region started to convert the ancient grassland and woodland into agricultural areas, which reduced available grazing land and put marginal lands under cultivation. This situation continued into the twentieth century, reaching a height of development in the 1950s and 1960s with a rapid expansion of human settlements and urban areas. In the beginning of the Great Leap Forward (1958–1960) and during the following two decades, expanding cultivation forced local nomadic herders to move into the border area, as most of the area was managed by agriculturalists. By the early 1980s, the rural reform program had played a key role in grassland overgrazing under the "household responsibility" system, and now the locally implemented "double responsibility" system may do little to reduce overgrazing (Hasi, 2010; Wang, 2013; Wang, 2004). With the development in the agricultural and industrial sectors, these essentially uncontrolled activities have resulted in destruction of woodland and grassland, degradation of surface soil, and increased water consumption (Wang, 2004). Since 2001, a series of large sandstorms have swept through much of northern China. The Chinese government and social media started to focus on desertification problems (Zhao, 2009). As part of its efforts to control desertification in affected regions, the Chinese government implemented a series of

ecological engineering programs, including the Three-North Shelter Forest Program (1978–2050), National Program on Combating Desertification (1991–2000), Beijing and Tianjin Sandstorm Source Treatment Program (2001–2010), Grain to Green Program (2003–present), Returning Grazing Land to Grassland Program (2003–present), and China's Western Development Strategy that focus on increasing vegetation coverage by prohibiting grazing, planting grasses and trees, and constructing shelter forest to protect farmland against blowing sand(Li, 2015).However, monitoring and assessment has identified that success has been achieved only in a few local regions (Zhao, 2005; Wang, 2006; Ellis, 1992; Jaime, 2013; Iqbal, 2014), while inappropriate measures have caused further desertification in other desertified areas.

Desertification in China has been aggravating. It is a major challenge facing humanity, because of the problems ranging from the scale of the problem, a shortage of national financing, and difficulties in land treatment and vegetation protection (Alatorre, 2009). Agricultural expansion and urbanization in this region led to dramatic changes in land use/land cover structure.

Land use/land cover (LULC) change analysis assists decision makers to ensure sustainable development and to understand the dynamics of our changing environment (Sharma, 2016). To date, however, previous studies on LULC structure spatial-temporal change pattern mainly based on spectral information of remote sensing data, improve the classification accuracy is necessity. Multitemporal coverage from remote sensing images over the large scale of Earth's surface provides substantial information to facilitate the monitoring of environmental problems, such as land degradation trends (Ran, 2004). In this study, moderate spatial resolution and multi-temporal Landsat archive images are uniquely ideal for identifying changes in LULC structure over time. The main objective of this study is analyzing spatiotemporal change patterns in LULC

structure in second-level land cover classes in Ongniud Banner. In the LULC mapping process, we use the Support Vector Machine to demonstrate the usefulness of multi-features for improving classification accuracy. The main second-level land cover classes mentioned in this study help us realize the desertification situation caused by human activities and the climate characteristics in this area.

1.2 Review of previous works

The Horqin Sandy Land is located in a fragile ecotone, such as the transitional zone between pastoral and animal husbandry areas, and desertification is a serious ecological problem in this region (Kou, 1994). There is an increasing need for monitoring and assessment of desertification processes as this can provide essential information for sustainable environmental management in arid and semi-arid regions.

Desertification progress is evaluated by several methods, such as direct observation and measurement, mathematical models, parametric equations, remote sensing (RS), and other indicators (Sepehr et al., 2007). Previous attempts to reveal the desertification status and intensity in the Horqin Sandy Land carried out desertification monitoring research from different subjects. Wulantuya (2000) analyzed cropland change related to cropland reclamation reform in the Horqin Sandy Land using statistical data from the last 50 years, and reported that cropland reclamation reform is an important factor affecting desertification. Zhang and Shao (2000) used China's land use dataset at a 1:1,000,000 scale to analyze land use change. However, these studies selected the prefecture as the study unit, and results did not present when and where the desertification process occurred or how it progressed.

Hasi (2010) used Landsat MSS/TM/ETM+ to analyze LULC change from 1987 to 2007, and detected significant LULC change occurring in the Horqin Sandy Land, with the population increasing and large areas of grassland and woodland converted to cropland. Moreover, sandy land expansion has slowed since 1987.

The susceptible area for desertification is mapped by combining desertification indices (Sepehr, 2007). In this process, desertification indicator selection is a crucial task (Rubio, 1998), but the relative contributions of driving forces for desertification remain unclear. Wang et al. (2006) proposed that two climate factors, drift potential and sand-

driving wind frequency, have a much stronger effect on environmental change than has been appreciated in previous research. However, the impact of human activity may have been overestimated during past the 5 decades. Qi et al. (2015) found that socioeconomic forces were dominant factors in desertification, accounting for 79.3% of the effects, whereas climate change accounted for 20.6% of the effects from 1983 to 2012. Plit et al. (1995) provided the quantity of desert affected area caused by various human activities in transitional and marginal zones of agriculture and animal husbandry. These activities include fuel wood collection (31.1%), overgrazing (28.3%), reclamation of sandy land (25.4%), and other activities (15 percent). Su et al. (2005a) conducted a comparative analysis of the effects of grazing and livestock exclusion on soil properties. The results suggest that livestock grazing exclusion is an alternative to grassland restoration. Steffens (2007) identified that the physical and chemical properties of steppe top soils remained stable after exclusion of livestock grazing and significantly recovered after 25 years of livestock exclusion. Su et al. (2005b) found that two types of shrub plantation in sandy lands effectively improve soil properties and vegetation restoration. Recently, Huang et al. (2008) identified that vegetation cover in the Horqin Sandy Land slightly increased with an undulating trend and that desert areas have been decreasing in recent decades. Zuo et al. (2008) studied soil properties under grazing and restoration. Zhao et al. (2005a) demonstrate through field experiments that long-term wind erosion and sand accumulation in farmland can result in an obvious reduction in soil infertility, dryness, and coarseness. Zhao et al. (2005b) concluded that the effect of little accumulated sand on crop yield is not significant. Crop biomass and seed production mainly correlated to soil organic matter, soil moisture, total N, and pH value in deteriorated soil environments. Zhang (2013) summarized the soil productivity reduction once sandy grassland has been converted to cropland.

Li et al. (2014) investigated the effects of soil moisture on sand saltation and dust emission, with results showing the potential of stronger saltation processes observed under wet soil conditions. Hasi et al. (2010) presented that significant LULC change occurred in the Horqin Sandy Land. Niu et al. (2015) experimental analysis revealed that land use plays a key role in controlling spatiotemporal changes in soil moisture. Zhao et al (2016) detected that significant LULC change and drought leads to groundwater resource depletion in desertified regions. Imuamirin et al. (2005) analyzed LULC change and clarified that deforestation and farmland policy led to land deterioration since 1988. Zhang et al. (2003) evaluate different measures of stabilizing sand dune, with placing wheat straw checkboard and planting *Artemisia halodendron* on the dunes as the most promising techniques for vegetation restoration in the Horqin Sandy Land. Zhang et al. (2012) discussed a series of ecological protection projects that have effectively improved different types of sandy dune.

More detailed LULC change information is needed to reflect the desertification process (Yan, 2005). However, most studies do not cover LULC change analysis in secondary sub-classes. Therefore, a time series comparison of the statistical record of desertification inventory could not reveal an accurate evolution of deserts because of the different inventory methods and survey scopes utilized at different times. On the contrary, dynamic change analysis over time thorough remote sensing data on the evolutionary history of the desertification process has been confirmed as reliable. In this research, detailed LULC change is treated as ecosystem degradation, combination of spectral data, spectral indices, spectral transformation, textural measures, and topographic to overcome the limitation of spectral based LULC classification to produce an accurate and detailed LULC map. At the same time, we calculated ground surface variations including surface soil grain size index, ground surface temperature,

ground surface water content, and ground water depth index to combine with LULC change and analyze the state of desertification in the study area between 2000–2009, 2009–2015, and 2000–2015.

1.3 Definition of Desertification

At present, the phenomenon known as desertification has attracted widespread attention from the public researchers.

The term desertification was first coined in 1927 by the French scientist and explorer Louis Lavauden, and was popularized by the French scientist Andre Aubreville as long ago as 1949 (Glantz, 1983; Aubreville, 1949). Others (e.g., Le Houerou) have discussed the phenomenon since the late 1950s.

In fact, Aubreville, a well-known botanist and ecologist, was the first to explain that desertification is not an extension of the existing desert. The Food and Agriculture Organization was the first international agency to use the word desertification in 1962. In 1977, The United Nations Conference on Desertification (UNCOD), held in Nairobi, Kenya, defined desertification as "the diminution or destruction of the biological potential of land, and (which) can lead ultimately to desert-like conditions."

It is an aspect of the widespread deterioration of ecosystems under the combined or interacting pressures of adverse and fluctuating climate and excessive exploitation. Such pressure has diminished or destroyed the biological potential, i.e., plant and animal production, for multiple use purposes at a time when increased productivity is needed to support growing populations in quest of development (Verstraete, 1986).

In February 1990, the UNEP (United Nation Environmental Program) formed an ad hoc committee for global evaluation of desertification (UNEP, 1992). It defined desertification as "land degradation in arid, semi-arid, and dry humid areas resulting mainly from adverse human impact."

Finally, this definition was accepted at the Conference on Environment and Development (UNCED, Agenda 21) held in Rio de Janeiro in 1992, which described desertification as land degradation in arid, semi-arid, and dry sub-humid areas resulting

from various factors, including climate variation and human activities. These definitions were agreed upon at the Intergovernmental Convention to Combat Desertification (ICCD, 1994).

1.4 Objective of This Study

The main objectives of this research regarded deterioration of ecological systems from the progress of desertification and presented sub-class LULC change analysis using time series Landsat data in spatial and temporal scales over the past 16 years after state and local governments implemented a series of policies to mitigate desertification and quantify the desertification in Ongniud Banner, in the western part of the Horqin Sandy Land. It was analyzed quantitatively and the result verified in conjunction with the land use dataset and SPOT-5 with 5 m high resolution image. At the same time, we calculated ground surface variations to analyze the state of desertification. In addition, this study discussed the links between desertification driving forces such as socio-economic factors and climate variations such as temperature and precipitation

The specific objectives:

1. Utilize Landsat Thermatic Mapper (TM) data from 2000 and 2009 and Landsat Operational Land Imager products acquired in 2015, to produce a LULC map for 17 categories of land sub-classes, including cropland (dry farm, irrigation land, paddy), grassland (dense grass, moderate grass, sparse grass), woodland (forest, shrub, other forest), built-up land (urban built-up, rural settlement), water body (stream and river, lake, tidal), and unused land (sandy land, bare area, salina, swampland).
2. In the LULC mapping process, estimate multiple features' (spectral data, spectral indices, spectral transformation, textural measures, and topographic) contribution using the Support Vector Machine to produce accurate LULC maps.
3. Analyze 17 categories of land sub-classes LULC change over the past 16 years to identify desertification in the study area.
4. Analyze the state of desertification by thorough study of ground surface variations

that can be calculated from Landsat satellite data.

5. Analyzing socioeconomic data and obvious interannual oscillations of climate variations, such as temperature and precipitation, linked to LULC change and desertification and understand their impact on desertification.

The result will be a basic dataset for regional managers to understand the LULC dynamic mechanisms. Further, this study aims to provide useful information for sustainable management of land resources and restoration of desertified areas in this region.

Chapter 2. Desertification in Horqin Sandy Land

Horqin Sandy Land was a desertified region resulted from irrational and intensified human activities in the background of uneven climate change. This region ever experienced obvious reverse progress during Jin Dynasty to Qing Dynasty due to diminution of human activity.

In this research according to understanding of historical desertification process to carry out characterizing of desertification present status of ongniud Banner, western part of Horqin Sandy Land and discusses the cause factors of desertification and controlling strategies.

2.1 Cause factor

Land degradation and desertification have become the increasingly server environmental and ecological problems in worldwide. These phenomenon resulting from combined insensitive and irrational human activities and the climate change.

In China, accelerating desertification is caused mainly by previous human activities: reckless land conversion to cropland, overgrazing, deforestation and irrational use of water resources, etc. (Wu Bo, 2002).

The percentage of the desertified land calculated according to each driving factors in 2000, the desertified land caused by excessive gathering of fuel wood, over grazing, over cultivation, water resource misuse and industry / mining-induced destruction, natural factors accounted for 31.8%, 28.3%, 25.4%, 9% and 5.5%, respectively (T. Wang, 2005; Behnke, 2016).

2.1.1 Human causes

According to UNEP (1992), the anthropogenic causes of desertification are over

cultivation, overgrazing, deforestation and poor irrigation practices (Darkoh, 1996). These factors are fuelled by local forces such as poverty, population pressure, and poorly conceived national policies and external forces such as protectionism and import restrictions in developed countries and the state of the world economy. The process may be aggravated by climate change, especially prolonged drought and desiccation.

2.1.1.1Over cultivation

Excessive cropping in arid and semi-arid region lead to exhaust the soil nutrient, agriculture productivity decrease season by season with the reduction of land return. Expansion agricultural land required to maintain the same agricultural productivities to sustain the large number of population and sustainable economic development, while the demand for food increasing with rapid increasing population number. Reducing fallow period and introducing irrigation measures are used to maintain output. On the other hand, farming expose the bare soils to wind erosion for many years, all these cultivation activities lead to further soil degradation and promoting salinization.

2.1.1.2 Overgrazing

Overgrazing occurred when the grazing intensity exceeds the carrying capacity of grassland because of pastoralists allow too many animals to graze on a fixed area of land (R.Z. Wang, 1995; H. L. Zhao, 1997).

Overgrazing is widely recognized as a one of the major cause factor of desertification in the worldwide. In china, there is about 3.9×10^5 km^2 of desertified land, in which 28.3% is caused by overgrazing (T.Wang, 2000).

Land surface vegetation damaged both by the large number of animal overgrazing itself and trampling. Specifically, the overgrazing resulted in considerable decreases in the plant diversity, vegetation cover, canopy height, standing crop biomass, and root biomass, and the proportion of poor quality herbages increased compared with

ungrazed grassland in the Horqin Sandy Land (T. Zhang, 2004).

The overgrazed lands fragile to water erosion and wind erosion as compaction of the soils reduces the infiltration, leading to greater runoff, while trampling increases wind erosion. Fencing/ enclosure of grassland, which confines animals to specific locations and the provision of water points and wells has led to severe localized overgrazing. Boreholes and wells also lower the water table, causing soil salinization.

Overgrazing may lead to a progressive reduction in the vegetation cover and increases wind erosion and runoff, which are conductive to desertification []. Another consequence of overgrazing is the destruction of native forage plants, which are then replaced either by annuals having little forage value or by unpalatable and toxic species (Y. Chen, 2005). For example, Cynanchum komarovii, a toxic annual, was associated with the rangeland subjected to heavy grazing in the Mu Us Sandy Land, north-central China.

2.1.1.4 Deforestation

Deforestation is most significant factor contribute to desertification, the removal of large area of forest or stand trees where the woodland has been converted to cultivated area or urban use and the trees surrounding the urban and rural settlement area stripped for firewood. The loss of vegetation cover lead to increase the land surface runoff, and the land become vulnerable to wind erosion and water erosion due to loss of root system in the land surface.

The people have continue stripping indigenous woodlands of their trees for use as fuel. At the same time, population pressure is forcing people to cut still more trees to clear land for agriculture. The disappearance of the trees adds to family labor, erodes the productivity of the land, and generally dose mischief to the economy and to people's lives.

2.1.1.5 Fuel wood collection and blind herb medicine

Fuel wood gathering is a primary cause factor for land degradation and desertification in developing country (Mallo, 2009).There have a linear relationship between fuel wood consumption with population growth and rates of fuel wood induced deforestation (Cline-Cole, 1990).

The local people harvested fuel wood for cooking, heating, and for steam engines and turbines for generate electricity. The transportation cost of the fuel wood from long distance to user household is rising, however the collecting indigenous wood is the cheapest compare to the commercial substitutes such as high cost either for the fuel itself electricity, kerosene, and energy plantation of wood, and for conversion devices for stoves and solar energy (F. David, 1986).The cost of fuel wood is rising as scarcity forces it to be transported long distances to users. However, indigenous wood will continue to be the cheapest fuel available, dung and crop residues expected. Commercial substitutes do exist: electricity, kerosene, coal, solar energy, wood from energy plantations. However, these imply a high cost either for the fuel itself (electricity, plantation wood, kerosene) or for conversion devices (solar collectors, stoves).

2.1.1.6 Policy for combating desertification

To combat desertification and implement the UNCCD, the Chinese government enacted the Law of Combating Desertification in 2002, and approved the National Plan for Combating Desertification in 2005, meanwhile, China launched a series of key national ecological engineering projects, such as the Three-North Shelterbelt development Project from1978 to 2050, National Program on Combating desertification from 1991 to 2000, Beijing and Tianjin Sandstorm Source Treatment project from 2001 to 2010,

Returning Farmland to Forest Project from 2003 to present and returning grazing land to grassland project from 2003 until present.

Also, China began the first national desertification survey in 1994 with repeat surveys planned at 5-year internals, in 1999, 2004 and 2009. The desertification areas at four surveys are, respectively, 2.622, 2.674, 2.636 and 2.634×10^6 km^2. Generally, the desertification area in China has kept stable in the past 20 years. Besides, in order to strengthen monitoring and research in desert region, the state forestry administration of China is now establishing the national desertification monitoring system and the China Desert Ecosystem Research Network (CDERN), which consist of 43 research stations across the arid, semi-arid and dry sub-humid areas in North China and the karst desertification areas in Southwest China. Finally, China has established the national desertification monitoring system and data bank, which will play an important role in the future (G.Q. Wang, 2012).

2.1.2 Climate cause

Land degradation and desertification is the result of combined effects of climate change and human activities. Climate change and other reasons (such as topography) can lead to precipitation changes which subsequently affect the vegetation productivity which is additionally deteriorated by human activities such as forestation or deforestation (Y.Z. An, 2014).

2.2 Consequence

Desertification brings many adverse impacts, it causes a decrees in farmland availability, declining crop productivity, falling incomes, disruptions to communications, and may eventually cause out-migration. Desertification also causes in increase in sand storms, silting of rivers and reservoirs, and increased soil erosion.

Chapter 3. Data sets and Method

3.1 Study area

This study was performed in Ongniud Banner, located in the western part of Horqin Sandy Land, in the southeastern part of the Inner Mongolia Autonomous Region of China. The location map of the study area shown in Figure 1. The study area was extent from 117°49′47″to 120°43′58″E, 42°26′42″to 43°25′31″N, and covers an area of 11882 km^2, which stretches 250 km from east to west, 84 km from south to north.

Ongniud Banner was belongs to transitional zone of pastoral and animal husbandry region, between the Inner Mongolia Plateau and the Northeast Plains, which is vulnerable to natural changes and anthropogenic activities. It is representative region suffering from sever soil erosion and improper industrial structure, mainly caused by over consumption and overexploiting land resource. In this region the degradation area about 47.91 ha, account for 40.88 percent of the Ongniud Banner. The altitude of this region decrease from 2025m in the west to 286m in the east and this region characterized by the three typical geomorphological features throughout the study area from west to east in the order of high elevation alluvial flats higher than 900m, low mountains and hills from 650m to 900m, and low Aeolian dunes lower than 650m (QL. Yan, 2011). The monsoon type of climate of this region characterized by temperate, semiarid, continental, and with windy and dry winters and springs, and warm and relatively rainy summers, and short and cool autumns. The mean annual temperature is 7 ℃; annual mean precipitation is 300 mm, of which 70 percent of precipitation falls between July and September. The mean annual potential evaporation about 2040.9 mm. The mean annual wind velocity is 4.2m s^{-1} (S. Yan, 2010). The windy season lasts from early March to late May. The growing season starts from late April end in late

September. The landscape is characterized by a mosaic of farmland and grassland. The main vegetation in this region is typical steppe and temperate steppe desert. The Soil consists of Aeolian sandy soil and chestnut. Additionally, The Wulanaodu Desertification Experiment Station of Chinese Academy of Science which located in the center of the Ongniud Banner can provide field survey data source to support the further reliable research on this region. Therefore, a comprehensive land cover change analysis in second level land cover classes will help reveal the regional sustainable land use potential, and promote the sustainable development for environments and social economic, and ecological security of northeast China.

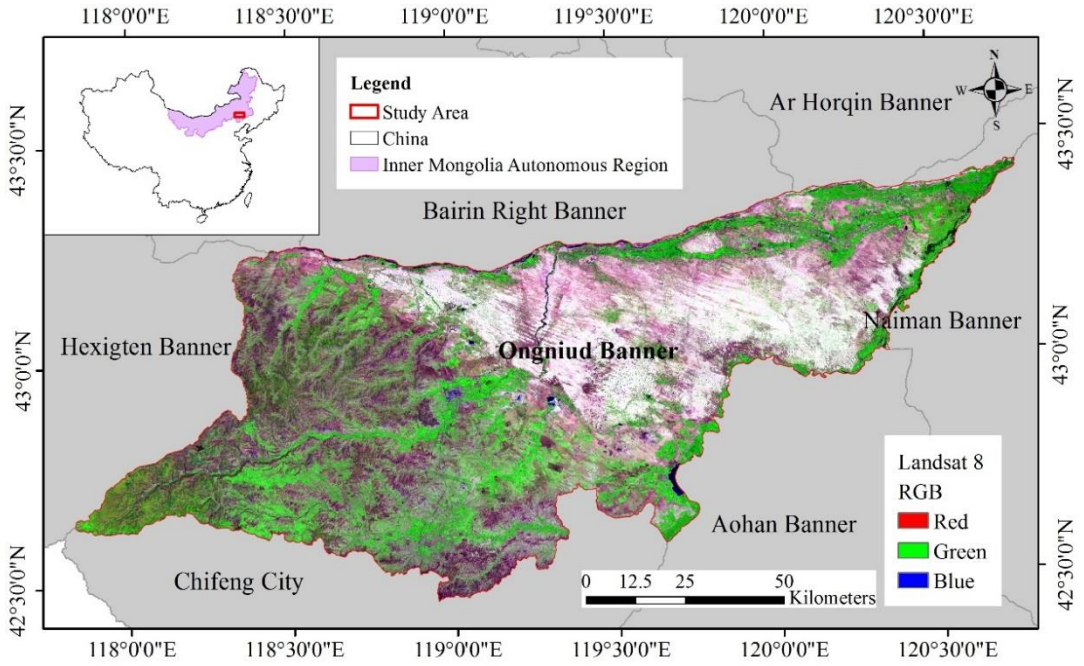

Figure 1 Location map of the study area (red polygon) displayed over the Landsat-8 data based false color composite (FCC) image.

3.2 Satellite data and preprocessing

The long term coverage remote sensing images are collected for almost everywhere on the earth, these characteristics promote to use of remote sensing images to monitor a wide range of environmental problems at local to global scales (S. Ran, 2004). The free of charge Landsat achieve products with moderate spatial resolution is the best option to monitor changes in land use/land cover over time.

In this study, the Landsat 5 thermal mapper(TM) datasets (path/row:121/30 and 122/30) observed in year 2000 and 2009; and Landsat 8 Operational Land Imager / Thermal Infrared Sensor (OLI/TIRS) datasets (path/row: 121/30、122/30 and 123/30) Observed in 2015 are available from the United Sate Geological Survey (USGS) website (http://glovis.usgs.gov/) were used. The time series of Landsat scenes with the 30m spatial resolution during the highest vegetation growing season (from July to September) and without cloud cover were available over the study area in study period. The details on the Landsat datasets used in the research are shown in Table 1.

Table 1 Description of satellite data used in study

Datasets	Year	Path/Row	Date acquired	Spatial resolution
Landsat 5 TM	2000	121/30	30-August-2000	Band 1-5 and 7 with 30m;
		122/30	6-September-2000	Band 6 with 120 m
Landsat 5 TM	2009	121/30	23-August-2009	Band 1-5 and 7 with 30m;
		122/30	15-September-2009	Band 6 with 120 m
Landsat 8 OLI/TIRS	2015	121/30	7-July-2015	Band 1- 7 with 30m;
		122/30	15-August-2015	Band 10 and 11 with 100 m
		123/30	15-September-2015	

First of all, choose the Landsat image (path/row: 122/30) which cover the main part of study area as the base image projected the projection system as Universal Transverse Mercator and zone number (N50), this work performed for neighbor images 122/30 and 123/30; Secondly, the co-registration work performed for two adjacent

images of 2000 by choosing about 20 ground control points (GCPs) from common area. GCPs were well dispersed throughout common area of both scene and yielded root-mean-square errors of less than 0.5 pixels. Similarly, this work performed for year 2009 and 2015. The images overly pixel by pixel not only between adjacent scene, and also between different time periods. Finally, mosaicking work conducted for neighbor imagery, and use the administrative boundary to subset the study area.

3.3 Reference Data for Mapping and Validation

In addition to Landsat 5 and 8 products, the Shuttle Radar Topography Mission (SRTM) with 30 m data based Digital Elevation Model (DEM) data available from the United Sate Geological Survey (USGS) website (http://glovis.usgs.gov/) and the SPOT-5 with 2.5 m high resolution image in 2009 provided from Inner Mongolia Key Laboratory of Remote Sensing and Geographic Information System, Hohhot, China, Google Earth based images, the land use dataset of Inner Mongolia Autonomous Region at 1:10 0000 in 1995 and 2000, The desert distribution dataset of China at 1:10 0000, The vegetation map of China at 1:400 0000, China Soil Map Based Harmonized World Soil Database (v 1.1) were provided by Environmental and Ecological Science Data Center for West China, National Natural Science Foundation of China (http://westdc.westgis.ac.cn) were used for land cover classification and validation process. The additional social-economic data between 1998 and 2014 from Inner Mongolia Statistical Bureau and Climate variations include precipitation and temperature data (1998-2014) of Chifeng meteorological station from Japan Meteorological Business Support Center (JMBSC) used to analysis driving factors cause land use land cover change and further desertification in the study area. According to the daily precipitation data, there were rainfall events 2 days preceding the Landsat data acquired date in 2000, however the precipitation were less than 3 mm. particularly, without rainfall events in September before the Landsat data acquired date in 2009.

Which proved that the precipitation have little or not at all effect on land surface temperature and soil moisture further groundwater after evaporation and infiltration.

Chapter 4. Analysis of desertification based on LULC change

4.1 Land Use/Cover Classification Technology

A wide range of methods for classification of remote sensing image continuously proposed. SVMs are particularly popular in the remote sensing field compare to the other classification methods such as maximum likelihood method, decision tree method, and neural network method. The principle of the SVM was originally introduced and improved by Vapnik and Chervonenkis. SVM is a non-parametric classification method which can also work with the small amount of training data and produce higher classification accuracy (G. Mountrakis, 2011; P. Mantero, 2005).

The success of the SVM method depends on how well the process is trained. Principally, SVM is a binary classifier that set an optimal separating hyperplane during classes to correctly separate the data point into two classes (Huang, C. et al, 2002). If the training data with k number of samples be represented as $(x_1, y_1), \cdots, (x_k, y_k)$, where $x \epsilon R^n$ is an n –dimensional space, and $y \in \{+1, -1\}$ is class label, then these training data will be separated by the two hyperplane parallel to the optimal hyperplane with maximum margin into the respective classes shown in equation (1a and 1b).

$$W \cdot x_i + b \geq +1 \; for \; y_i = +1, i = 1, 2, \cdots, k \quad (1a)$$

$$W \cdot x_i + b \leq -1 \; for \; y_i = -1 \quad (1b)$$

The original idea of SVM presented in figure 2.

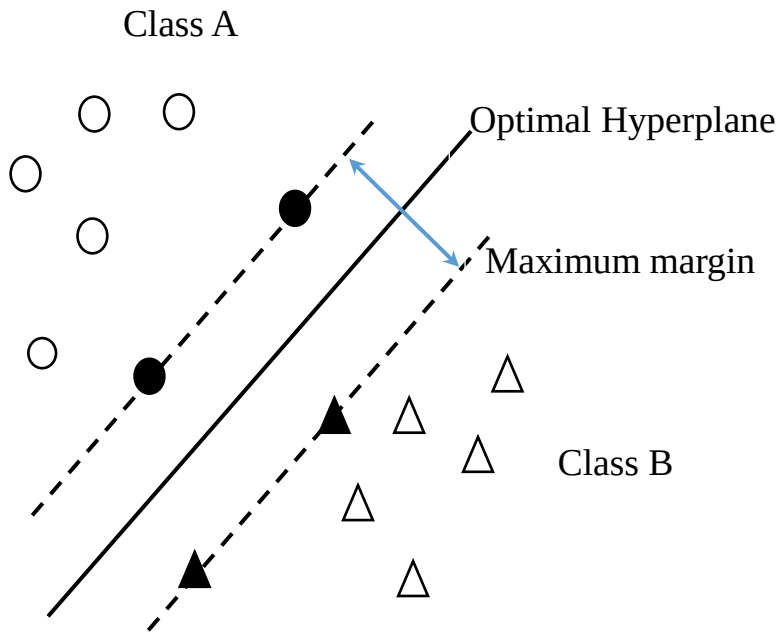

Figure 2 Original idea of SVM

SVM can classify the data linearly and nonlinearly, and kernel function is used for nonlinear classification. The SVM provide four types of kernels: linear, polynomial, and radial basis function (RBF), and sigmoid. According to the previous studies, radial basis function kernel works better for remote sensing image classification (Kavzoglu, T., 2009). The equation of radial basis function kernel presented as follow (equation 2):

$$K\left(x_{i,}\ x_{j.}\right) = \exp\left(-g\left\|x_i - x_j\right\|^2\right), g > 0 \qquad (2)$$

Where, g indicate the gamma term in the radial basis kernel function.

The supervised classification was conducted using the Support Vector Machine (SVM) (T. Kavzoglu, 2003) algorithm. In this study utilized the default parameter provided by ENVI software to perform supervised classification on Landsat images. LULC classification and mapping was conducted for each years (2000, 2009, and 2015) using the above mentioned 25 feature images and the training data collected. The processes of Land use land cover mapping and change analysis shown in figure 3.

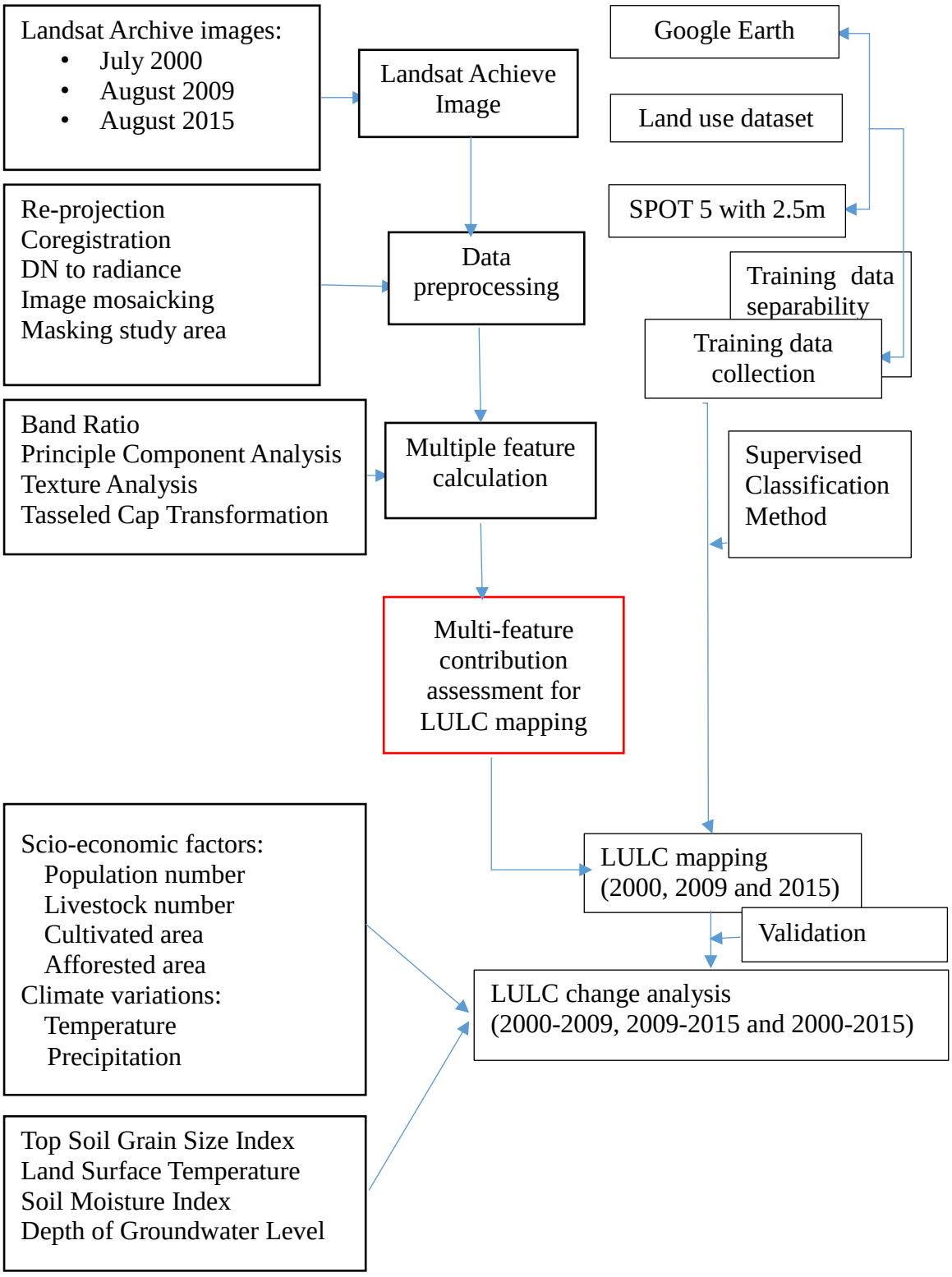

Figure 3 Flow chart of the land use land cover change analysis in this research

4.2 Land Use/Cover Mapping in Study Area

4.2.1 Land use/cover classification system

The land use land cove classification system used in this study defined by the Chinese Academy of Science through the field survey. This multi-hieratical classification system covered the 6 main land cover classes, 31secondary sub-classes, this is the highest detail classification system in China. According to the landscape of the study area 17 categories of sub-classes land use land cover presented in Ongniud Banner. The detail description of land use land cover classes presented in Table 2.

Table 2 Land use land cover classification system and description

1st level classes	2nd level classes	Descriptions
Cropland		Cultivated lands for crops. Including mature cultivated land, newly cultivated land, fallow, shifting cultivated land; intercropping land such as crop-fruiter, crop-mulberry, and crop-forest land in which a crop is a dominant species; bottomland and beach that cultivated for at least 3 years.
	Paddy land	Cropland that has enough water supply and irrigation facilities for planting paddy rice, lotus etc., including rotation land for paddy rice and dry farming crops.
	Dry land	Cropland for cultivation without water supply and irrigating facilities; cropland planting vegetables; fallow land.
	Irrigation land	cropland that has water supply and irrigation facilities and planting dry farming crops;
Woodland		Lands growing trees including arbor, shrub, bamboo and for forestry use.
	Forest	Natural or planted forests with canopy cover greater than 30%.
	Shrub	Lands covered by trees less than 2 m high, the canopy cover > 40%.
	Woods	Lands covered by trees with canopy cover between10-30%.
Grassland		Lands covered by herbaceous plants with the coverage of shrub canopies less than 10%.
	Dense grass	Grassland with canopy coverage greater than 50%.

	Moderate Grass	Grassland with canopy coverage between 20% and 50%.
	Sparse grass	Grassland with canopy cover between 5% and 20%.
Water body		Lands covered by natural water bodies or lands with facilities for irrigation and water reservation.
	Stream and rivers	Lands covered by rivers including canals.
	Lakes	Lands covered by lakes.
	Reservoir and ponds	Man-made facilities for water reservation.
	Bottomland	Lands between normal water level and flood level.
Built-up land		Lands used for urban and rural settlements, factories and transportation facilities.
	Urban built-up	Lands used for urban.
	Rural settlements	Lands used for settlements in villages.
Unused land		Lands that are not put into practical use or difficult to use.
	Sandy land	Sandy land covered with less than 5% vegetation cover.
	Salina	Lands with salina accumulation and sparse vegetation.
	Swampland	Lands with a permanent mixture of water and herbaceous or woody vegetation that cover extensive areas.
	Bare land	Bare exposed soil with less than 5% vegetation cover; Bare exposed rock with less than 5% vegetation cover.

In this study, desertification regraded as natural vegetation coverage degradation between 6 categories of general land use land cover and within 17 categories of sub-classes land use and land cover in semi-arid desertification area primarily destroyed by unsustainable human social –economic activities such as irreversible land resource exploitation for variety of utility combined with the effect of significant interannual change of climate variations including temperature and precipitation.

4.2.2 The Classification Scheme and Training Data

Collection of the highly representative training data is one of the major factors determining to what degree the classification rules can be generalized to unseen samples (Paola and Schowengerdt, 1995). A previous study showed that this factor could be more important for obtaining accurate classifications than the selection of classification algorithms (Hixson et al. 1980).

In this research, following the land cover classification system defined by the Chinese Academy of Sciences, training data belonging to 17 categories of secondary land cover classes were collected for each year 2000, 2009 and 2015. Existing land use and vegetation maps, false color composite images prepared from Landsat 5 and 8 data, Google Earth images, and high resolution Spot-5 images were used as the reference datasets while collecting the training and validation data. The classification scheme used in the research and the number of training data (polygons/pixels) collected are listed in Table 2.

We carefully examined the reference data and spectral signatures of each land cover classes across the image of study area to collect the training site from three period images. Spectral feature of the 17 categories of sub-class land use land cove presented in figure 4. In order to ensure the training data they were the representative of the entire image, a sufficient number of pixels for each land cover class must be collected. To enhance the comparability of land cover classification results between three periods we tried to use the same training sites as much as possible when no change had occurred.

The reliability of the training data over the entire study area was further ensured by using the Jeffries-Matusita transformed divergence index to assess the separability of training data for each year 2000, 2009 and 2015. We confirmed that land cover classes water, sandy with the high separability, but other land cover classes with the much lower separability.

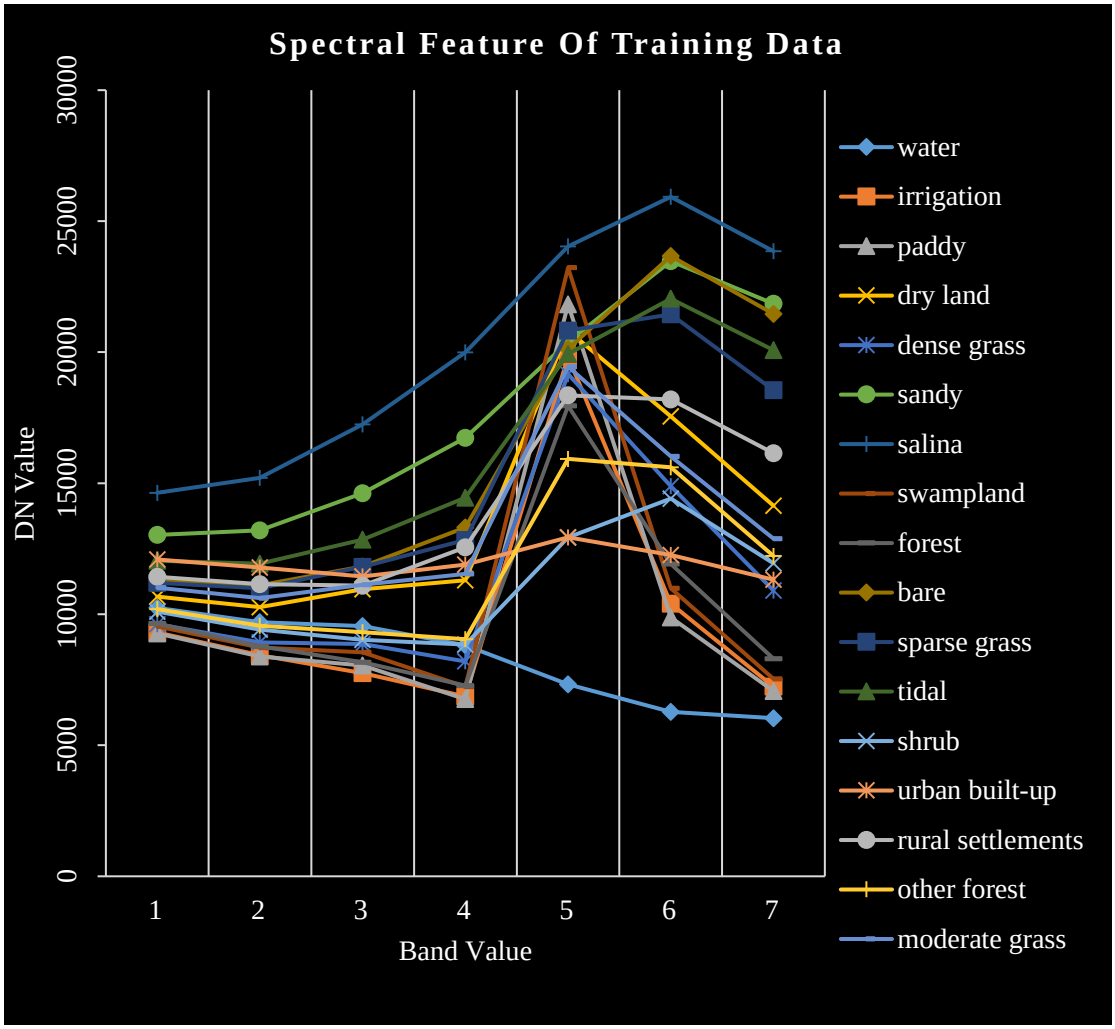

Figure 4 spectral feature of 17 categories of sub-class LULC

Table 3 LULC classification system and the number of training data (polygons/pixels) used in the research for year 2000, 2009 and 2015

1st level classes	2nd level classes	Color composition (Red-Green- Blue)	Training data(polygon/pixel)		
			2000	2009	2015
Cropland	Paddy	139-90-0	18/3641	21/2969	17/3684
	Dry land	235-180-0	43/7489	57/9793	64/10792
	Irrigation land	255-100-0	35/3919	51/4643	57/7686
Woodland	Forest	45-139-87	50/4113	39/4347	52/7150
	Shrub	97-181-140	29/2852	30/8171	27/6396
	Other forest	150-255-171	26/4194	27/3969	31/5370
Grassland	Dense grass	0-139-0	34/5085	31/3573	29/5936
	Moderate grass	0-205-0	32/3005	32/3005	26/5933
	Sparse grass	0-255-0	33/2369	34/2671	35/8244
Water body	Rivers and lakes	0-0-255	24/5379	18/4682	21/6118
	Tidal	110-180-238	20/1181	19/1340	25/1835
Built-up land	Urban built-up	139-0-0	15/1877	10/3312	10/4385
	Rural settlements	238-0-0	40/3846	37/3527	40/4548
Unused land	Sandy land	238-238-142	31/7993	31/9423	46/16651
	Salina	255-255-255	22/3121	22/3121	19/2913
	Swampland	216-191-216	11/1588	9/560	5/742
	Bare	210-181-155	43/1837	50/3283	37/3909

4.2.3 Feature calculation and combination

The study area is mixed of the diverse types of LULC. Considering the spectral complexity such as same object with different spectra, different objects with same spectrum of ground object, we calculated multi-feature such as NDVI (Normalized Difference Vegetation Index), NDBI (Normalized Difference Built-Up Index), NDBaI (Normalized Difference Bareness Index), NDWI (Normalized Difference Water Index)，NDSI (Normalized Difference Salinity Index), tasseled cap transformation features (Greenness, Brightness, Wetness), topography feature (Elevation, Slope and Aspect).

The six spectral bands of the Landsat data were used for the principal component analysis, and the first principal component which included more than 90% spectral information was used to calculate textural features. Eight textural measures (Mean, Variance, Homogeneity, Contrast, Dissimilarity, Entropy, Second moment, and Correlation) were calculated using the Gray Level Co-occurrence Matrix (GLCM) with

the moving window size of 3 by 3 pixels, moving direction 45℃ and moving distance 1 pixel as ancillary information support the higher accuracy land cover classification.

4.2.3.1 NDVI (Normalized Difference Vegetation Index)

The NDVI is one of the first successful vegetation indices based on band ratioing. It was calculated using the equation 3:

$$\text{NDVI} = \frac{(NIR-Red)}{(NIR+Red)} \quad (3)$$

Where,

Landsat 5 :(band 4-band 3) / (band 4+band 3)

Landsat 8: (band5-band4) / (band 5 +band 4)

4.2.3.2 NDBI (Normalized Difference Built-Up Index)

NDBI (Normalized Difference Built-Up Index), Zha et al. (2003) calculated with following equation 4:

$$NDBI = \frac{(MIR-NIR)}{(MIR+NIR)} \quad (4)$$

Where MIR indicate mid infrared band in Landsat TM, NIR indicate near infrared band in Landsat TM.

NDBI derived image show that buil-up area have the higher reflectance in MIR wavelength range than in NIR wavelength range.

4.2.3.3 NDBaI (Normalized Difference Bareness Index)

Recognize different types of bare area is crucial task for accurate land use land cover classification. The primary bare area are area there no vegetation cover existed due to physiographic factors such as climate, hydrology; the humus bare lands were mainly influenced by anthropogenic disturbance such as heavily farming and urban construction. Therefore, normalized difference bareness index (H.M. Zhao, 2005) proposed to distinguish the different types of bare areas as follows (equation 5):

$$NDBaI = \frac{(SWIR-TIR)}{(SWIR+TIR)} \quad (5)$$

Where,

SWIR is indicate band 5 of Landsat TM;

TIR is indicate band 6 of Landsat TM.

4.2.3.4 NDSI (Normalized Difference Salinity Index)

The concept of Normalized difference soil salinity index (NDSI) shown in equation 6 is designed to suppressing the vegetation and highlight the saline zones. NDSI is the ratio of difference of red band and near infrared band and divided by the accumulation of red band and near infrared band.

$$NDSI = \frac{(Red-NIR)}{(Red+NIR)} \times 100 \quad (6)$$

Where,
Landsat 5: (band 3-band 4) / (band 3+band 4)

Landsat 8: (band4-band5) / (band 4 +band 5)

4.2.3.5 NDWI (Normalized Difference Water Index)

NDWI (Normalized Difference Built-Up Index) proposed by McFeeters (1996) to delineate open water features, which is expressed as follows (equation 7)

$$NDBI = \frac{(Green-NIR)}{(Green+NIR)} \quad (7)$$

Where Green is indicate a green band of Landsat TM, and NIR is indicate a near infrared band of Landsat TM.

This index enhanced the water body with positive reflectance value and suppressed the vegetation and soil with zero or negative reflectance value.

4.2.3.6 Tasseled Cap Transformation

The tasseled cap index was calculated from the related six Landsat bands, the parameter for the first three tasseled cap component such as Tasseled Cap Brightness (TCB), Tasseled Cap Greenness (TCG) and Tasseled Cap Wetness (TCW) for each band of Landsat 5 and Landsat 8 products presented in table 4 (Crist,1986; Baig,2014).
Brightness, measure of soil; Greenness, measure of vegetation; Wetness,

interrelationship of soil and canopy moisture, the wetness component contrast the sum of the visible and near-infrared bands with the sum of the longer-infrared bands to determine the amount of moisture being held by the vegetation or soil.

The tasseled cap transformation of the first three tasseled cap component of the Landsat imagery carried out using the tasseled cap function of the Environment for Visualizing Images (ENVI 4.8) image processing software.

Table 4 Tasseled Cap Transformation parameter for Landsat imagery

		Band 1	Band 2	Band 3	Band 4	Band 5	Band 7
Landsat 5 (TM)	TCB	0.2909	0.2493	0.4806	0.5568	0.4438	0.1706
	TCG	-0.2728	-0.2174	-0.5508	0.7220	0.0733	-0.1648
	TCW	0.1446	0.1761	0.3322	0.3396	-0.6210	-0.4186
		Band 2	Band 3	Band 4	Band 5	Band 6	Band 7
Landsat 8 (OLI)	TCB	0.3029	0.2786	0.4733	0.5599	0.508	0.1872
	TCG	-0.2941	-0.243	-0.5424	0.7276	0.0713	-0.1608
	TCW	0.1511	0.1973	0.3283	0.3407	-0.7117	-0.4559

The combination of the multiple features (spectral, spectral indices, spectral transformations, textures, and topographic) calculated from the satellite data were used to improve the accuracy of the LULC classification. The list of spectral features used in the research are shown in table 5. Altogether, 25 feature images were used as an input dataset in the research. These features were calculated separately for each years (2000, 2009, and 2015) using the satellite data of the corresponding years.

Table 5 List of feature images used in the research.

Features	Descriptions	Total
Spectral	Blue, Green, Red, Near Infrared, Shortwave Infrared, and Thermal Infrared	6
Spectral indices	Normalized Difference Vegetation Index (NDVI), Normalized Difference Built-Up Index (NDBI), Normalized Difference Bareness Index (NDBaI), Normalized Difference Salinity Index (NDSI), Normalized Difference Water Index (NDWI)	5
Spectral transformations	Tasseled cap-wetness, Tasseled cap-Greenness, Tasseled cap-brightness	3
Textural	Mean, Variance, Homogeneity, Contrast, Dissimilarity, Entropy, Second moment, Correlation	8
Topographic	Slope, altitude, aspect	3
Total		25

The above mentioned multi-features combined to basic spectral data of Landsat 5 and Landsat 8 one by one. The combination of the multiple features with basic spectral data shown in table 6.

Table 6 Multi-feature contribution scheme in the research

	Spectral data (Landsat 5 or Landsat 8)	Additional feature
Group 1	band 1-5,7 or band 1-7	
Group 2	band 1-5,7 or band 1-7	DEM
Group 3	band 1-5,7 or band 1-7	Slope
Group 4	band 1-5,7 or band 1-7	Aspect
Group 5	band 1-5,7 or band 1-7	NDVI
Group 6	band 1-5,7 or band 1-7	NDWI
Group 7	band 1-5,7 or band 1-7	NDSI
Group 8	band 1-5,7 or band 1-7	NDBI
Group 9	band 1-5,7 or band 1-7	NDBaI
Group 10	band 1-5,7 or band 1-7	Greenness
Group 11	band 1-5,7 or band 1-7	Brightness
Group 12	band 1-5,7 or band 1-7	Wetness
Group 13	band 1-5,7 or band 1-7	Mean
Group 14	band 1-5,7 or band 1-7	Variance
Group 15	band 1-5,7 or band 1-7	Homogeneity
Group 16	band 1-5,7 or band 1-7	Contrast
Group 17	band 1-5,7 or band 1-7	Dissimilarity
Group 18	band 1-5,7 or band 1-7	Entropy
Group 19	band 1-5,7 or band 1-7	Second moment
Group 20	band 1-5,7 or band 1-7	Correlation

LULC classification and mapping was conducted for each years (2000, 2009, and 2015) using the above mentioned 25 feature images and its combination method and the training data collected. The supervised classification was conducted using the Support Vector Machine (SVM) algorithm.

Chapter 5. Analysis of desertification based on physical properties' change

Desertification resulted in reduction of productivity in a desert steppe thorough affect the soil physical and chemical properties directly and UN -directly. Remote sensing techniques not only used for detecting changes in land use and land cover category, but also identify the physical properties changes of the land surface by utilizing associated indices.

5.1 Top Soil Grain Size Index

In arid and semiarid area, wind erosion strongly affects the land surface soil physical properties. Therefore, spectral reflectance of the land surface soil can be potentially used as an indicator to land degradation. So it is possible to monitor land desertification by topsoil grain size index change in arid and semiarid area using remote sensing technique (Xiao, J., 2005).

Increasing of the spectral reflectance of land surface soil imply land degradation or desertification. Xiao et al (2005) introduced the top soil grain size index that manifest the physical properties (grain size composition) of top soil very well. This index was not like normalized difference vegetation index, bare soil index, and percentage grass coverage which has large spatial and temporal variability and uncertainty in arid regions due to these indices very sensitive to precipitation. GSI was proposed to monitoring desertification process in arid region.

However, this index designed to monitoring the change in surface soil texture by analyzing the correlation between soil grain size distribution and surface soil reflectance data. The GSI calculate by using bellowing equation (8):

$$\mathrm{GSI} = \frac{\rho_{red} - \rho_{blue}}{\rho_{red} + \rho_{blue} + \rho_{green}} \quad (8)$$

Where, R, B, and G are the reflectance of the red, blue and green bands of the Landsat TM or ETM + and Landsat 8 products that band 3, band 1 and band 2 for Landsat TM/ETM+ and band 4, band 2 and band 3 for Landsat 8, respectively.

In general, within visible and near infrared wavelength range the spectral reflectance value increasing with the fine sand percentage increase in top soil, while the reflectance value decreasing with the clay and silt content increasing.

In principle, in the GSI formula, the difference value between red band and blue band designed to distinguish the area covered with vegetation or water and bare soil. The difference value between red band and blue band will be close to 0 in vegetated area, and the deference value will be negative for water body; while the difference value large for bare soil. The accumulation reflectance value of the red, green and blue bands designed to distinguish the topsoil with different grain size composition. The accumulation value of visible bands reflectance is positively correlated to fine sand content of the topsoil. There are no explicit upper limit for GSI value.

In this study, the experimental result showed that GSI index negatively related to vegetation coverage, so GSI index possible to monitor land desertification in arid and semiarid area using remote sensing technique.

5.2 Land Surface Temperature Derivation

Satellite TIR sensors measure top of the atmosphere (TOA) radiances, from which brightness temperatures (also known as blackbody temperatures) can be derived using Plank's law (Dash et al., 2002).

The TOA radiance are the mixing result of three fractions of energy:

(1) Emitted radiance of the Earth's surface, (2) upwelling radiance from the atmosphere, and (3) down welling radiance from the sky.

The difference between the TOA and land surface brightness temperatures ranges generally from 1 to 5 K in the 10-12 micrometer spectral region, subject to the influence of atmosphere effects, including absorption, upward emission, and downward irradiance reflected from the surface (Franca & Cracknell, 1994), must be corrected before land surface brightness temperatures are obtained. These brightness temperature should be further corrected with spectral emissivity values prior to the computation of LST to account for the roughness properties of the land surface, the amount and nature of vegetation cover, and the thermal properties and moisture content of the soil (Friedl, 2002).

Two approaches have been developed to recover LST from multispectral TIR imagery (Schmugge et al., 1998). The first approach utilizes a radiative transfer equation to correct the at-sensor radiance to surface radiance, followed by an emissivity model to separate the surface radiance into temperature and emissivity (Schmugge et al., 1998). The second approach applies the split-window technique for sea surfaces to land surfaces, assuming that the emissivity in the channels used for the split window is similar (Dash et al., 2002). In other words, a set of thermal responses for a specific landscape phenomenon or process measured using a specific TIR sensor cannot be extrapolated to predict the same TIR measurements either from other sensors, or from

images recorded at different times using the same sensor (Quattrochi & Goel, 1995).

5.2.1 Convert digital number (DN) to spectral radiance

The Landsat thermal infrared (TIR) band 6 of Landsat 5 and Landsat thermal infrared sensors (TIRS) band 10 and band 11 of Landsat 8 were converted to top of atmosphere (TOA) spectral radiance using the radiometric rescaling coefficients, multiplicative rescaling factor and additive rescaling factor provided in the metadata file (MTL file), the detail process described as below (equation 9):

$$L_\lambda = M_L Q_{cal} + A_L \quad (9)$$

Where:

L_λ is indicate TOA spectral radiance (Watts/(m^2 * srad * μm))

M_L is band-specific multiplicative rescaling factor from the metadata (radiance_mult_band_10/11)

A_L is band-specific additive rescaling factor from the metadata (radiance_add_band_10/11)

Q_{cal} is quantized and calibrated standard product pixel values (DN).

The values of M_L and A_L for Landsat imagery for our study area is extracted from the metadata.

5.2.2 Conversion to at-satellite Brightness temperature

TIRS band data can be converted from spectral radiance to brightness temperature using the thermal constants provided in the metadata file (equation 10):

$$\mathrm{T} = \frac{K_2}{\ln\left(\frac{K_1}{L_\lambda}+1\right)} \quad (10)$$

Where:

T is at-satellite brightness temperature (K)

L_λ is the TOA spectral radiance (Watts/ (m^2 * srad * μm))

K_1 is Band-specific thermal conversion constant from the metadata

K_2 is Band-specific thermal conversion constant from the metadata

5.2.3 Fractional Vegetation Coverage

Fractional vegetation cover (FVC) was estimated for a pixel. FVC for an image was calculated by according to (Carlson & Ripley, 1997) (Valor, 1996) (equation 11):

$$P_V = \left(\frac{NDVI - NDVI_{min}}{NDVI_{max} - NDVI_{min}}\right)^2 \quad (11)$$

Where $NDVI_{max} = 0.5$ and $NDVI_{min} = 0.2$.

Where,

$NDVI_S$ NDVI reclassified for soil

$NDVI_V$ NDVI reclassified for vegetation

5.2.4 Land Surface Emissivity

To calculate the LST it is essential to understand the emissivity knowledge of ground object. Previous researchers introduced different methods to calculate LSE such as: the temperature and emissivity separation (TES) method (Gillespie, 1985), temperature-independent spectral indices (TISI) (Becker & Li, 1990), spectral ratio method (Watson, 1992), Alpha residual method (Kealy & Gabell, 1990), method based on NDVI image (Valor & Caselles, 1996), method based on classification image (Snyder et al., 1998), and the temperature and emissivity separation (TES) method (Gillespie et al., 1998).

In which, an alternative, operative method is to obtain the land surface emissivity from NDVI, the NDVI threshold method shows a good working in comparison to a reference method as the one based on TISI indices (Becker & Li, 1990), as is pointed by Sobrino et al. (2001). In this study, assume that the pixel is composed by a mixture of vegetation and bare soil, and the land surface emissivity equation provided as bellow:

$$\varepsilon = 0.004P_V + 0.986$$

Where,

ε_V is the vegetation emissivity and ε_S is the soil emissivity, P_V is the vegetation proportion

Derivation of Land surface temperature from Landsat 5 and Landsat 8 imagery

The LST were derived from the Landsat 5 Thermal Infrared band 6 (10.40-12.50 μm) collected at 120 m and Landsat 8 Thermal Infrared Sensor (TIRS) bands 10 (10.60-11.19 μm) and band 11 (11.50-12.51μm) collected at 100 meters, these band resampled to 30 meters to match multispectral bands. The local time of satellite overpass was in the morning (approximately 11:14 AM) (this was the best image available), so that the chance for detecting a weaken UHI is maximized. However, (Roth et al., 1989) has demonstrated that satellite detection of land surface temperature using thermal infrared sensors the heat island intensity is greatest in the daytime and in the warm season.

The Landsat 5 and Landsat 8 image used in this research is therefore appropriate although not optimal. The following equation was used to convert the digital number (DN) of Landsat 5 TIR band and Landsat 8 TIRS band into spectral radiance (equation 12):

$$T_B = \frac{K_2}{\ln\left(\frac{K_1}{L_\lambda}+1\right)} \quad (12)$$

Where T_B is effective at-satellite temperature in K, L_λ is spectral radiance in W/ (m^2 ster Am); and K_2 and K_1 are pre-launch calibration constants. The values of calibration constant for Landsat imagery shown in table 7 (Chander, 2003).

Table 7 the calibration constants of thermal band for Landsat imagery

		K_1 (W m^{-2} sr^{-1}μm $^{-1}$)	K_2 (Kelvin)
Landsat 5 TM		607.76	1260.56
Landsat 7 ETM+		666.09	1282.71
Landsat 8 TIRS	Band 10	774.89	1321.08
	Band 11	480.89	1201.14

The temperature values obtained above are referenced to a black body. Therefore, corrections for spectral emissivity (e) became necessary according to the nature of land cover. Each of the LULC categories was assigned an emissivity value by reference to the emissivity classification scheme by Snyder et al. (1998). The emissivity corrected land surface temperatures were computed as follows (Artis & Carnahan, 1982) (equation 13):

$$S_t = \frac{T_B}{1+(\lambda+T_B/\rho)\ln\varepsilon} \quad (13)$$

Where: λ is wavelength of emitted radiance (for which the peak response and the average of the limiting wavelengths (11.5) (Markham & Barker, 1985) will be used),

5.3 Land Surface Soil Moisture

This suggests that the surface soil particle size distribution can be changed by soil moisture. Under wet soil conditions, the particles appear to have a larger size, and hence more potential saltating particles are available. This explains the occurrence of stronger saltation processes observed under wet soil conditions (X.L. Li, 2014).

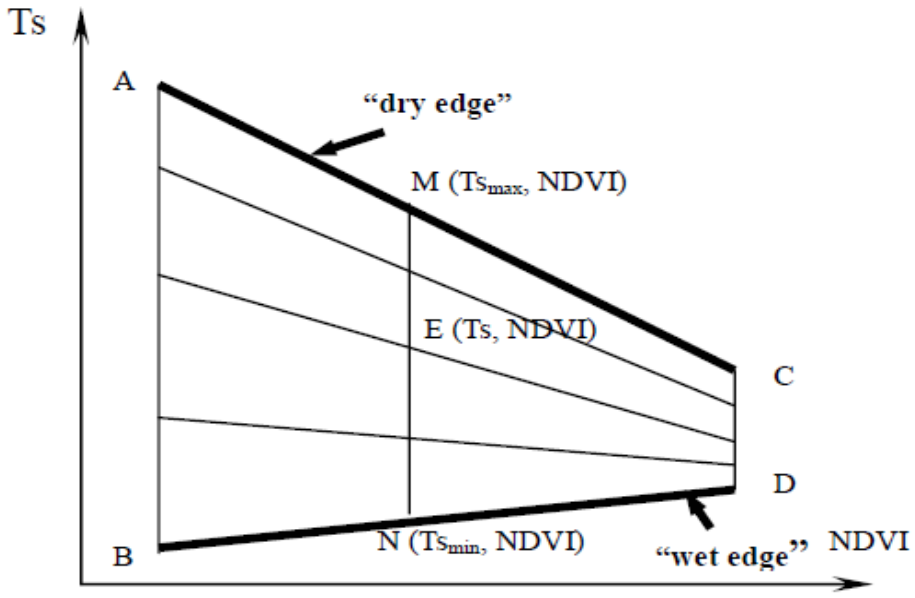

Figure 5 The scatterplot in Ts- NDVI space and the definition of *SMI*

The line from point A to point C in Figure 5 represents the driest conditions, namely "dry edge", under different vegetation coverage. The line from points B to point D in Fig. 2 represents the wettest conditions, namely "wet edge", under different vegetation coverage. Ts is positively correlated with NDVI along the wet edge (from point B to point D) and negatively correlated with NDVI along the dry edge (from point A to point C). The Ts and NDVI relationships along the dry edge and wet edge (Figure 5) assured our confidence that soil moisture could be estimated with the Ts-NDVI space. We thus propose a soil moisture index (SMI) in Ts-NDVI space to estimate soil moisture. The

soil moisture index (SMI), whose value is 0 along “dry edge” and 1 along the “wet edge”, is defined as following (equation 14):

$$SMI = \frac{T_{s_{max}} - T_s}{T_{s_{max}} - T_{s_{min}}} \quad (14)$$

Where $T_{s_{max}}$, $T_{s_{min}}$ are the maximum and minimum surface temperature for a given NDVI. T_s is the remotely-sensed data derived surface temperature at a given pixel for a given NDVI. In other words, SMI is the ratio of two temperature difference ($T_{s_{max}} - T_s$) and ($T_{s_{max}} - T_{s_{min}}$) at a given pixel for a given NDVI. For example, ($T_{s_{max}} - T_s$) at the point E in Fif.2 is the temperature difference between point M and point E, and ($T_{s_{max}} - T_{s_{min}}$) is the temperature difference between point M and point N (equation 15a and 15b).

$$T_{s_{max}} = a_1 NDVI + b_1 \quad (15a)$$

$$T_{s_{min}} = a_2 NDVI + b_2 \quad (15b)$$

Where, a_1, a_2, and b_1, b_2 are empirical parameters that can be obtained by linear regression of known remotely-sensed data for both the dry and wet edges.

5.4 The depth of ground water table derivation

The groundwater table is one of the most important input parameter for regional ecological and hydrological modeling, especially in arid and semi-arid region characterized by scarce precipitation and insufficient surface water resources. Which is subject to irrigation, drainage, water consumption and land reclamation measures. The monitoring of groundwater level change is assist to understanding the desertification with the significant land use land cover change caused by irrational human activity and uneven climate change occurred in Horqin Sandy Land cover the study area Ongniud Banner (Zhao, 2016).

It is critical to estimate the groundwater levels at the regional scale to assess the potential suitable distribution. The optical satellite data have the advantages of spatial, spectral, and temporal availability and the ability to obtain data covering large and inaccessible areas in a short period of time. Therefore, (Yan Y. et al 2015) developed the empirical model through field survey and laboratory experiment.

The principle of the groundwater level calculation model as follow:

First, based on the surface soil moisture derived from remote sensing data, create the correlation between the tasseled cap wetness derived from Landsat data and the soil water content to calculate the soil water content (SWC) image by using the correlation between Soil water content (SWC) and Tasseled Cap Transformation Wetness (TCW) (equation 16):

$$SWC=0.1099\ \ TCW+9.3522 \qquad (16)$$

Next, consider the well-known principle of how the groundwater affects the surface soil moisture to develop the relationship of surface soil moisture and groundwater level;

finally, the relationship between tasseled cap wetness and the groundwater levels were developed based on field survey and laboratory analysis to produce the groundwater table image for study area (equation 17).

$$H = d + H_m \times \frac{W_{max}^2 - (0.1099TCW + 9.3522)^2}{W_{max}^2 - W_{min}^2} \quad (17)$$

$W_{max} = 10.6\%$ Maximum soil moisture

$W_{min} = 1.8\%$ Minimum soil moisture

$H_m = 5.8m$ The rising of the capillary edge, it is related to the soil physical and chemical properties, especially the soil texture.

Considering the applicability of empirical model established based on Landsat TM imagery, in this study calculate the ground water level for year 2000 and 2009.

Chapter 6. The main driving factors cause land degradation and desertification

6.1 Climate variations

In the arid and semi-arid regions, temperature and precipitation are important climatic factors of the land degradation and desertification. The analysis of the mean annual precipitation and mean annual temperature in the study area shown in figure 6.

Figure 6 shows that mean annual precipitation has the oscillation change trend from 1998 to 2014. The mean annual precipitation value with the decreasing rates of 47.25 mm per year from 1998 to 2001, while its value with the growing rates of 28 mm per year from 1998 to 2005. Between 2005 and 2009, its value with the decreasing rate 30mm per year, while increasing from 2011 to 2014 with the 14.88 mm.

The lowest mean annual precipitation value of 253 mmm occurred in year 2009, while the highest mean annual precipitation value of 532 mm occurred after one year in 2010.

Simultaneously, the fluctuation characteristics of mean annual temperature change also detected from 1998 to 2014. From 1998 to 2000, the mean annual temperature decreasing with rate of 0.31℃ per year, while its value increasing with rate of 0.17 ℃ from 2000 to 2007. In which, the mean annual temperature reached the highest value of 8.825℃ in 2007. The mean annual temperature dropped down with the rate of 0.42 ℃ per year, whereas the lowest mean annual temperature of 6.3℃ observed in 2012.

Finally, the analysis result show that the mean annual temperature and mean annual precipitation with the significant innterannual fluctuation change from 1998 to 2014.

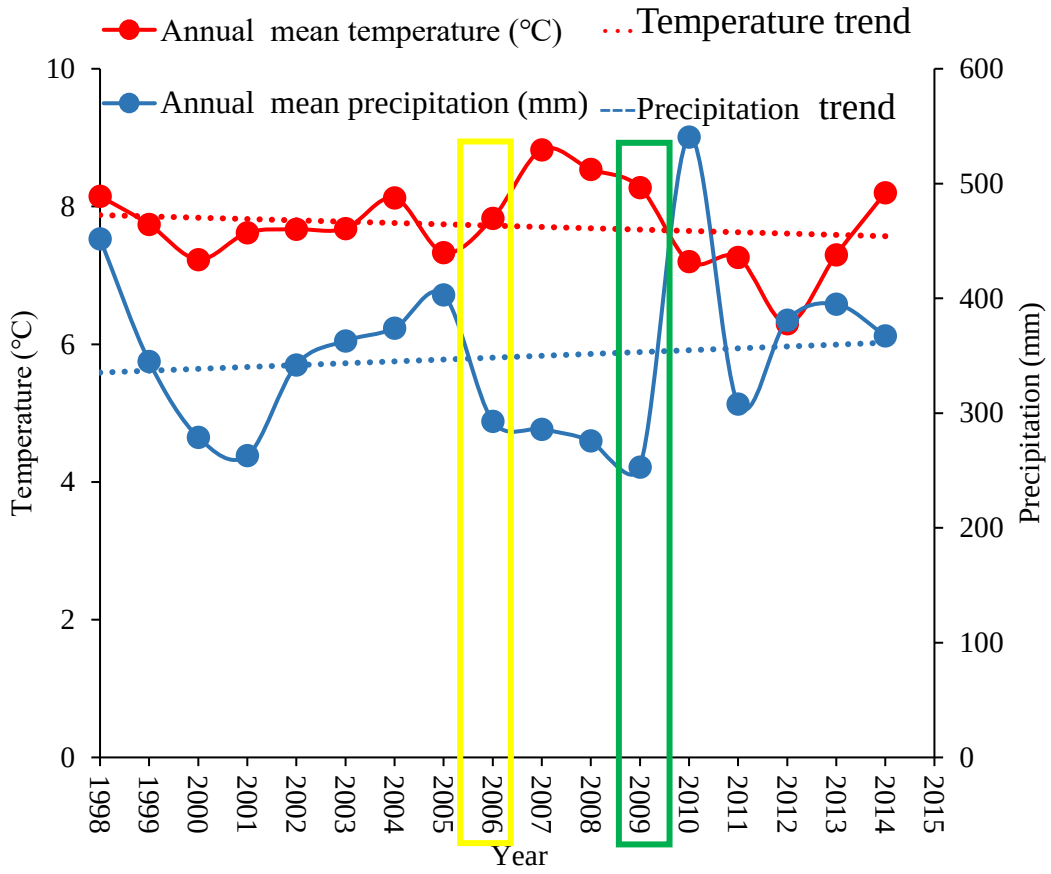

Figure 6 Temporal change pattern of mean annual climate variations (mean annual precipitation and mean annual temperature) in Ongniud Banner from 1998 to 2014.

A minimum 30 year data series is needed. A double 30-year period or longer period would be better to be used to analysis climate change (Ren, 2015). In this study, innterannual change of precipitation and temperature is considered to the climate cause factor of driving land use and land cove change and desertification.

6.2 Socio-Economic factors

The primary cause of desertification in Horqin Sandy Land is identified as irrational and intensified human economic activities with a rapidly increasing of population number. The increase of the population and livestock numbers and expanding of cultivated area in the study are the major proxies of anthropogenic activities.

According to the Inner Mongolia Statistical Yearbook record, the total population number of Ongniud Banner increased from 473,460 in 1999 to 482,114 in 2014 as shown in Figure 14; and the population density increased from 35.6 persons per km^2 in 1986 to 41 persons per km^2 in 2014.

In order to meet the demand of basic food, meat, shelter, and energy for the ever growing population a large amount of grain production, household necessary for sustain large number of population using limited natural resources.

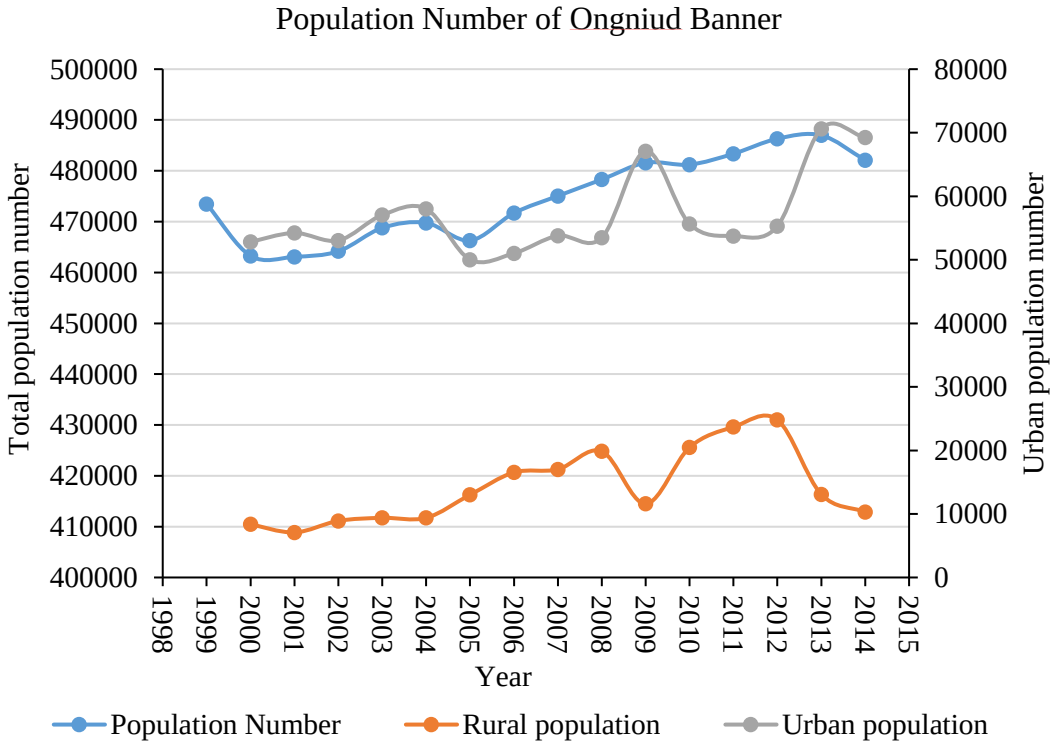

Figure 7 Evolution of the population number in Ongniud Banner from 1999 to 2014 (source: Inner Mongolia Autonomous Region Bureau of Statistics, People's Republic of China, 2015)

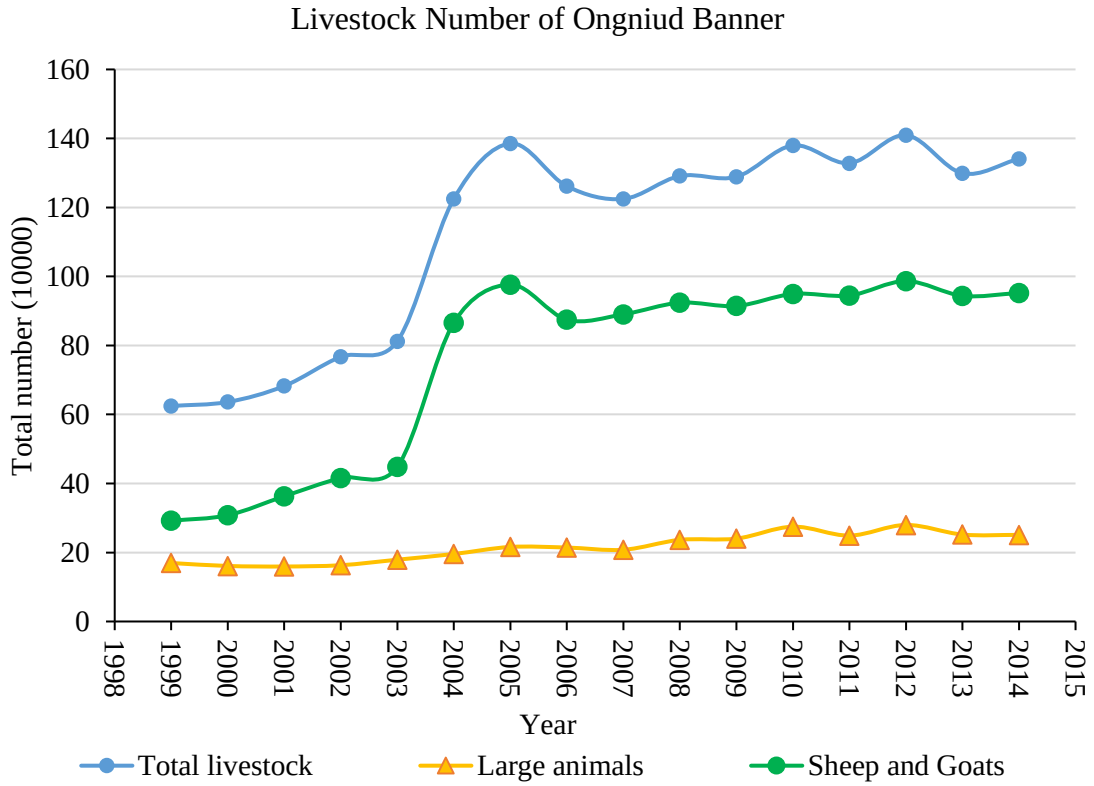

Figure 8 Evolution of the livestock number in Ongniud Banner from 1999 to 2014 (source: Inner Mongolia Autonomous Region Bureau of Statistics, People's Republic of China, 2015)

Beside the increase in population number, the increase in livestock number is another cause of irrational human -induced land deterioration through overgrazing on limited grassland. The total number of livestock increasing steadily from 62.46 in 1999 to 134.12 in 2014, it is two times greater than 1999. In which large animal number slightly increasing or with non-significant change between 1999 and 2014, in contrast, the number of sheep and coats increasing significantly over the whole study period, the total number of both animal population and sheep and goats reached the largest number of 138.54 and 97.63 respectively, in 2005.

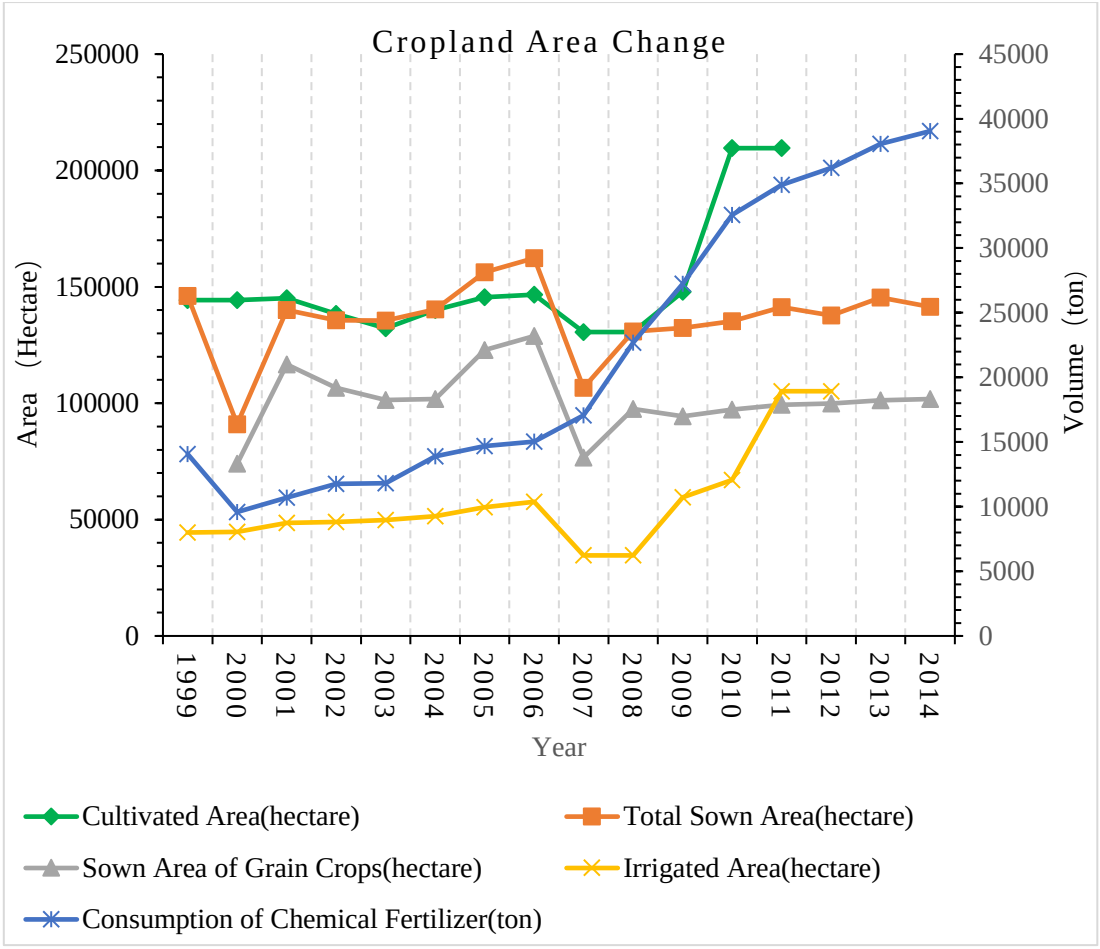

Figure 9 Evolution of the cultivated area in Ongniud Banner from 1999 to 2014 (source: Inner Mongolia Autonomous Region Bureau of Statistics, People's Republic of China, 2015)

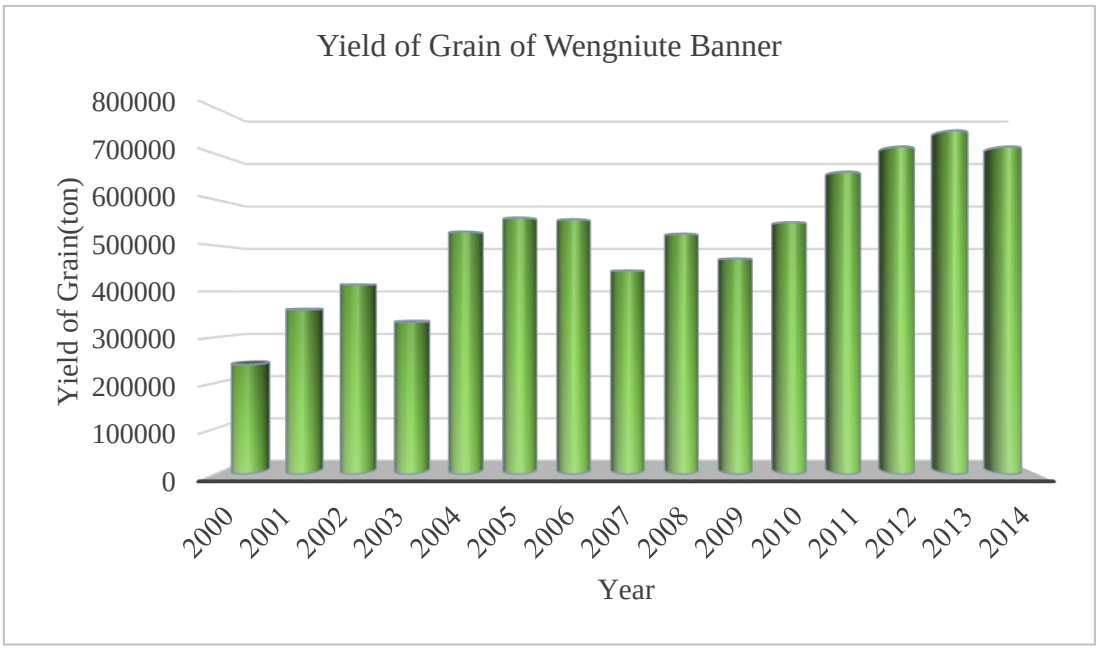

Figure 10 Evolution of the grain yield in Ongniud Banner from 1999 to 2014 (source: Inner Mongolia Autonomous Region Bureau of Statistics, People's Republic of China, 2015)

According to the statistical results recorded that shown in figure 9, the total area of cultivated land steadily increasing from 144,270 km^2 in 1999 to 2070,000 km^2 in 2014, in which irrigation land increasing of same change pattern with total area of cultivated land. The area of sown area reached the maximum value 57713 km^2 in 2006, drop down to 34614 km^2 one year after in 2007, while the lowest value of sown area occurred in 2000. But the amount of chemical fertilizer used for cropland is steadily increasing with the expansion of cultivated land. With the increasing of the area of sown area, grain yield with the increasing trend except drop down in year 2007 and 2009 (figure 10). This result indicate that innter annual change of mean annual precipitation and the mean annual temperature were affected the area change of the cropland and grain yield from 1998 to 2014.

Chapter 7. Results and discussion

7.1 LULC classification results

The LULC classification maps of year 2000, 2009, and 2015 produced in the research are displayed in figures 11, 12, and 13 respectively. Each of these maps includes 17 secondary classes in the study area.

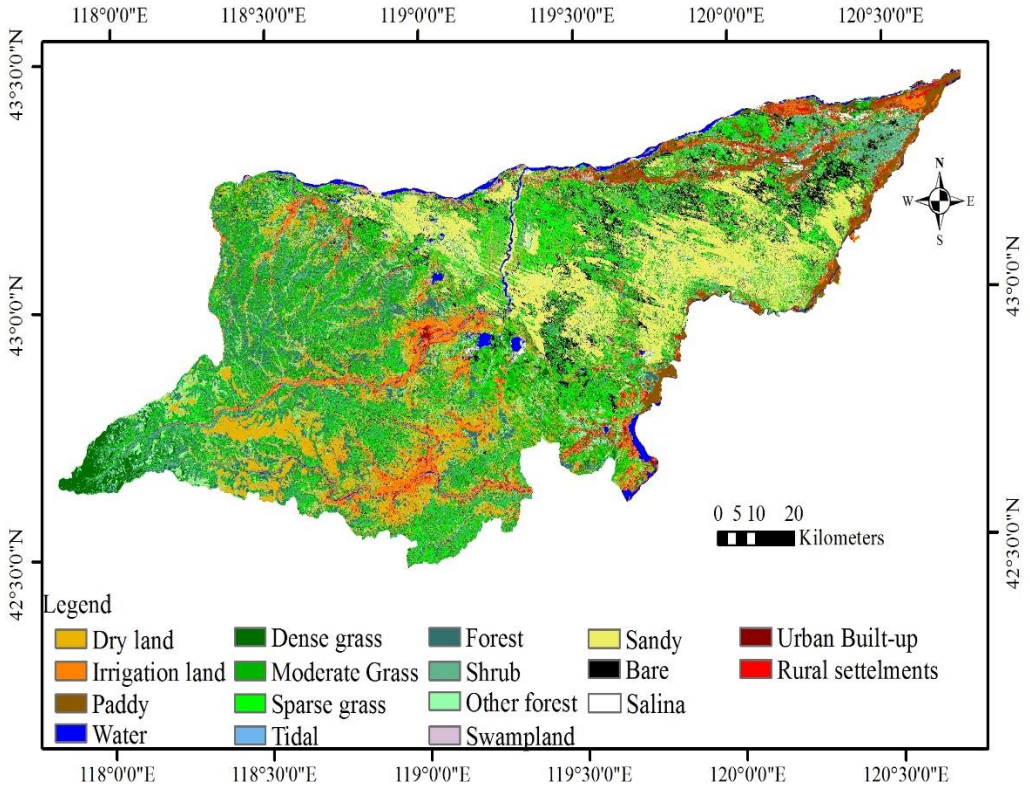

Figure 11 LULC classification map of year 2000 in the study area.

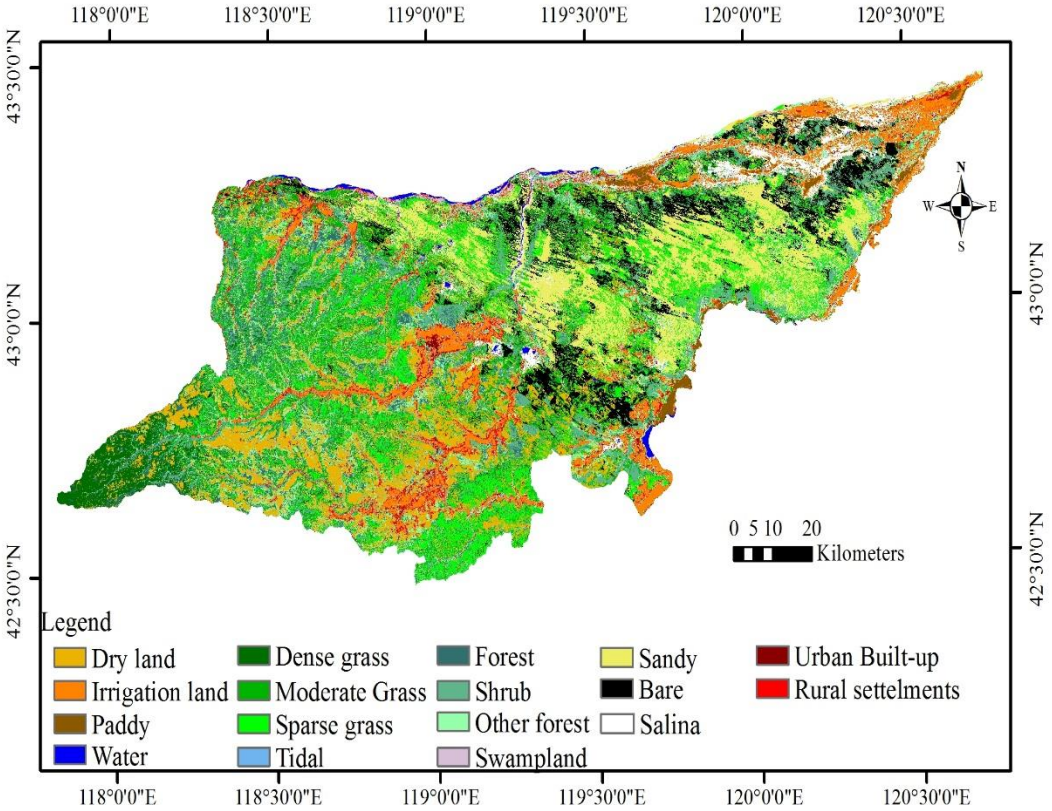

Figure 12 LULC classification map of year 2009 in the study area.

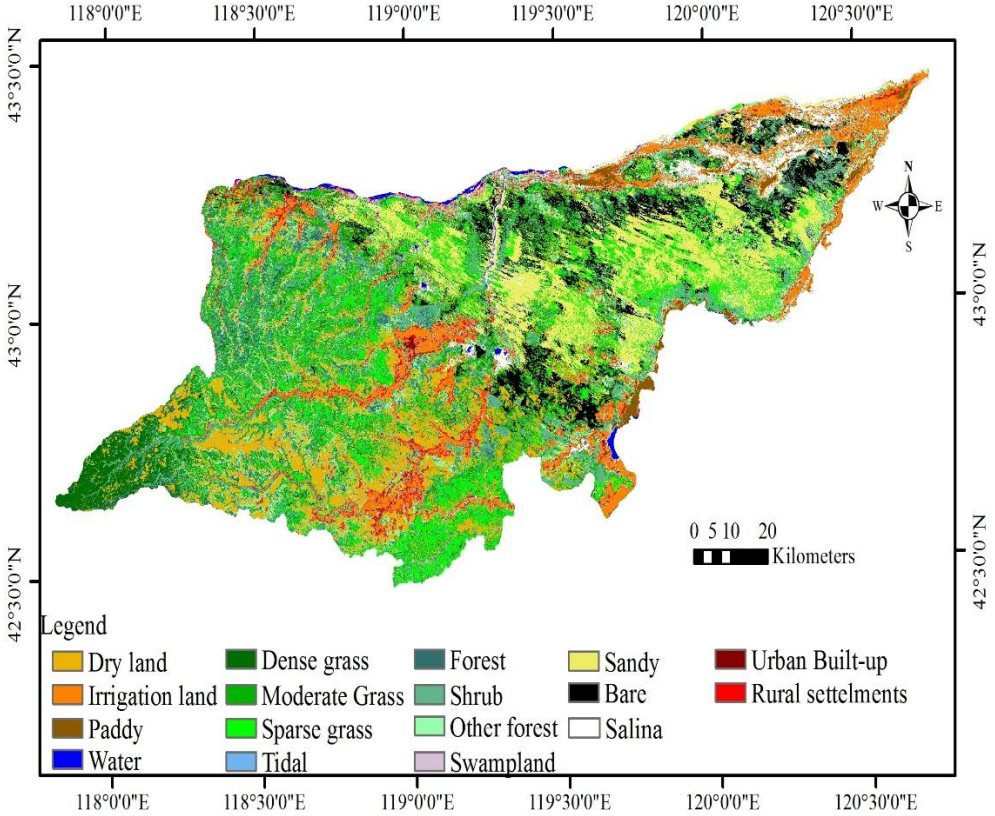

Figure 13 LULC classification map of year 2015 in the study area.

The areal coverage and proportion of 17 LULC secondary classes for each year (2000,

2009, and 2015) are presented in Figure 14 and Table 8.

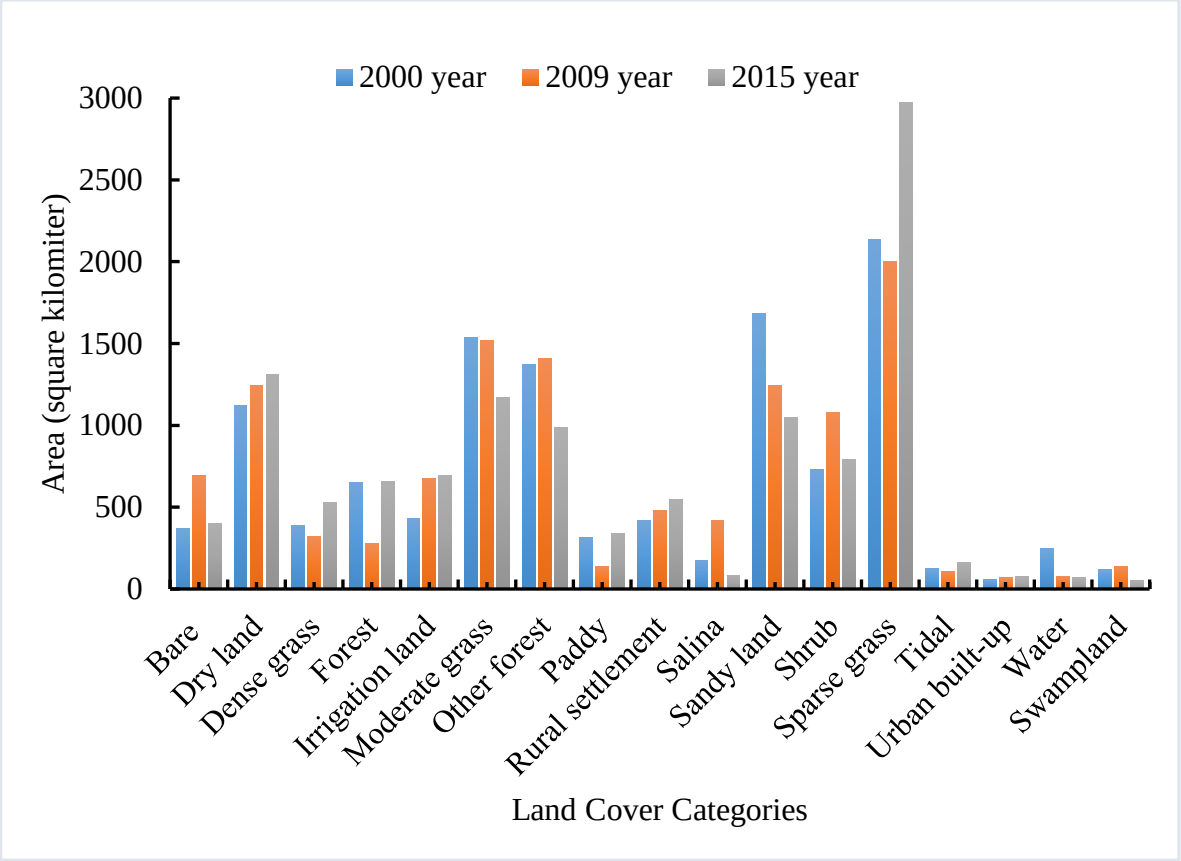

Figure 14 Areal coverage of the 17 LULC secondary classes of years 2000, 2009, and 2015 in the study area.

According to the LULC classification maps of each year (2000, 2009 and 2015) and statistical figure present clearly dry land, irrigation land, sparse grass, urban built-up, and rural settlement and tidal expanding continuously over the study period from 2000 to 2015. Meanwhile, moderate grass, water, swampland, and sandy shrank from 2000 to 2015.

Table 8 the areal coverage and proportion of the 17 LULC secondary classes of years 2000, 2009, and 2015 in the study area.

	Area (Square kilometers)			Proportion (%)		
LULC types	2000	2009	2015	2000	2009	2015
Bare	370.32	691.94	398.99	3.12	5.82	3.36
Dry land	1123.82	1241.67	1310.58	9.46	10.45	11.03
Dense grass	390.56	321.36	526.04	3.29	2.70	4.43
Forest	650.07	277.11	654.82	5.47	2.33	5.51
Irrigation land	430.31	674.35	693.33	3.62	5.67	5.83
Moderate grass	1537.22	1520.58	1169.51	12.93	12.79	9.84
Other forest	1370.81	1407.63	989.34	11.53	11.84	8.32
Paddy	313.58	138.46	341.18	2.64	1.16	2.87
Rural settlement	421.63	477.35	548.19	3.55	4.02	4.61
Salina	175.09	419.46	85.02	1.47	3.53	0.72
Sandy land	1684.27	1245.83	1051.09	14.17	10.48	8.84
Shrub	728.48	1078.00	790.45	6.13	9.07	6.65
Sparse grass	2135.63	2001.15	2971.38	17.97	16.84	25.00
Tidal	124.93	108.95	162.29	1.05	0.92	1.37
Urban built-up	60.22	67.63	74.36	0.51	0.57	0.63
Water	250.60	76.84	67.47	2.11	0.65	0.57
Swampland	118.35	137.56	51.87	1.00	1.16	0.44

The main LULC classes of the study area in the year 2015 were found to be grassland (dense grass, moderate grass and sparse grass), woodland (forest, shrub, and other forest), and cropland (dry farmland, irrigated farmland, and paddy) with the coverage of 39.3%, 20.5%, 19.7% of the study area respectively.

7.2 Validation of LULC Map

The LULC classification was carried out for each year by accounting the contribution of each of the additional features (spectral indices, spectral transformations, textural, and topographic) to the basic Landsat based spectral features (Landsat 6 bands). The one by one performance of these additional features is shown in table 9. Based on this analysis, only highly performed features were chosen for the production of the LULC maps. The exclusion of the less contributed features could reduce the data volume for further processing.

Table 9 Contribution of the additional features for the LULC classification in the study area.

Additional features	Contribution
DEM	Improve discrimination among irrigation land, swampland, and paddy
Slope	Improve discrimination of grassland and forest, and bare area and tidal
Aspect	Less contribution
NDVI	Improve discrimination between grassland and forest
NDWI	Improve discrimination between irrigated land and swampland
NDSI	Improve discrimination between salina land and sandy land
NDBI	Enhance discrimination of built-up and rural settlement area
NDBaI	Improve discrimination between bare area and salinized area
Greenness	Less contribution
Brightness	Less contribution
Wetness	Less contribution
Mean	Improve discrimination between rural settlements and urban built-up area
Variance	Less contribution
Homogeneity	Improve discrimination between rural settlements and urban built-up area
Contrast	Less contribution
Dissimilarity	Improve discrimination between cropland and built-up area
Entropy	Improve discrimination between artificial grassland and cropland
Second moment	Enhance discrimination of the tidal and rural settlement
Correlation	Less contribution

The performance of the resulted LULC maps assessed through the confusion matrix based analysis using the validation data is shown in Table 110.

Table 10 Confusion matrix of the LULC classification for each years in the study area

	Year 2000		Year 2009		Year 2015	
Classes	User's accuracy	Producer's accuracy	User's accuracy	Producer's accuracy	User's accuracy	Producer's accuracy
Bare	0.88	0.61	0.86	0.77	0.88	0.56
Dryland	0.74	0.8	0.88	0.75	0.86	0.57
Dense grass	0.96	0.76	0.88	0.92	0.8	0.83
Forest	0.94	0.86	0.88	0.86	0.8	0.85
Irrigation land	0.94	0.82	0.92	0.81	0.96	0.65
Moderate grass	0.92	0.88	0.92	0.87	0.84	0.84
Other forest	0.74	0.93	0.92	0.92	0.68	0.92
Paddy	0.88	1	0.94	0.96	0.64	1
Rural settlements	0.8	0.89	0.82	0.8	0.76	0.79
Salina	0.84	0.98	0.88	0.96	0.74	0.97
Sandy land	0.82	0.91	0.98	0.88	0.96	0.91
Shrub	0.86	0.88	0.92	0.92	0.86	0.84
Sparse grass	0.92	0.7	0.9	0.87	0.84	0.76
Tidal	0.86	0.93	0.82	0.89	0.82	0.91
Urban built-up	0.62	1	0.78	1	0.76	1
Water	1	1	0.96	1	1	1
Swampland	0.84	0.93	0.86	0.98	0.78	0.98
Overall accuracy	0.86		0.89		0.82	
Kappa coefficient	0.85		0.88		0.81	

The overall accuracy (Kappa coefficient) obtained for 17 secondary classes in the study area were 0.86(0.85), 0.89(0.88), and 0.82(0.81) for years 2000, 2009, and 2015 respectively.

Accuracy of LULC map in 2009 higher than both LULC map in 2000 and in 2015. The LULC map in 2000 with the higher accuracy than LULC map in 2015 due to the high resolution SPOT 5 image provide the high quality training data for 2009. Visual interpretation land use dataset of 2000 provide the high quality training data for 2000. Lack of ground truth reference data for 2015 resulted in LULC map of 2015 with relatively low accuracy. But, the comparison between previous LULC classification result [13] cover the study area with the overall accuracy of 86.83% and the result of this research confirmed that this research successfully produce the accurate and reliable

LULC map for further analysis of LULC change and desertification in study area.

7.3 Spatio-temporal changes of LULC.

The annual rate of change (%) of the 17 LULC secondary classes between 2000-2009, 2009-2015, and 2000-2015 are presented in Table 11.

Table 11 The annual rate of change (%) of the 17 LULC secondary classes between 2000-2009, 2009-2015, and 2000-2015 in the study area. Positive (negative) value indicates increasing (decreasing) trend over the time period.

LULC classes	Annual rate of change (%)		
	2000-2009	2009-2015	2000-2015
Bare	9.65	-7.06	0.52
Dry land	1.17	0.92	1.11
Dense grass	-1.97	10.62	2.31
Forest	-6.37	22.72	0.05
Irrigation land	6.30	0.47	4.07
Moderate grass	-0.12	-3.85	-1.59
Other forest	0.30	-4.95	-1.86
Paddy	-6.20	24.40	0.59
Rural settlement	1.47	2.47	2.00
Salina	15.51	-13.29	-3.43
Sandy land	-2.89	-2.61	-2.51
Shrub	5.33	-4.45	0.57
Sparse grass	-0.70	8.08	2.61
Tidal	-1.42	8.16	1.99
Urban built-up	1.37	1.66	1.57
Water	-7.70	-2.03	-4.87
Swampland	1.80	-10.38	-3.74

As shown in table 11, significant changes in the LULC secondary classes over the past 16 years (2000 -2015) have been detected in the study area. Over this period (2000 -2015), dry land, irrigated land, urban built-up areas, and rural settlement were expanded with an annual rate of 1.11 %, 4.07%, 1.57% and 2.00%, respectively, in which irrigation land expanding most fast. However, at the same period (2000 -2015), water, swampland, sandy land, and moderate grass were reduced at an annual rate of 4.87%, 3.74%, 2.51%, and 1.59 % respectively, in which, water shrank fast.

The fluctuation trend of the LULC classes was also detected in the study area. During

the period 2000-2009, bare, salina, and shrub expanded significantly (positive annual changes) with an annual rate of 9.65%, 15.51%, and 5.33%; however, they decreased (negative annual changes) in next 6 years (2009-2015). On the other hand, dense grass, forest, paddy, sparse grass and tidal decreased between 2000 and 2009; however, these classes expanded during 2009-2015.

The increase of the salinized area and bare area between 2000 and 2009; and the decrease of dense grasses, and swamp land between 2000 and 2009 can be linked to the climatic variation such as increasing temperature and low precipitation. On the other hand, between 2009 and 2014, the decrease of annual mean temperature and the increase of annual mean precipitation could also be linked to the climatic variations because the sparse grasses increased between 2009 and 2015. The decrease of the precipitation and soil moisture in warm and dry climate restrict the growth of vegetation resulting exposed soil, shrinkage of water body, and the increase of barren and tidal areas. In contrast, the increase of the precipitation is favorable to the growth of vegetation and biodiversity with high soil moisture and less soil erosion.

Desertification phenomenon represented by different types of land degradation processes include water erosion, wind erosion, soil fertility decline, water logging, salinization, lowering of water table, deforestation, grassland degradation, soil destruction by mining and urban and industrial encroachment onto agricultural land.
The Ongniud Banner region located in the western part of the Horqin Sandy Land is a typical transition zone of agricultural and animal husbandry. Over the past five decades, this region is affected by land degradation and desertification due to climate change and irrational human activities.

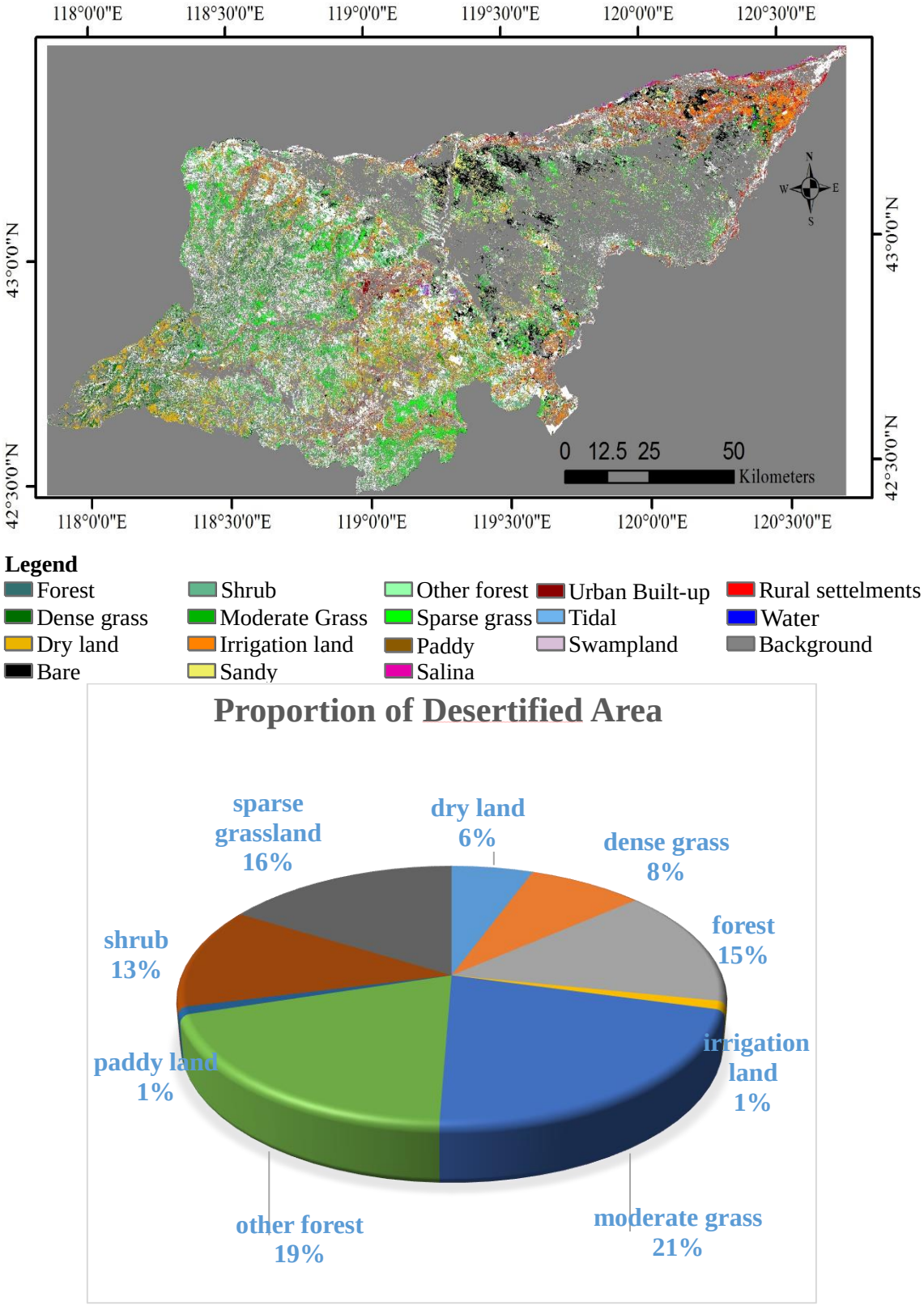

Figure 15 Changes in water bodies between 2000 and 2015 in the study area.

In this study the most evident spatial-temporal change of the water bodies, irrigation lands, sandy lands, and salina (salinized lands), grassland over the period of 2000-2015

considered to be desertification phenomenon occurred in study area, the desertification maps are presented in figures 16-23 respectively.

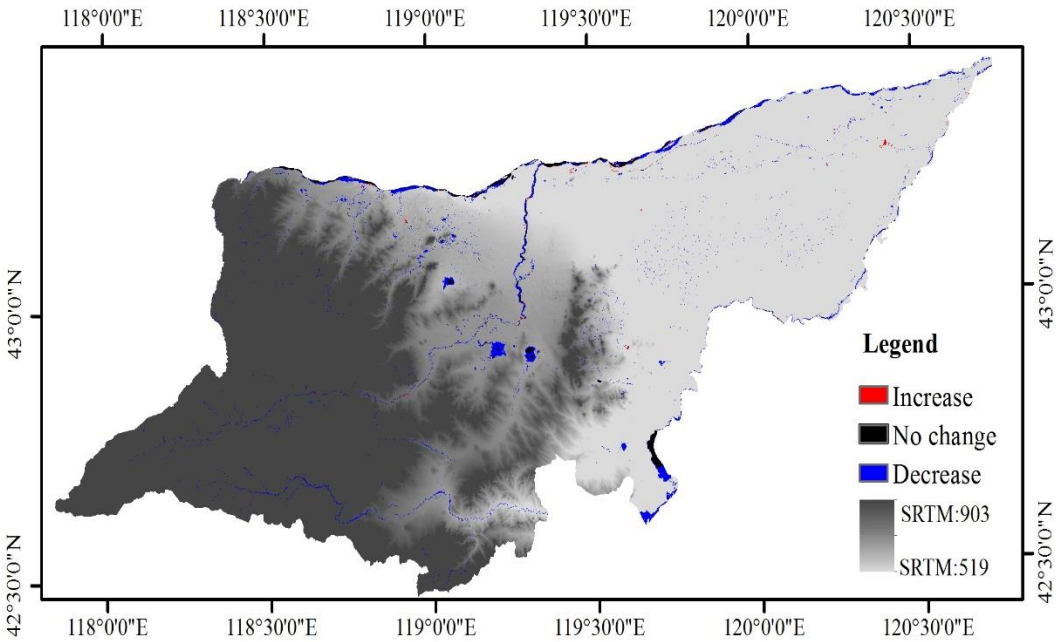

Figure 16 Changes in water bodies between 2000 and 2015 in the study area.

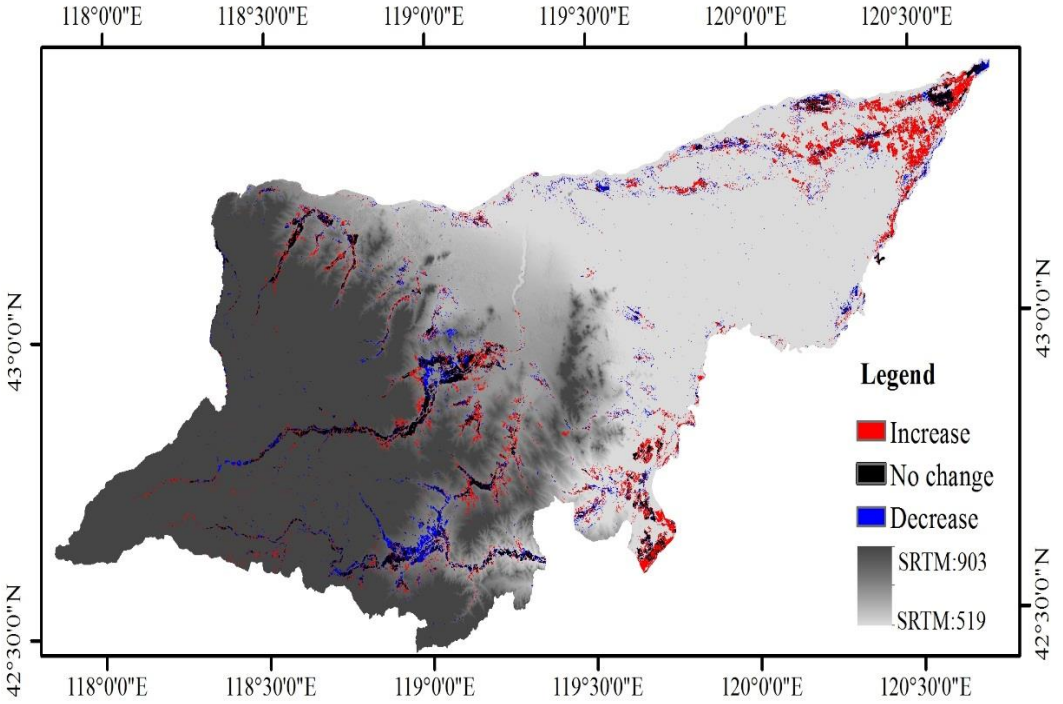

Figure 17 Changes in irrigated lands between 2000 and 2015 in the study area.

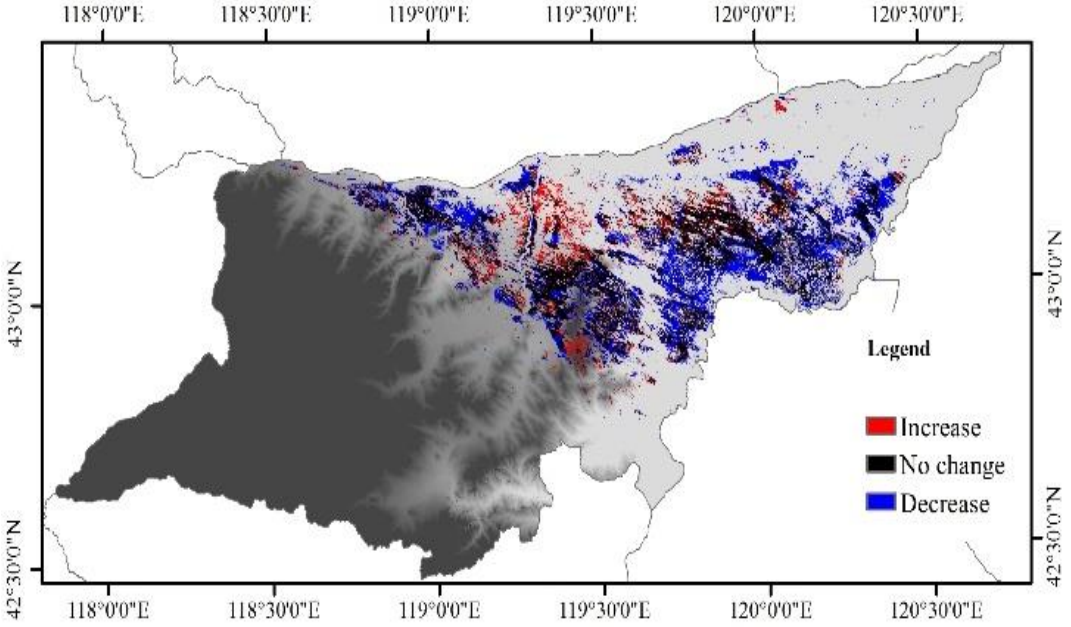

Figure 18 Changes in sandy lands between 2000 and 2015 in the study area.

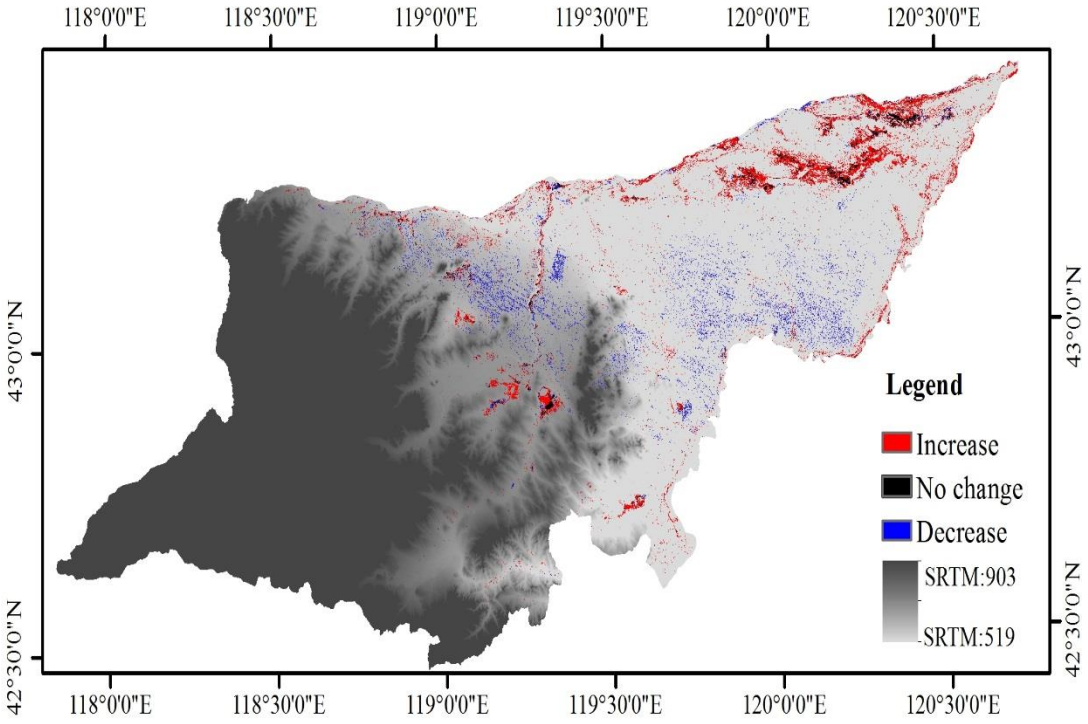

Figure 19 Changes in salina between 2000 and 2015 in the study area.

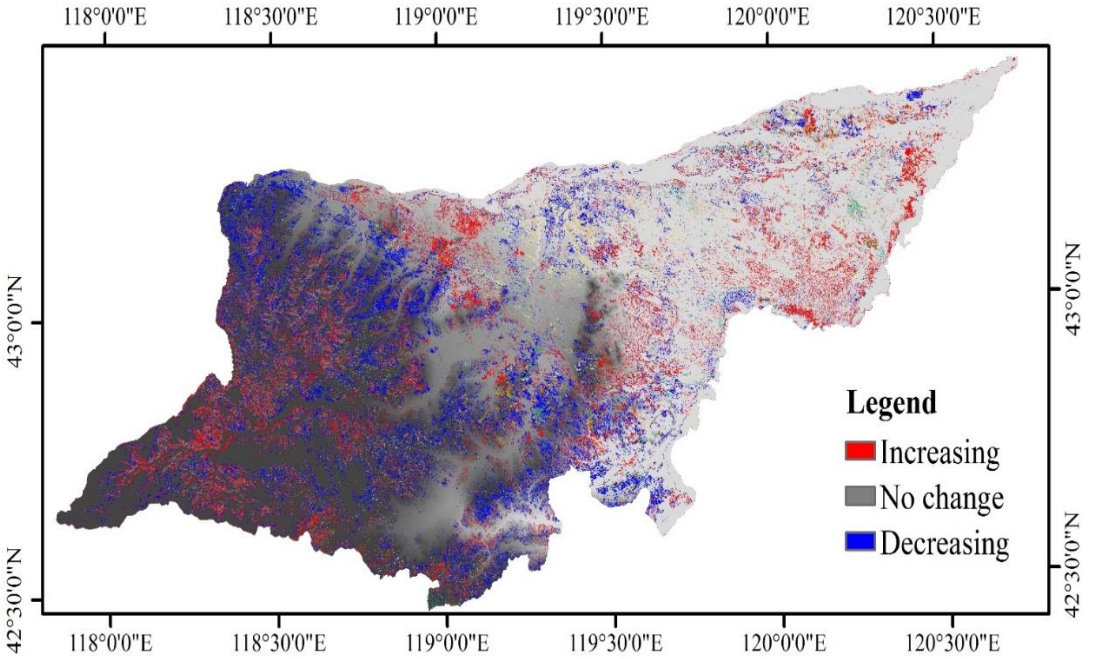

Figure 20 Changes in moderate grass between 2000 and 2015 in the study area.

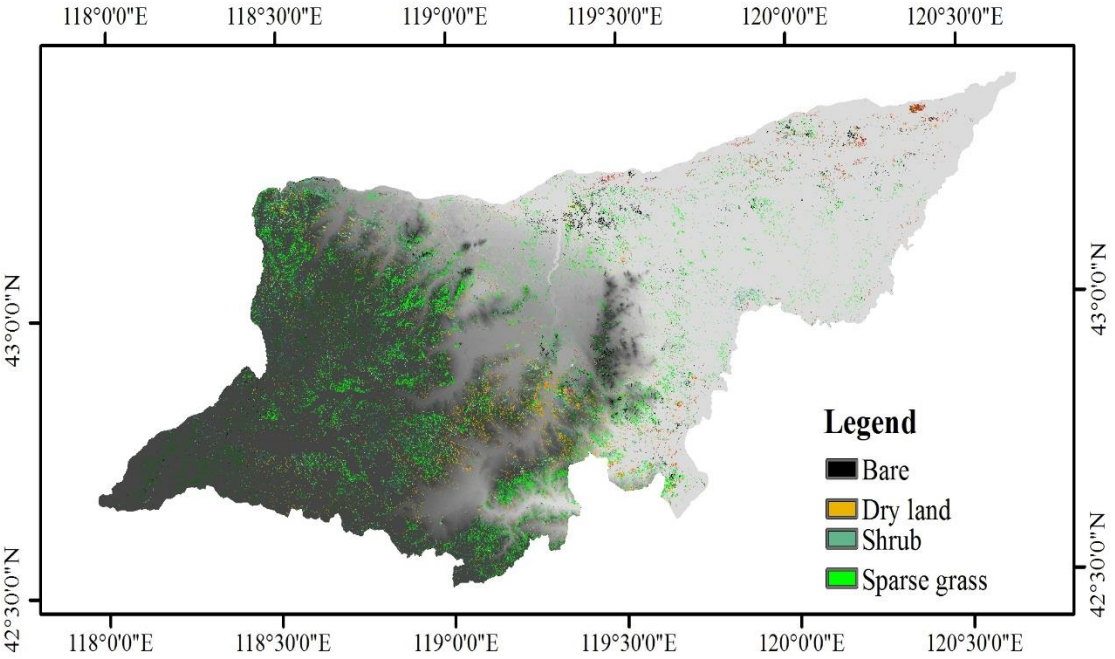

Figure 21 Degradation of moderate grass between 2000 and 2015 in the study area.

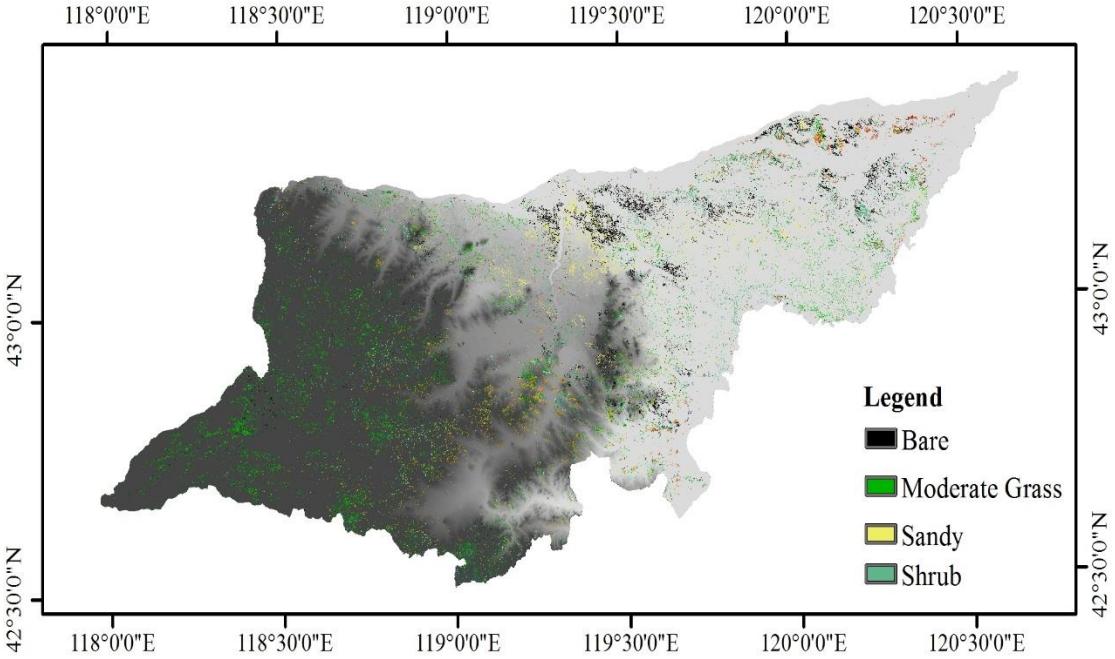

Figure 22 Conversion of sparse grass to other land cover types from 2000 to 2015

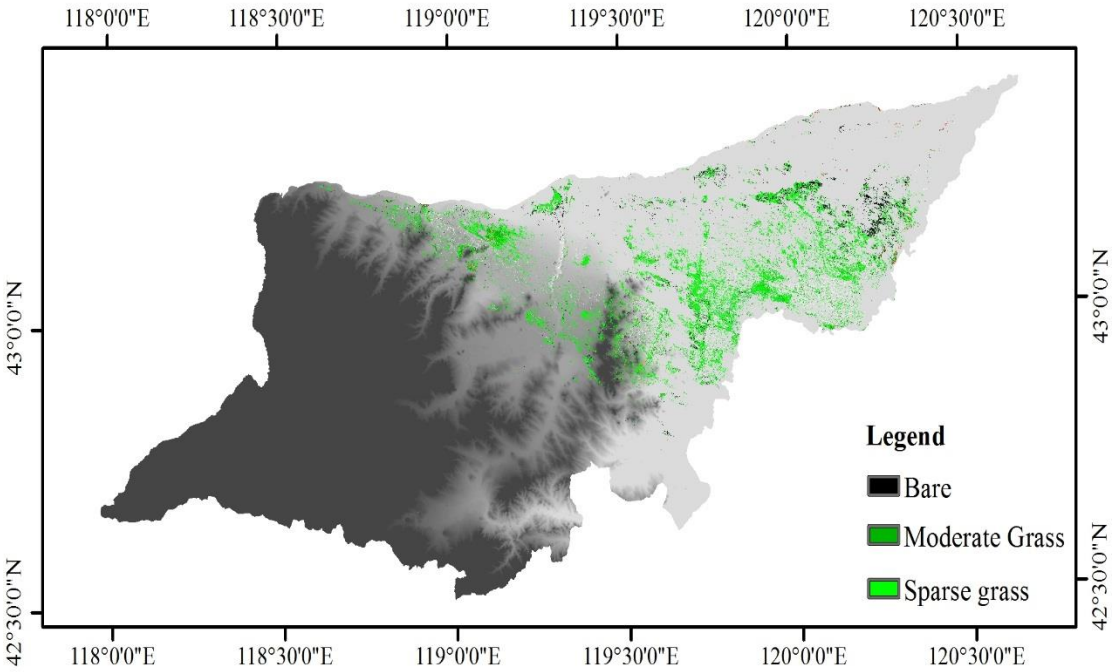

Figure 23 Reversion of Sandy from 2000 to 2015

Form the above mentioned land cover type changes, we can identify the main land degradation and desertification process from 2000 to 2015 appeared in salinization in irrigation land; moderate grass degraded to sparse grass, dry land, bare and shrub;

sparse grass degraded to bare, sandy land and shrub. In contrast, small area of sandy land reversed to sparse grass and moderate grass.

As shown in figure 15 the desertification map based on desertification definition defined in this study that produced result confirmed that, a 3051 km2 area suffered from desertification in the study area from 2000 to 2015, and desertification of moderate grass was the most common type of desertification (21% of total desertified area), followed by desertification of other forest, sparse grass, and forest areas at 19%, 16%, and 15% respectively. And less desertification occurred in dense grass (8%) and dry land (6%) areas.

7.4 Desertification analysis based on Top Soil Grain Size Index

This study applies the proposed GSI to produce three top soil grain size index distribution maps for Ongniud Banner in the year 2000, 2009 and 2015 respectively. The top soil grain size distribution maps of year 2000, 2009 and 2015 presented in figure 24, figure 25, and figure 26.

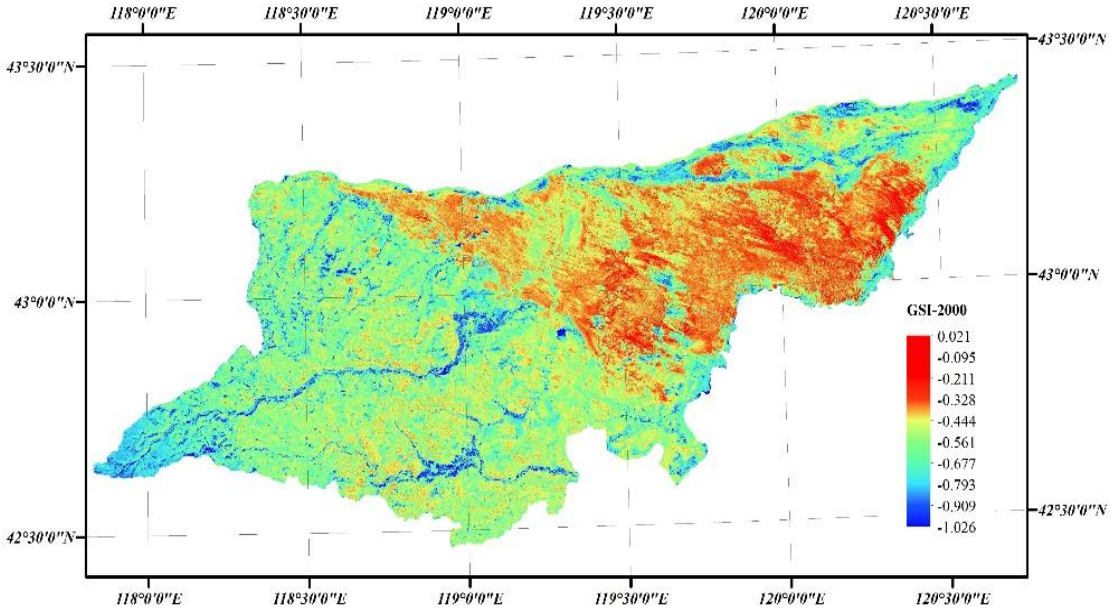

Figure 24 Top soil grain size distribution of 2000

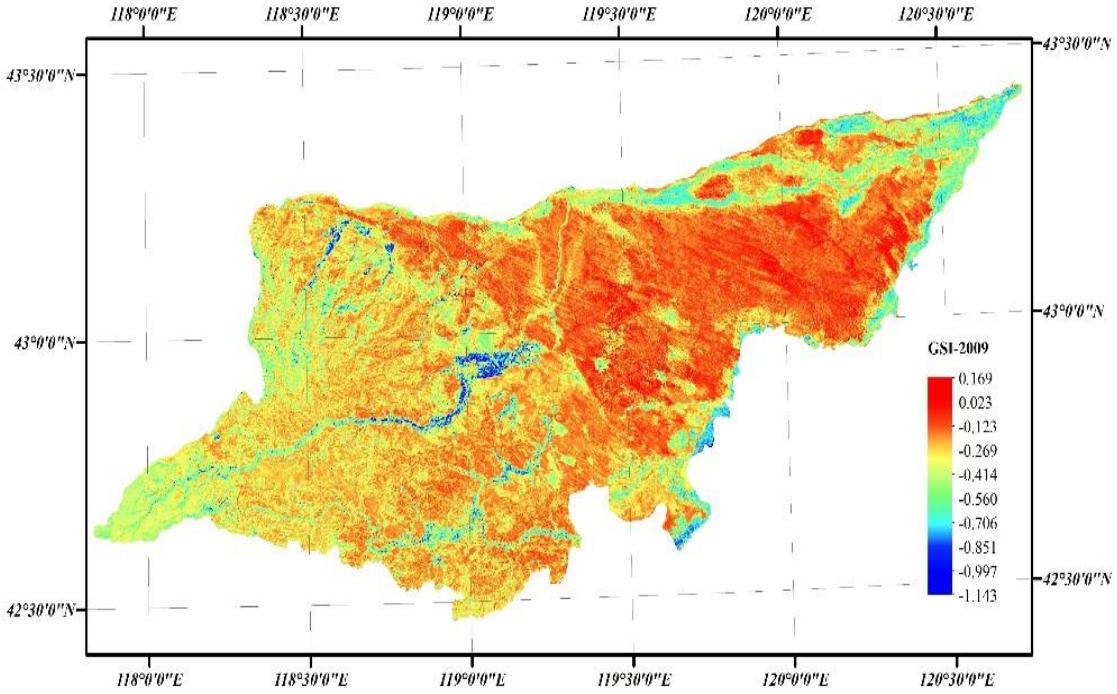

Figure 25 Top soil grain size distribution of study area in 2009

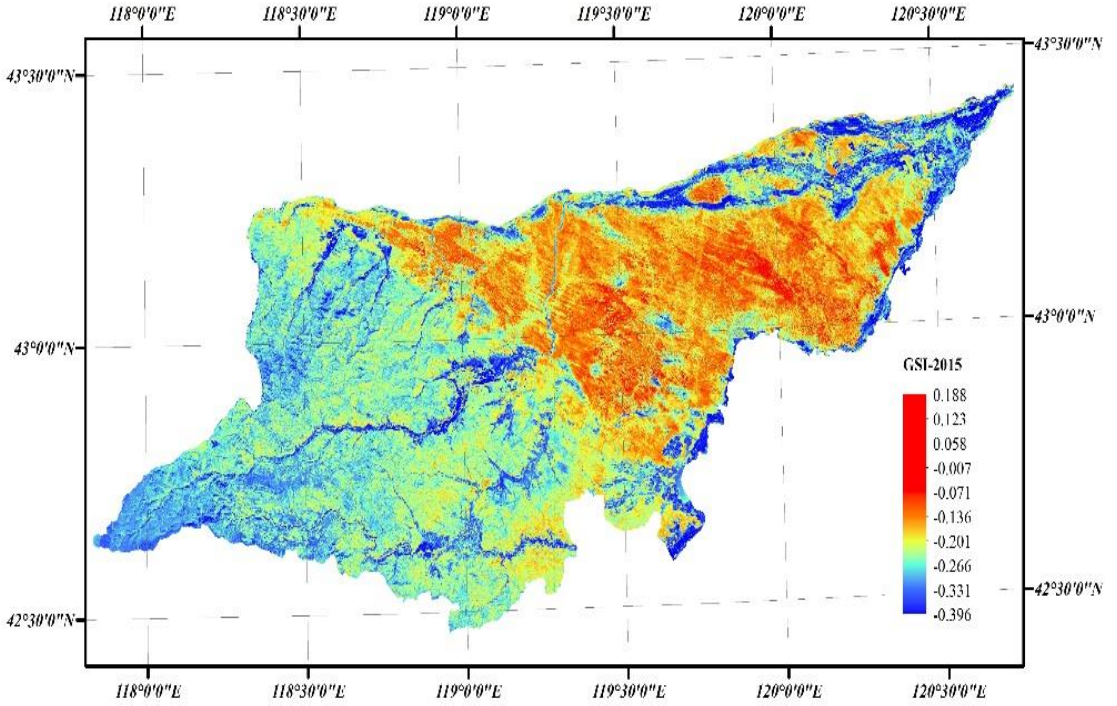

Figure 26 Top soil grain size distribution of study area in 2015

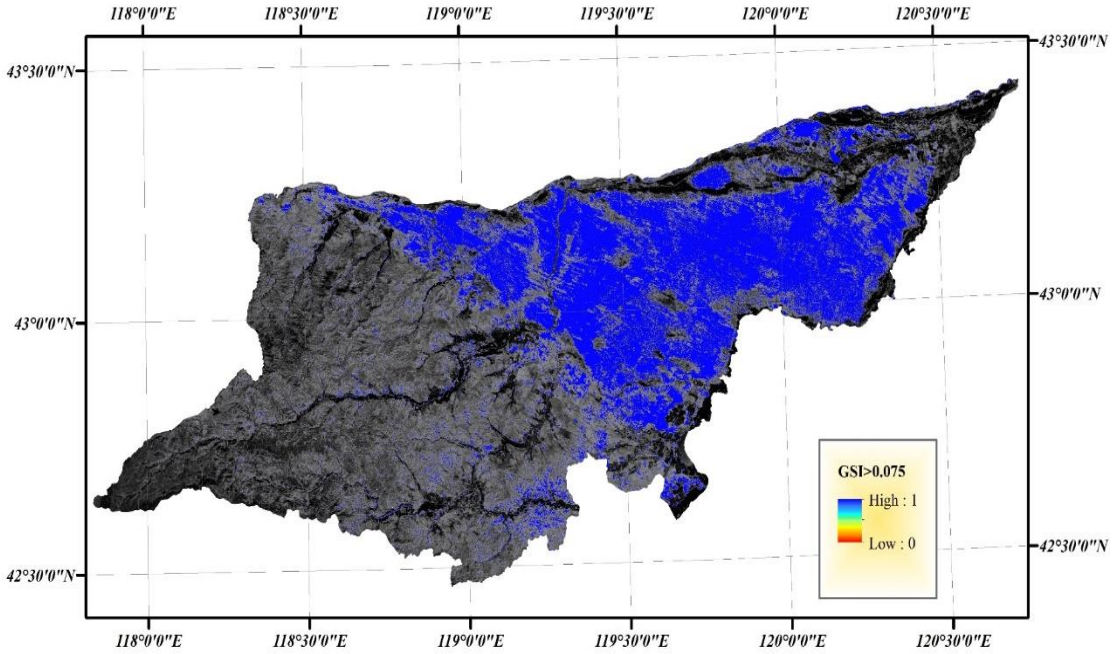

Figure 27 Fine sand mask of study area

As we can see from figure 24, figure 25 and figure 26, the result show that a high GSI value area concentrated in the northeast flat area of the Ongniud Banner, and GSI value increasing from the southwest to the northeast direction, it means the fine sand content of the topsoil is increasing from southwest to northeast direction. This distribution is coherent with the Land cover category change from grassland in mountain area to cropland in hilly area to sandy land in flat area.

The attempt made to understanding the soil physical change in desertified area we produce the top soil grain size index change maps from the year 2000 to 2009, from year 2009 to 2015 and from year 2000 to 2015 through differentiating the top soil grain size maps in the year 2000, 2009 and 2015. The topsoil grain size change maps presented in figure 21, figure 22 and figure 23.

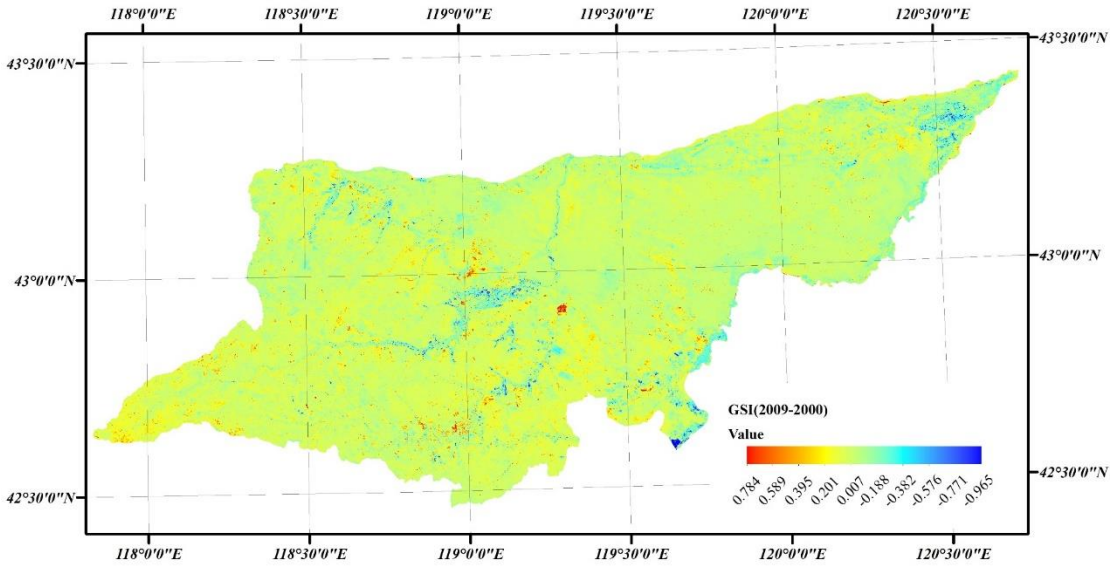

Figure 28 Top Soil Grain Size change of Ongniud Banner between 2000 and 2009

From 2000 to 2009, the GSI value increased significantly in the whole study area except the small area covered by irrigation farming area and paddy, especially surrounding of water body distributed in the center of study area, indicate that soil grain size of top soil to increase significantly with salinization area appeared while water body shrank. In study area, vegetation coverage decreased, large area of soil surface less protected by grass and exposed to wind erosion. Desertification developed in study area which lead to water body shrinking and salinization increasing.

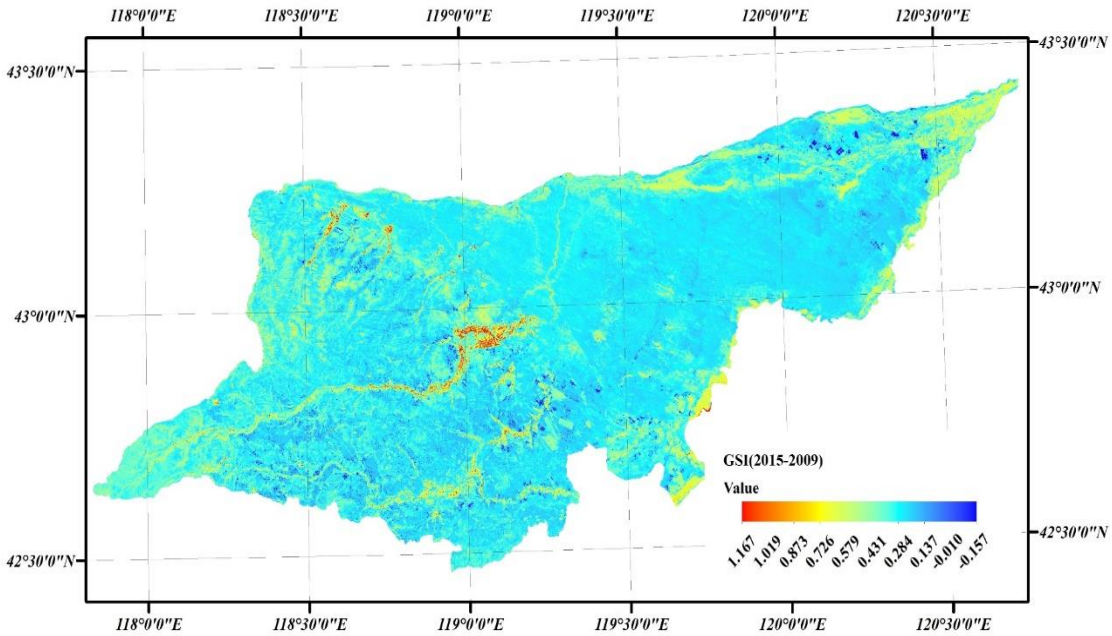

Figure 29 Top Soil Grain Size change of Ongniud Banner between 2009 and 2015

During the period 2009-2015, the GSI value of top soil increased significantly around the urban built-up area, this result linked to the intensity and irrational human activities such construction of household for increasing urban population, and cleaned out the forest land convert to cultivated land to satisfy the demand for food. Soil grain size in sandy land and hilly mountain area restored duo to the local people planted artificial shrub and grassland in sandy land to protect the sandy desertification.

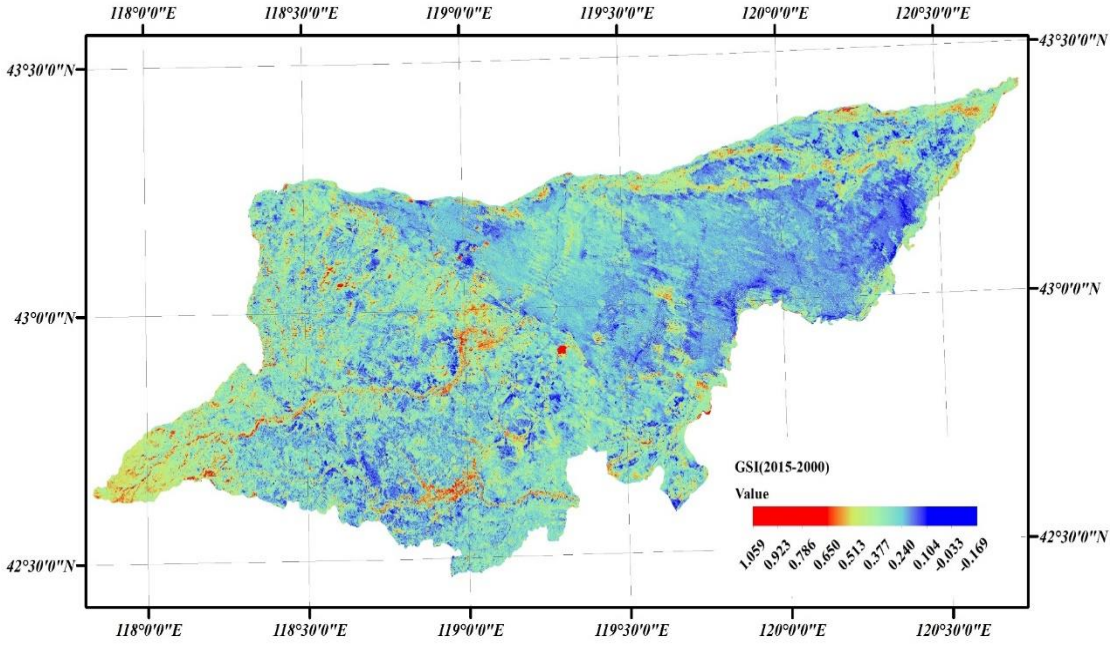

Figure 30 Top Soil Grain Size change of Ongniud Banner between 2000 and 2015

Change value of top soil grain size index between 2000 and 2015 in Ongniud Banner presented in table 12.

Table 12 Change of top soil grain size index between 2000 and 2015 in Ongniud Banner

	Top soil grain Size index	Minimum	Maximum	Mean	Standard deviation
Ongniud Banner	2000	-1.3333	0.04201	-0.122940	0.169946
	2009	-3.320755	0.50000	-0.124731	0.174216
	2015	-0.455951	0.312278	0.012907	0.047310

During the past 16 years such as from 2000 to 2015, GSI value of topsoil coarsening continuously in Ongniud Banner, in which around the farming area and the water body due the destruction of natural vegetation cover in large scale lead to expose the bare area eroded by wind easily and salina appeared with the water shrank duo to the over consumption of water resource and high temperature and less precipitation situation. The top soil grain size index value extracted from sandy land in each year 2000, 2009 and 2015 to eliminate the water and vegetation effect. The top soil grain size index

value in sandy land presented in table 13.

However, in the desertified sandy land even the area of sandy land decreasing from 1684.3 km^2 in 2000, 1245.8 km^2 in 2009 to 1051.1 km^2 in 2015 , but the top soil grain size index present increasing trend, the top soil grain size index with the positive change trend in sandy land. It is indicating the ecology protecting measures launched by state and local government effectively control the sandy encroachment in study region, exposed sandy replaced by sparse grass (figure 18 and 23). But the top soil grain size index present increasing trend, this result indicates that sandy soil physical properties worsening, soil organic matter and silt and clay transported over the great distance by wind-blown, desertification severity accelerating over the study period.

Table 13 Change of top soil grain size index between 2000 and 2015 in sandy land

	Top soil grain size index	Minimum	Maximum	Mean	Standard deviation
Sandy land	2000	-0.308943	0.04201	-0.092246	0.0331083
	2009	-0.544304	0.290837	-0.115455	0.0302483
	2015	-0.176482	0.233134	0.006959	0.029958

7.5 Land Surface Temperature and LULC

In this study calculate the land surface temperature of study area using the Landsat image for each year 2000, 2009 and 2015. The different parameter used form metadata of Landsat 5 and Landsat 8. The snap short land surface temperature images shown in from figure 31 to figure 35.

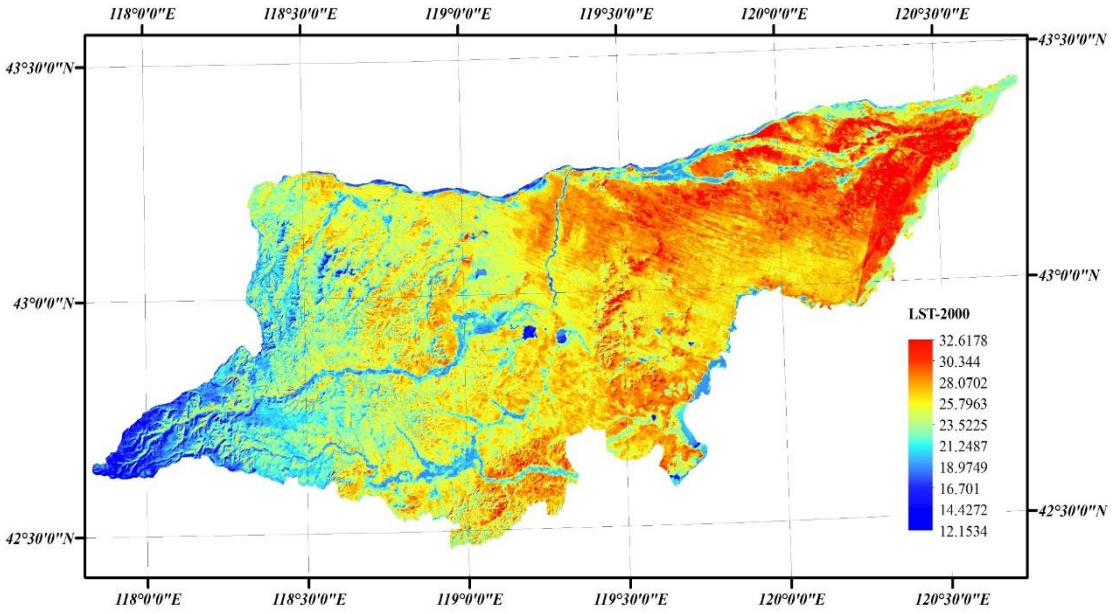

Figure 31 Land surface temperature of study area in 2000

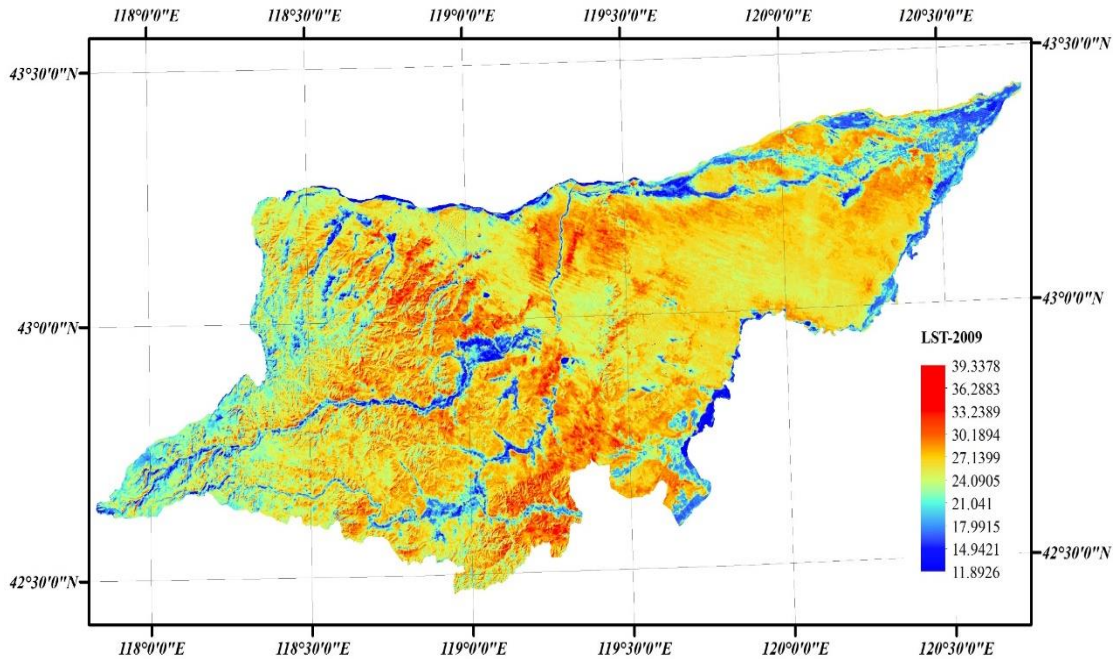

Figure 32 Land surface temperature of study area in 2009

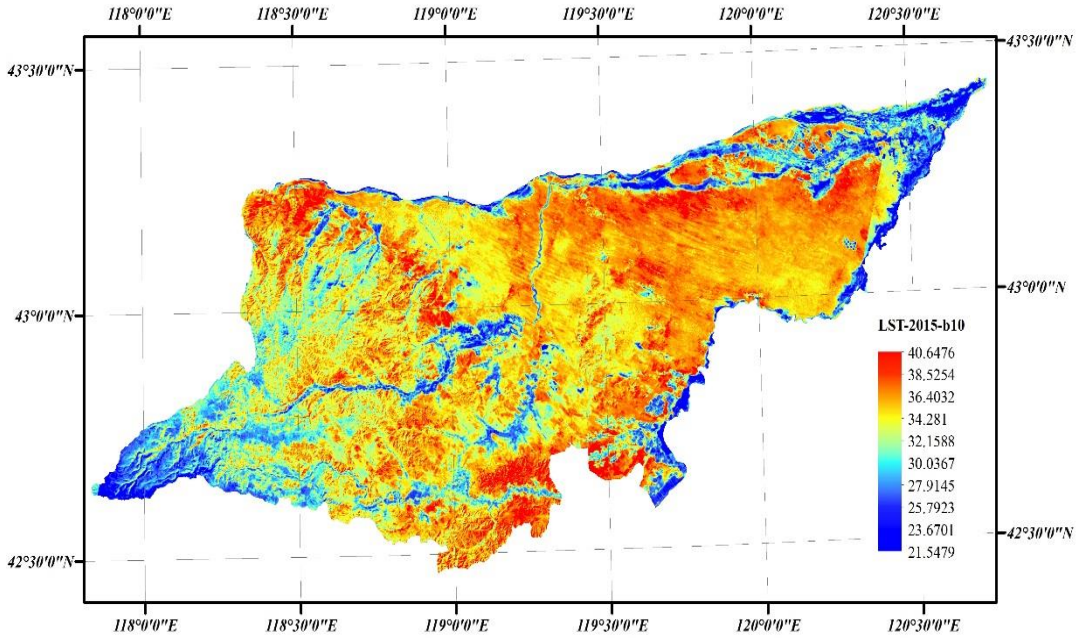

Figure 33 Land surface temperature of study area in 2015(band 10)

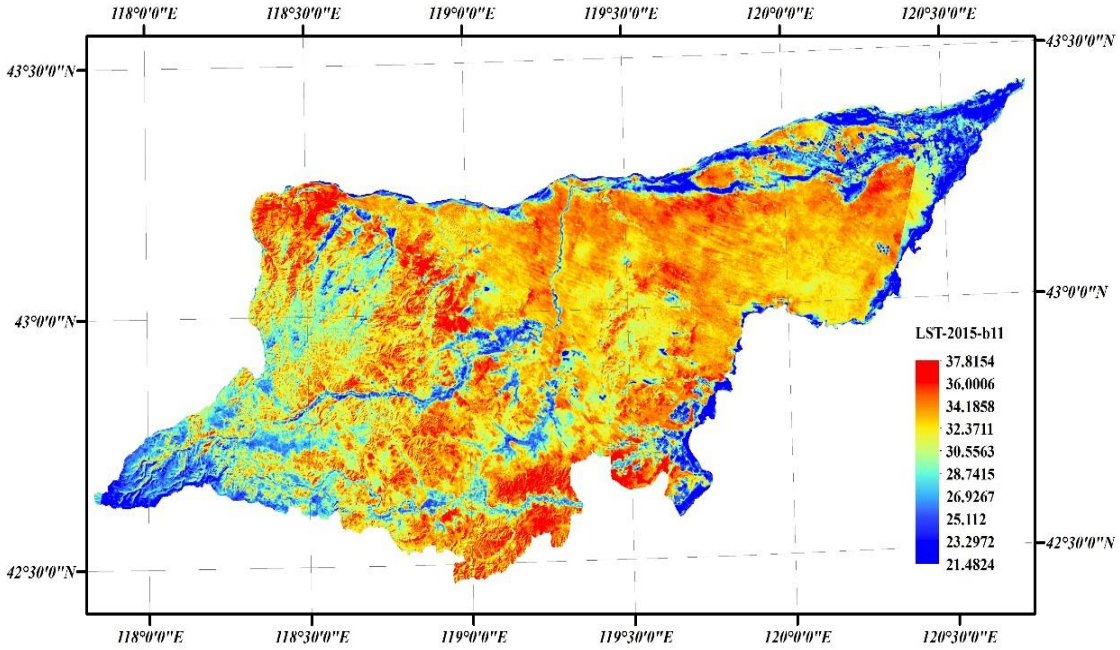

Figure 34 Land surface temperature of study area in 2015 (band 11)

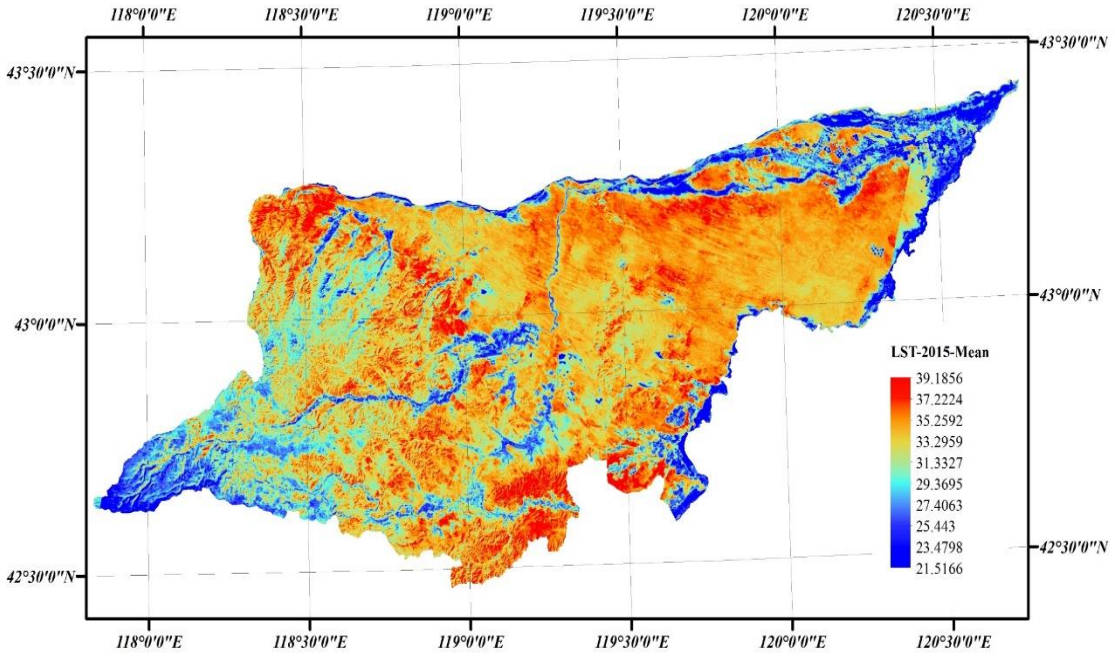

Figure 35 Average Land surface temperature of study area in 2015

The land surface temperature image for year 2000, 2009 and 2015 show that surface soil temperature in high in exposed sandy land, dry farmland and area with low vegetation cover area. Land surface temperature linear positively correlated to vegetation coverage. Land surface temperature as much as high the top soil become dry, all these factor lead to the soil grain size coarsening.

7.6 Desertification analysis based on Land Surface Soil Moisture

Our repeated experiment show that the scatterplot of remotely sensed surface temperature (Ts) and normalized difference vegetation index (NDVI) forms a typical trapezoid in the Ts-NDVI space (Figure. 2) being very similar to the one described by Lambin (1996).

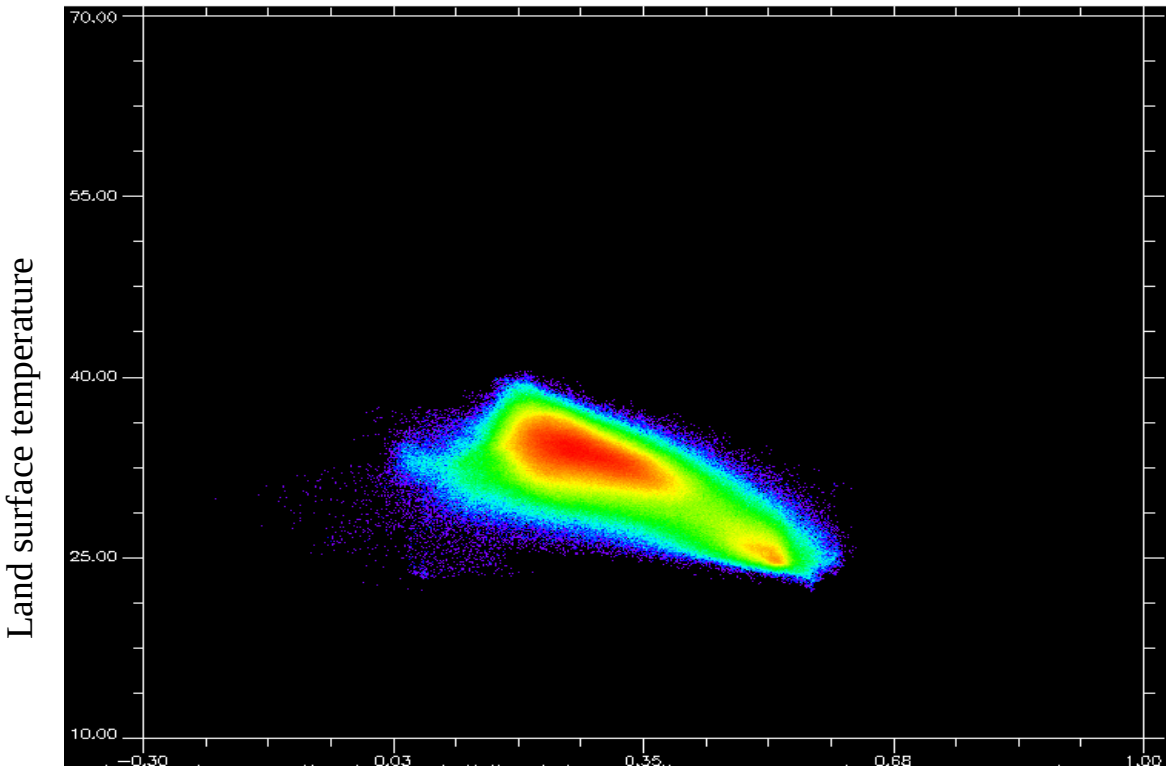

Figure 36 NDVI－temperature distribution in study area

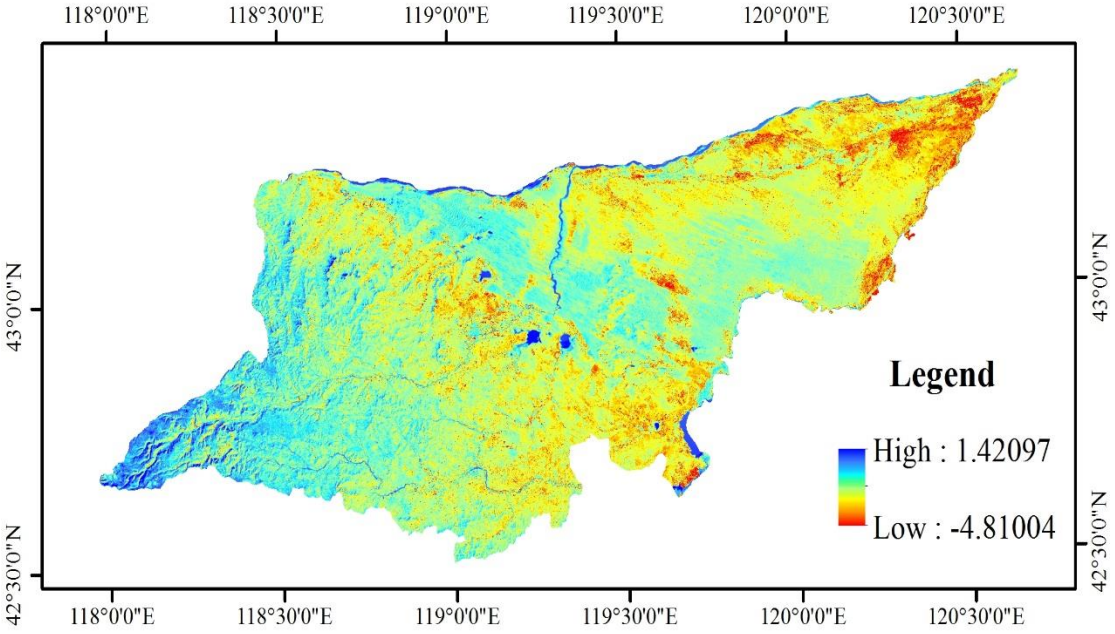

Figure 37 Soil moisture index of study area in 2000

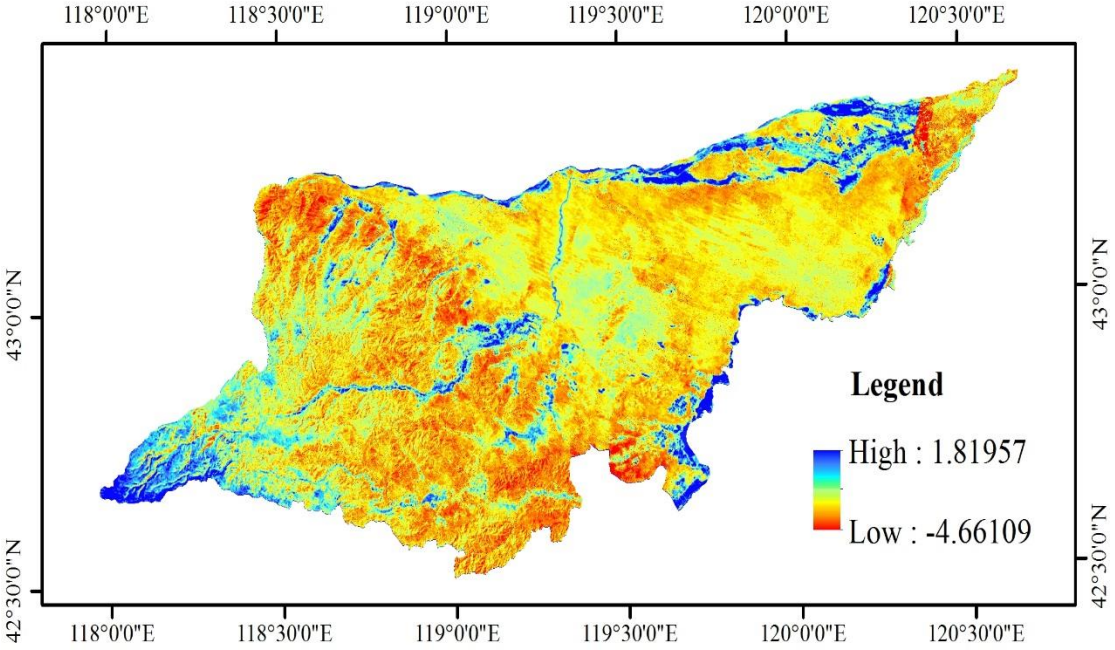

Figure 38 Soil moisture index of study area in 2000

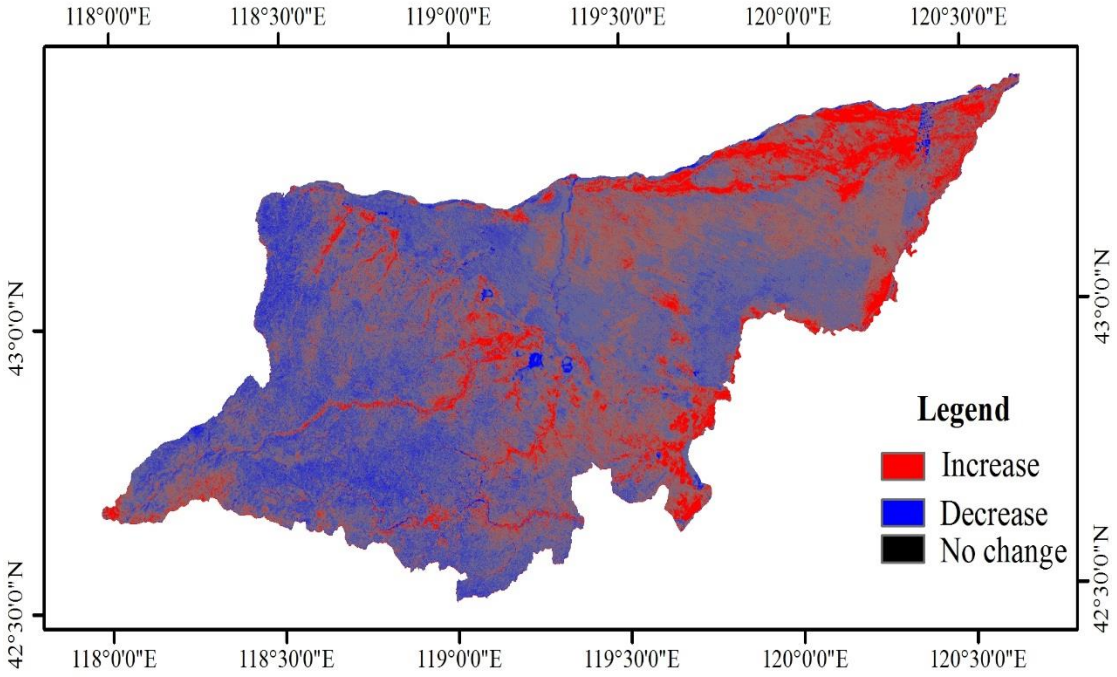

Figure 39 Change of soil moisture index between 2000 and 2015

The soil moisture derived image show that high soil moisture value occurred in river, lake, irrigation farming land and high coverage vegetation area due to water and water supply sufficiently.

Comparison of the statistical result of table 13 and figure 39 indicate that, sandy land with the increasing top soil grain size index value present the soil moisture decreasing. With the moderate grass degradation presented in figure 20 the soil moisture decreasing in degraded area.

7.7 Desertification analysis based on Groundwater Level Change

In this study, the groundwater level maps calculated by utilizing the experimental model based on the Landsat TM imagery of year 2000 and 2009.

Groundwater table image throughout the study area in year 2000 and 2009 shown in figure 40 and 41.

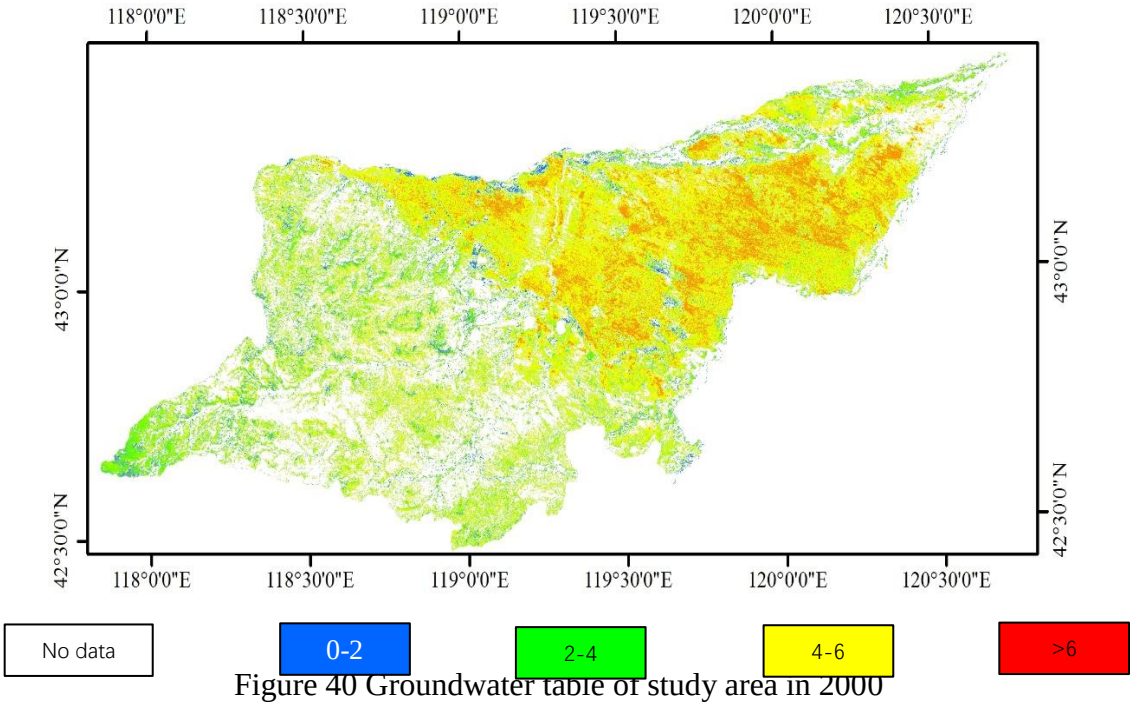

Figure 40 Groundwater table of study area in 2000

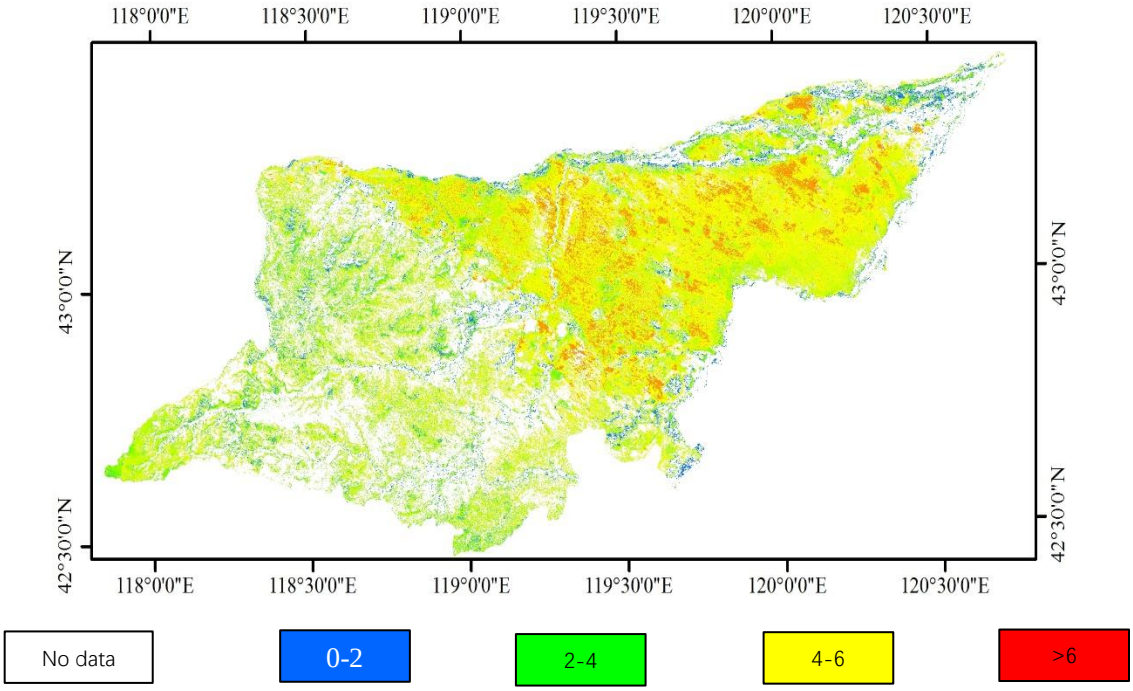

Figure 41 Groundwater table of study area in 2009

The groundwater level in study region is consistent with the soil moisture distribution in figure 40 and 41. In groundwater table in river, lake and irrigation farming land and paddy land ranging from 0-2; in dry farmland the groundwater table ranging from 2 to 4; in grassland area the groundwater table ranging from 4 to 6 and in exposed sandy land and shrub the groundwater table more than 6.

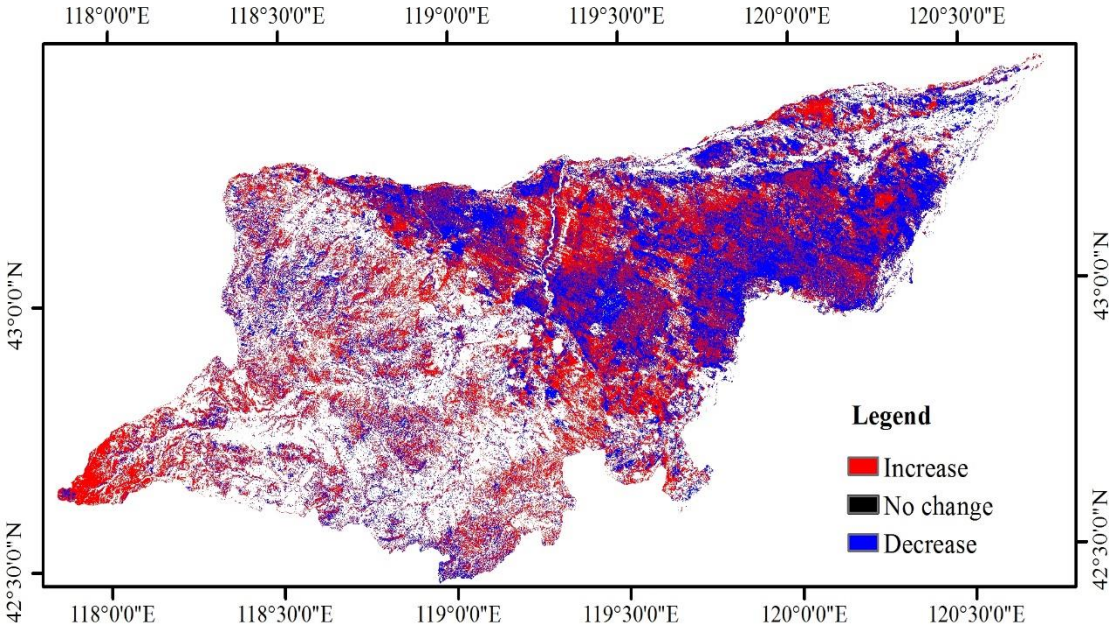

Figure 42 Groundwater level change between 2000 and 2009 in Ongniud Banner

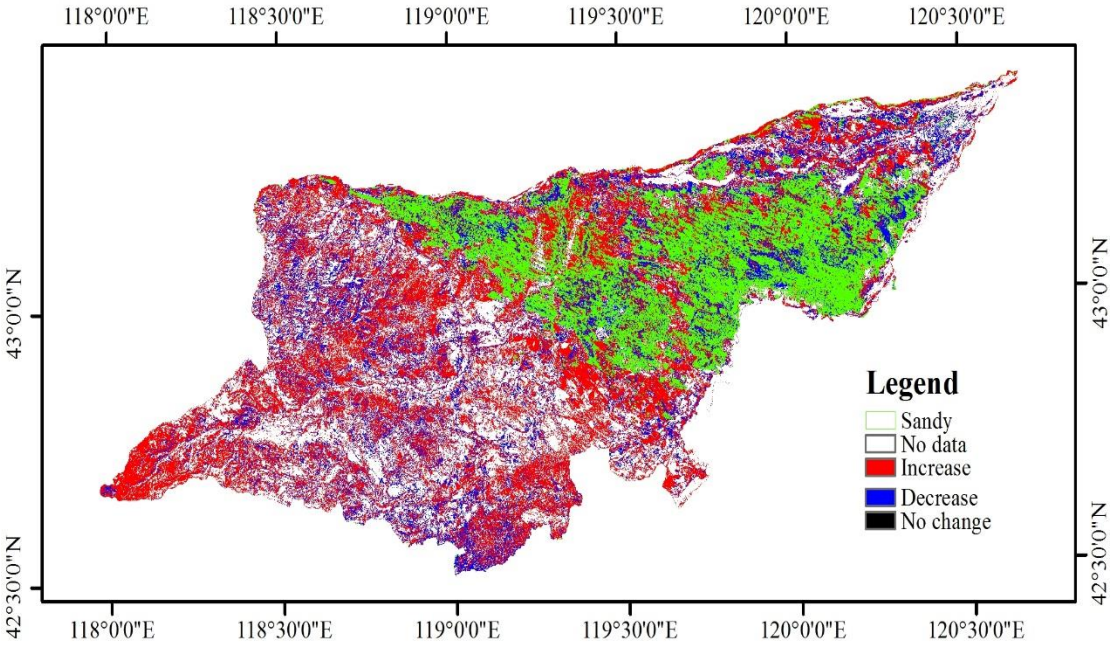

Figure 43 Groundwater level change between 2000 and 2009 in sandy land

The comparison of the map 14-15 and the figure 35-36, the result showed that ground water level declining in moderate grass decreased to sparse grass or other land cover types such as bare and in exposed sandy land with the surface soil moisture decreasing and the soil physical properties coarsening.

The previous researcher identified that the groundwater level in Horqin Sandy Land draw down due to the significant Land use land cover change coupled with persistent drought phenomenon (Zhao, Z.Z., 2016).

Chapter 8. Conclusion

Ongniud Banner is located in the western part of the Horqin Sandy Land, which belongs to a transitional zone of pastoral and animal husbandry regions and is vulnerable to anthropogenic activities and natural changes. It is representative of regions experiencing desertification, mainly caused by unsustainable human socioeconomic activities and significant interannual change in climate variations such as temperature and precipitation.

In this study, we attempted to understand desertification by analyzing changes of 17 categories of land sub-class LULC between 2000 and 2015 in Ongniud Banner. We studied changes in 17 categories of sub-class LULC to identify the desertification situation from 2000 to 2015. The analysis of land cover change based on "change to" categories between 2000 and 2015 images revealed that desertification extended to 3051 km^2 after 2000 due to a series of policies implemented to mitigate desertification in the Horqin Sandy Land. Desertification in moderate grasslands was the most common type (21% of total desertified area), followed by desertification in other forest, sparse grass, and forest areas at 19%, 16%, and 15%, respectively. Less desertification occurred in dense grass (8%) and dry land (6%) areas.

At the same time, we calculated ground surface variations including surface soil grain size index, ground surface temperature, ground surface water content, and ground water depth index to combine with LULC change and analyze the state of desertification in the study area between 2000–2009, 2009–2015, and 2000–2015.

Integration of physical properties indices, such as the surface soil grain size index, ground surface temperature, soil moisture index, and ground water depth index, with LULC change data revealed key findings:

Physical property indices are limited by only representing short land surface

phenomena change, but results successfully identified that the area of sandy land decreased during the analysis period. However, the deterioration of the sandy land was processing, while the LULC change is difficult to detect desertification processing occurred.

In addition, we discussed the driving causal forces of LULC change and desertification in the study area, such as socioeconomic situation, policy, and interannual oscillation of climate variations in the Horqin Sandy Land in the study period.

8.1 Advantages of the method used in this study

Previous studies in the Horqin Sandy Land utilized only the spectral bands of the satellite data used for change analysis of general LULC classes. In this study, we used a combination of multi-features (spectral indices, spectral transformations, textural, and topographic) of the LULC mapping process. The verification of the contribution of each feature in the research showed that using only the spectral features from Landsat data is not enough for improving the classification accuracy, as the misclassification between the secondary classes, such as irrigated land and swampland, swampland and paddy, bare area and tidal, cropland and bare area, bare area and urban, and grassland and forest were significant. The additional features (spectral indices, spectral transformations, textural, and topographic) could support production of a reliable LULC map.

8.2 Accuracy of LULC map change and cause factor

The overall accuracy (Kappa coefficient) obtained for 17 categories of land sub-class LULC in the study area were 0.86(0.85), 0.89(0.88), and 0.82(0.81) for the years 2000, 2009, and 2015 respectively.

The overall accuracy of LULC mainly depended on the expert knowledge of LULC interpretation based on available reference data. The accuracy of the 2009 LULC map is higher than the 2000 and 2015 LULC maps. The 2009 LULC map has the best overall

accuracy due to the high-resolution SPOT-5 image used as evidence of LULC in the study area providing high quality training data for 2009. The 2000 LULC map had better overall accuracy than 2015 due to the visual interpretation land use dataset of 2000 providing high quality training data for 2000. A lack of high-resolution ground truth reference data for 2015 resulted in a LULC map of 2015 with relatively lower accuracy than the 2000 and 2009 maps. But the comparison between previous LULC classification results [13] covers the study area with an overall accuracy of 86.83% and our results confirmed that this research successfully produced an accurate and reliable LULC map with 17 categories of land sub-classes for further analysis of LULC change and desertification in the study area.

8.3 LULC change between 2000 and 2015

The secondary class level LULC change analysis performed in the research provides very detailed information on LULC changes over the past 16 years. The high resolution (30 m) LULC change analysis in this study showed a significant LULC change in Ongniud Banner in the western part of the Horqin Sandy Land in Inner Mongolia. We also detected different LULC change trends over three periods, 2000–2009, 2009–2015, and 2000–2015. Over the past 16 years, irrigated farming lands and salinized areas expanded, whereas water bodies shrank, and exposed sandy lands were replaced by sparse grass and moderate grass converted to sparse grass.

8.4 The Ground surface variations and LULC change and desertification indicator

Additional physical property indices of ground surface variations, such as surface soil grain size index, ground surface temperature, soil moisture index, and ground water level depth revealed LULC change and desertification in this study. The top soil grain size index identified that soil physical properties were still worsening based on the

average GSI value (−0.09 in 2000 to 0.007 in 2015), whereas the area of sandy land decreased from 1684.3 km^2 in 2000 to 1051.1 km^2 in 2015. The increase of the top soil grain size index was accompanied by a ground surface temperature increase, whereas soil moisture and groundwater level depth decreased. The results show that ground surface condition indicators proved useful for monitoring desertification process for quantitative and qualitative changes.

8.5 Driving cause of LULC change and desertification

Human activities are the primary cause of 17 categories of LULC change and desertification. There was a significant change of interannual climate variations, including temperature and precipitation, which played a key role for changes in land use.

8.6 Perspective of this study

The satellite remote sensing-based detailed LULC change analysis performed in the study is important for assessing the performance of ecological protection and restoration programs.

Spatiotemporal change analyzes of detailed secondary classes in the research are expected to contribute to policy makers for the protection and sustainable management of environmentally sensitive ecological resources in the Horqin Sandy Land. This research has confirmed the expansion of irrigated farming lands and salinized areas over the past 16 years, whereas water bodies and sandy lands decreased. This trend implies an increasing demand for water. Therefore, a continuous and long-term monitoring of LULC changes related to water resources and salinization is suggested to promote sustainable development and the ecological security of northeast China.

Reference

Alatorre, L. C., & Beguería, S. (2009). Identification of eroded areas using remote sensing in a badlands landscape on marls in the central Spanish Pyrenees. Catena, 76(3), 182-190.

An, Y., Gao, W., & Gao, Z. (2014). Characterizing land condition variability in Northern China from 1982 to 2011. Environmental earth sciences, 72(3), 663-676.

Aubréville, A. (1949). Climats, forêts et désertification de l'Afrique tropicale.

Bagan, H., Takeuchi, W., Kinoshita, T., Bao, Y., & Yamagata, Y., (2010). Land cover classification and change analysis in the Horqin Sandy Land from 1975 to 2007. IEEE Journal of Selected Topics in Applied Earth Observations and Remote Sensing, 3(2), 168-177.

Baig, M. H. A., Zhang, L., Shuai, T., & Tong, Q. (2014). Derivation of a tasselled cap transformation based on Landsat 8 at-satellite reflectance. Remote Sensing Letters, 5(5), 423-431.

Becker, F., & Li, Z. -L. (1990). Temperature-independent spectral indices in TIR bands. Remote Sensing of Environment, 32, 17– 33.

Behnke, R., & Mortimore, M. (2016). The End of Desertification.

Bing. J., (2012), Chinese newspaper report for the issue of desertification of Inner Mongolia," *Bulletin of the Graduate School*, *Toyo University*, vol. 49, pp.25-39. (in Japanese)

Bullock, P., & Le Houérou, H., (1996). Land degradation and desertification.

Chander, G., & Markham, B. (2003). Revised Landsat-5 TM radiometric calibration procedures and postcalibration dynamic ranges. IEEE Transactions on geoscience and remote sensing, 41(11), 2674-2677.

Chen, Y., & Tang, H. (2005). Desertification in north China: background, anthropogenic impacts and failures in combating it. Land Degradation & Development, 16(4), 367-376.

Chen, Y., & Tang, H., (2005). Desertification in north China: background, anthropogenic impacts and failures in combating it. Land Degradation & Development, 16(4), 367-376.

Cline-Cole, R. A., Main, H. A. C., & Nichol, J. E. (1990). On fuelwood consumption, population dynamics and deforestation in Africa. World Development, 18(4), 513-527.

Crist, E. P., Laurin, R., & Cicone, R. C. (1986, September). Vegetation and soils information contained in transformed Thematic Mapper data. In Proceedings of IGARSS'86 Symposium (pp. 1465-1470). Paris: European Space Agency Publications Division.

Darkoh, M. B. K. (1996). The human dimension of desertification in the drylands of Africa. *Journal of Social Development in Africa*, *11*(2), 89-106.

Darkoh, M. B. K., (1998). The nature, causes and consequences of desertification in the drylands of Africa. Land Degradation & Development, 9(1), 1-20.

Duan, H. C., Wang, T., Xue, X., Liu, S. L., & Guo, J., (2014). Dynamics of aeolian desertification and its driving forces in the Horqin Sandy Land, Northern China. Environmental monitoring and assessment, 186(10), 6083-6096.

El-Karouri, M. O. H., (1986). The impact of desertification on land productivity in Sudan. In Physics of desertification (pp. 52-58). Springer Netherlands.

Fan, S. Y., & Zhou, L. H., (2001). Desertification control in China: possible solutions. Ambio, 30(6), 384-385.

French, D. (1986). Confronting an unsolvable problem: Deforestation in Malawi. World Development, 14(4), 531-540.

Ghulam, A., Qin, Q., Zhu, L., & Abdrahman, P. (2004). Satellite remote sensing of groundwater: quantitative modelling and uncertainty reduction using 6S atmospheric simulations. International Journal of Remote Sensing, 25(23), 5509-5524.

Gillespie, A., Rokugawa, S., Matsunaga, T., Cothern, J. S., Hook, S., & Kahle, A. B. (1998). A temperature and emissivity separation algorithm for Advanced Spaceborne Thermal Emission and Reflection Radiometer (ASTER) images. IEEE transactions on geoscience and remote sensing, 36(4), 1113-1126.

Glantz, M. H., & Orlovsky, N. S. (1983). Desertification: A review of the concept. *Desertification Control Bulletin*, *9*, 15-22.

Han, Z., Wang, T., Yan, C., Liu, Y., Liu, L., Li, A., & Du, H., (2010). Change trends for desertified lands in the Horqin Sandy Land at the beginning of the twenty-first century. Environmental Earth Sciences, 59(8), 1749-1757.

Huang, C., Davis, L. S., & Townshend, J. R. G. (2002). An assessment of support vector machines for land cover classification. International Journal of remote sensing, 23(4), 725-749.

Huang, F., Wang, P., & Liu, X. N., (2008). Monitoring vegetation dynamic in Horqin sandy land from spot vegetation time series imagery. The International Archives of the

Photogrammetry, Remote Sensing and Spatial Information Sciences, 37, 915-920.

Imuamirin, Takafumi Miyasaka, (2005). Discussion of the impact of time-series analysis and the agricultural policy of the desert KaSusumu line by satellite data - as a case study of China in Mongolia Autonomous Region Horqin sand -,Comprehensive Policy Studies word over King Paper Series, 65.5.

Iqbal, M. F., & Khan, I. A. (2014). Spatiotemporal land use land cover change analysis and erosion risk mapping of Azad Jammu and Kashmir, Pakistan. the Egyptian journal of remote sensing and space science, 17(2), 209-229.

Jaime, PG., Mas, JF., More, G. J. Cristobal, M. Martinez, A. Luz, M. Gueze, M. Macia and V. Garcia, (2013). Enhanced land use/land cover classification of heterogeneous tropical landscapes using support vector machines and textural homogeneity. *International Journal of Applied Earth Observation and Geoinformation*, 23, 372-383.

Kavzoglu, T., & Colkesen, I. (2009). A kernel functions analysis for support vector machines for land cover classification. International Journal of Applied Earth Observation and Geoinformation, 11(5), 352-359.

Kavzoglu, T., & Mather, P. M. (2003). The use of backpropagating artificial neural networks in land cover classification. International journal of remote sensing, 24(23), 4907-4938.

Kealy, P. S., & Gabell, A. R. (1990, June). Estimation of emissivity and temperature using alpha coefficients. In Proc. 2nd TIMS Workshop (pp. 90-55). Jet Propul. Lab..

Li, J., Xu, B., Yang, X., Jin, Y., Zhao, Zhao, L., Zhao, F., Shi, C., Jian, G., Qin, Z., & Ma, H., (2015). Characterizing changes in grassland desertification based on Landsat images of the Ongniud and Naiman Banners, Inner Mongolia. *International Journal of Remote Sensing*, *36*(19-20), 5137-5149.

Li, X., & Zhang, H. (2014). Soil moisture effects on sand saltation and dust emission observed over the Horqin Sandy Land area in China. Journal of Meteorological Research, 28, 444-452.

Li, X., & Zhang, H. (2014). Soil moisture effects on sand saltation and dust emission observed over the Horqin Sandy Land area in China. Journal of Meteorological Research, 28, 444-452.

M. Sciortino, (2001). Desertification in the Mediterranean. *Contributed Paper of the 22th International School on Disarmament and Research on Conflicts (ISODARCO) Summer Course*, Candriai, Italy.

Mallo, I. I. Y., & Ochai, B. C. (2009). An Assessment of the Effects of Urbanization on

Deforestation in Bwari Council, Abuja–FCT, Nigeria. Abuja Journal of Geography and Development, 3(1), 1-19.

Mantero, P., Moser, G., & Serpico, S. B. (2005). Partially supervised classification of remote sensing images through SVM-based probability density estimation. IEEE Transactions on Geoscience and Remote Sensing, 43(3), 559-570.

Mountrakis, G., Im, J., & Ogole, C. (2011). Support vector machines in remote sensing: A review. ISPRS Journal of Photogrammetry and Remote Sensing, 66(3), 247-259.

National Research Council. (1992). Grasslands and grassland sciences in northern China. National Academies Press.

Nicholson, S. E., Tucker, C. J., & Ba, M. B., (1998). Desertification, drought, and surface vegetation: an example from the West African Sahel. Bulletin of the American Meteorological Society, 79(5), 815-829.

Niu, C. Y., Musa, A., & Liu, Y. (2015). Analysis of soil moisture condition under different land uses in the arid region of Horqin sandy land, northern China. *Solid Earth*, *6*(4), 1157-1167.

Niu, C. Y., Musa, A., & Liu, Y. (2015). Analysis of soil moisture condition under different land uses in the arid region of Horqin sandy land, northern China. Solid Earth, 6(4), 1157-1167.

Plit, F., Plit, J., & Żakowski, W., (1995). Drylands Development and Combating Desertification: Bibliographic Study of Experiences in Countries of the CIS (No. 14). Food & Agriculture Org..

Qi, F., Ma, H., Jiang, X., Wang, X. & Cao, S., (2015). What Has Caused Desertification in China? *Sci. Rep.* **5**, 15998; doi: 10.1038/srep15998.

RM. Pink, Water Rights in Southeast Asia and India, Palgrave Macmillan, US, 2016. pp. 1-253.

Ran, S. H., & Jin, J. J. (2004). Evolvement and control of vulnerable ecological region. Chinese Geographical Science, 14(2), 135-141.

Ran, S., and Jin, J. (2004). Evolvement and control of vulnerable ecological region. Chinese Geographical Science, 14(2), 135-141.

Roth, M., Oke, T. R., & Emery, W. J. (1989). Satellite-derived urban heat islands from three coastal cities and the utilization of such data in urban climatology. International Journal of Remote Sensing, 10(11), 1699-1720.

Rubio, J. L., & Bochet, E. (1998). Desertification indicators as diagnosis criteria for

desertification risk assessment in Europe. Journal of Arid Environments, 39(2), 113-120.

Sepehr, A., Hassanli, A. M., Ekhtesasi, M. R., & Jamali, J. B. (2007). Quantitative assessment of desertification in south of Iran using MEDALUS method. Environmental monitoring and Assessment, 134(1), 243-254.

Sharma, R. C., Tateishi, R., Hara, K., & Iizuka, K. (2016). Production of the Japan 30-m Land Cover Map of 2013–2015 Using a Random Forests-Based Feature Optimization Approach. Remote Sensing, 8(5), 429.

Snyder, W. C., Wan, Z., Zhang, Y., & Feng, Y. Z. (1998). Classification-based emissivity for land surface temperature measurement from space. International Journal of Remote Sensing, 19(14), 2753-2774.

State Forestry Administration, (2011). A Bulletin of Status Quo of Desertification and Sandification in China. Government Report.

Steffens, M., Kölbl, A., Totsche, K. U., & Kögel-Knabner, I. (2008). Grazing effects on soil chemical and physical properties in a semiarid steppe of Inner Mongolia (PR China). Geoderma, 143(1), 63-72.

Su, Y. Z., Zhang, T. H., Li, Y. L., & Wang, F. (2005). Changes in soil properties after establishment of Artemisia halodendron and Caragana microphylla on shifting sand dunes in semiarid Horqin Sandy Land, Northern China. Environmental Management, 36(2), 272-281.

Su, Y. Z., Zhao, H. L., Zhang, T. H., & Zhao, X. Y. (2004). Soil properties following cultivation and non-grazing of a semi-arid sandy grassland in northern China. Soil and Tillage Research, 75(1), 27-36.

Szirmai, A. (2005). The dynamics of socio-economic development: an introduction. Cambridge University Press.

Takeuchi, K., Katoh, K., Nan, Y., & Kou, Z. (1995). Vegetation cover change in desertified Kerqin sandy lands, Inner Mongolia. Geog. Rep. Tokyo Metropolitan Univ, 30, 1-24.

Tashpolat, T., & Abduwasit, G. (2002). Research on model of groundwater level distribution in the oasis and desert ecotone using remote sensing. JOURNAL OF REMOTE SENSING-BEIJING-, 6(4), 299-306.

UNCOD. Secretariat, (1977). Desertification: Its Causes and Consequences. *Secretariat of United Nations Conference on Desertification (Ed.)*, Pergamon Press, Oxford, UK.

Valor, E., & Caselles, V. (1996). Mapping land surface emissivity from NDVI:

Application to European, African, and South American areas. Remote sensing of Environment, 57(3), 167-184.

Valor, E., & Caselles, V. (1996). Mapping land surface emissivity from NDVI: Application to European, African, and South American areas. Remote sensing of Environment, 57(3), 167-184.

Verstraete, M. M. (1986). Defining desertification: a review. *Climatic Change*, *9*(1), 5-18.

WANG, Tao, and Ha-lin ZHAO. "Fifty-year History of China Desert Science [J]." *Journal of Desert Research* 2 (2005): 000.

WRI, IUCN. (1995). UNEP. 1992. Global Biodiversity Strategy .

Wang, F., Pan, X., Wang, D., Shen, C., & Lu, Q., (2013). Combating desertification in China: past, present and future. Land Use Policy, 31, 311-313.

Wang, G., Wang, X., Wu, B. & Lu, Q., (2012). Desertification and its mitigation strategy in China. Journal of Resources and Ecology, 3(2), 97-104.

Wang, G., Wang, X., Wu, B., & Lu, Q. (2012). Desertification and its mitigation strategy in China. Journal of Resources and Ecology, 3(2), 97-104.

Wang, R. Z., & Li, J. D. (1995). Study on grazing succession law in Songnen grassland. Chinese Journal of Applied Ecology, 6, 277-281. (In Chinese)

Wang, S. J., Liu, Q. M., & Zhang, D. F., (2004). Karst rocky desertification in southwestern China: geomorphology, landuse, impact and rehabilitation. Land degradation & development, 15(2), 115-121.

Wang, T. (2000). Land use and sandy desertification in the north China. J. Desert Res., 20(2), 103-107. (In Chinese).

Wang, T., & Zhao, H., (2005). Fifty-year history of China desert science. *Journal of Desert Research*, *25*(2), 145-165.

Wang, T., Wu, W., Xue, X., Han, Z., Zhang, W., & Sun, Q., (2004). Spatial-temporal changes of sandy desertified land during last 5 decades in northern China. ACTA GEOGRAPHICA SINICA-CHINESE EDITION-, 59(2), 203-212.

Wang, X., Chen, F., & Dong, Z. (2006). The relative role of climatic and human factors in desertification in semiarid China. Global Environmental Change, 16(1), 48-57.

Warren, A., & Agnew, C., (1988). An assessment of desertification and land degradation in arid and semi-arid areas. London: IIED 72p. En IIED Drylands Programme, Drylands Paper, (2).

Watson, K. (1992). Spectral ratio method for measuring emissivity. Remote Sensing of Environment, 42(2), 113-116.

World Health Organization (WHO), (1992). United Nations Environment Programme (UNEP)," *Urban air pollution in megacities of the world*, Cambridge, MA: Blackwell Publishers, Oxford.

Wu, B., & Ci, L. J. (2002). Landscape change and desertification development in the Mu Us Sandland, Northern China. Journal of Arid Environments, 50(3), 429-444.

Xiao, J., Shen, Y., Tateishi, R., & Bayaer, W. (2006). Development of topsoil grain size index for monitoring desertification in arid land using remote sensing. International Journal of Remote Sensing, 27(12), 2411-2422.

Yan, Q. L., Zhu, J. J., Hu, Z. B., & Sun, O. J. (2011). Environmental impacts of the shelter forests in Horqin Sandy Land, Northeast China. Journal of environmental quality, 40(3), 815-824.

Yan, S., & Liu, Z. (2010). Effects of dune stabilization on the plant diversity of interdune wetlands in northeastern Inner Mongolia, China. Land Degradation & Development, 21(1), 40-47.

Yan, Y., Zhu, J., Yan, Q., Zheng, X., & Song, L. (2014). Modeling shallow groundwater levels in Horqin Sandy Land, North China, using satellite-based remote sensing images. Journal of Applied Remote Sensing, 8(1), 083647-083647.

Yong-Zhong, S., Yu-Lin, L., Jian-Yuan, C., & Wen-Zhi, Z. (2005). Influences of continuous grazing and livestock exclusion on soil properties in a degraded sandy grassland, Inner Mongolia, northern China. Catena, 59(3), 267-278.

Zhang, G., Dong, J., Xiao, X., Hu, Z., & Sheldon, S. (2012). Effectiveness of ecological restoration projects in Horqin Sandy Land, China based on SPOT-VGT NDVI data. *Ecological Engineering*, *38*(1), 20-29.

Zhang, T. H., Zhao, H. L., Li, S. G., & Zhou, R. L. (2004). Grassland changes under grazing stress in Horqin sandy grassland in Inner Mongolia, China. New Zealand Journal of Agricultural Research, 47(3), 307-312.

Zhang, T. H., Zhao, H. L., Li, S. G., Li, F. R., Shirato, Y., Ohkuro, T., & Taniyama, I. (2004). A comparison of different measures for stabilizing moving sand dunes in the Horqin Sandy Land of Inner Mongolia, China. *Journal of Arid Environments*, *58*(2), 203-214.

Zhao, H. L., Masayuki, N., & Toshiya, O. (1997). Study on desertification mechanism of grazing grassland in Kerqin sandy land in inner Mongolia, China. Grassland of China, 3, 15-23.

Zhao, H. L., Yi, X. Y., Zhou, R. L., Zhao, X. Y., Zhang, T. H., & Drake, S. (2006). Wind erosion and sand accumulation effects on soil properties in Horqin Sandy Farmland, Inner Mongolia. Catena, 65(1), 71-79.

Zhao, H. L., Zhao, X. Y., Zhou, R. L., Zhang, T. H., & Drake, S., (2005). Desertification processes due to heavy grazing in sandy rangeland, Inner Mongolia. Journal of Arid Environments, 62(2), 309-319.

Zhao, H. L., Zhou, R. L., Zhang, T. H., & Zhao, X. Y. (2006). Effects of desertification on soil and crop growth properties in Horqin sandy cropland of Inner Mongolia, north China. Soil and Tillage Research, 87(2), 175-185.

Zhao, H. L.; Nemoto, M.; Ohkuro, T. 1997: Study on desertification mechanism of grazing grassland in Horqin Sandy Land. Journal of Desert Research 17 (Supplement 1): 15-21. (In Chinese)

Zhao, H., & Chen, X. (2005, July). Use of normalized difference bareness index in quickly mapping bare areas from TM/ETM+. In Geoscience and Remote Sensing Symposium, 2005. IGARSS'05. Proceedings. 2005 IEEE International (Vol. 3, pp. 1666-1668). IEEE.

Zhao, X., Zhang, C., Zuo, X., Huang, G., Huang, Y., Luo, Y., Wang, S., & Huang, Q., 2009. Challenge to the desertification reversion in Horqin Sandy Land. *Chinese Journal of Applied Ecology*, 20(7)

Zhao, Z., Lin, A., Feng, J., Yang, Q., & Zou, L. (2016). Analysis of Water Resources in Horqin Sandy Land Using Multisource Data from 2003 to 2010. *Sustainability*, *8*(4), 374.

Zhao, Z., Lin, A., Feng, J., Yang, Q., & Zou, L. (2016). Analysis of Water Resources in Horqin Sandy Land Using Multisource Data from 2003 to 2010. Sustainability, 8(4), 374.

Zhao, Z., Lin, A., Feng, J., Yang, Q., & Zou, L., (2016). Analysis of Water Resources in Horqin Sandy Land Using Multisource Data from 2003 to 2010. Sustainability, 8(4), 374.

Zhenda, Z., (1989). Advance in desertification research in China. Journal of Desert Research, 1, 000.

Zhu, Z. (1989). Advance in desertification research in China. Journal of Desert Research, 1, 000.

Zuo, X., Zhao, H., Zhao, X., Zhang, T., Guo, Y., Wang, S., & Drake, S. (2008). Spatial pattern and heterogeneity of soil properties in sand dunes under grazing and restoration in Horqin Sandy Land, Northern China. Soil and Tillage Research, 99(2), 202-212.